Purdue University
Purdue e-Pubs

Open Access Dissertations | Theses and Dissertations

5-2018

Morphological Changes of Neuronal Growth Cones by Intracellular Signaling and Cell Culture Conditions

Yuan Ren
Purdue University

Follow this and additional works at: https://docs.lib.purdue.edu/open_access_dissertations

Recommended Citation
Ren, Yuan, "Morphological Changes of Neuronal Growth Cones by Intracellular Signaling and Cell Culture Conditions" (2018). *Open Access Dissertations*. 1809.
https://docs.lib.purdue.edu/open_access_dissertations/1809

This document has been made available through Purdue e-Pubs, a service of the Purdue University Libraries. Please contact epubs@purdue.edu for additional information.

MORPHOLOGICAL CHANGES OF NEURONAL GROWTH CONES BY INTRACELLULAR SIGNALING AND CELL CULTURE CONDITIONS

by

Yuan Ren

A Dissertation

Submitted to the Faculty of Purdue University

In Partial Fulfillment of the Requirements for the degree of

Doctor of Philosophy

Department of Biological Sciences

West Lafayette, Indiana

May 2018

THE PURDUE UNIVERSITY GRADUATE SCHOOL

STATEMENT OF COMMITTEE APPROVAL

Dr. Donna Fekete, Chair

Department of Biological Sciences

Dr. Daniel Suter

Department of Biological Sciences

Dr. Chris Staiger

Department of Biological Sciences

Dr. Taeyoon Kim

Department of Biomedical Engineering

Approved by:

Dr. Daniel Suter

Head of the Graduate Program

Neurons of the world, unite!

ACKNOWLEDGMENTS

I would like to acknowledge the invaluable support I got from my PhD advisor Dr. Daniel Suter. His passion for science, attention to details and work ethics are exemplary of a true scientist and everlasting lessons for me learn from. He is encouraging and kind to everyone, and always available to help. I'm grateful for the freedom he granted for scientific exploration, especially in the early years of my PhD, and the generosity he displays to his students. He is a good companion in science as well as in life, and I feel fortunate to have had him as a mentor.

I would like to express gratitude to my committee members, Dr. Chris Staiger, Dr. Donna Fekete and Dr. Taeyoon Kim, whose constructive criticism made this dissertation possible. I also thank them for being inspiring scholars and conscientious instructors, and for raising my appetite for science.

I appreciate the help from members of Suter lab and Hollenbeck lab, who inspired my research and made my PhD years fulfilling. My thanks goes to Dr. Peter Hollenbeck, Dr. Yingpei He, Dr. Cory Weaver, Dr. Ahmad Athamneh, Haley Summers Roeder, Aslihan Terzi, Kristi McElmurry, Dr. Vidhya Munnamalai, Dr. Swathi Devireddy, Dr. Hyun Sung, Dr. Pin Chao Liao, Elizabeth Garland-Kuntz, Autumn Beachy, Melissa Casella, and Sabbir Alam.

I'm also grateful to help from lab of Dr. Fang Huang for super-resolution imaging. I thank Dr. Michael J Mlodzianoski and Dr. Donghan Ma for image acquisition and reconstruction. Many thanks to Dr. Seema Mattoo and Dr. Anwesha Sanyal for their help with Src kinase assay.

My sincere gratitude to my parents and my wife, who believed in me and supported me with deep love. I love you too.

Thank *you* for reading.

TABLE OF CONTENTS

LIST OF TABLES

LIST OF FIGURES

LIST OF ABBREVIATIONS

AFM	Atomic force microscopy
apCAM	*Aplysia* cell adhesion molecule
ASW	Artificial sea water
BSA	Bovine serum albumin
CB	Cytochalasin B
CCD	Charge-coupled device
C domain	Central domain
DIC	Differential interference contrast
DMSO	Dimethyl sulfoxide
ECM	Extracellular matrix
EGTA	Ethylene glycol tetra-acetic acid
F-actin	Filamentous actin
FBS	Fetal bovine serum
FSM	Fluorescent speckle microscopy
G-actin	Globular actin
HEPES	4-(2-Hydroxyethyl)-1-piperazineethanesulfonic acid
IgCAM	Immunoglobulin superfamily cell adhesion molecule
LatA	Latrunculin A
MT	Microtubule
NPF	Nucleation-promoting factor
NTA	N-terminal acidic

PBS	Phosphate-buffered saline
P domain	Peripheral domain
PLL	Poly-L-lysine
RBI	Restrained bead interaction
RT	Room temperature
sCMOS	scientific complementary metal-oxide-semiconductor
SH	Src homology
STORM	Stochastic optical reconstruction microscopy
T zone	Transition zone
WASP	Wiskott-aldrich syndrome protein

ABSTRACT

Author: Ren, Yuan. PhD

Institution: Purdue University

Degree Received: May 2018

Title: Morphological Changes of Neuronal Growth Cones by Intracellular Signaling and Cell Culture Conditions.

Major Professor: Daniel Suter

Proper wiring of neurons is key to the functionality of nervous system. This is achieved by a highly motile structure referred to as the neuronal growth cone located at the tip of axons and dendrites during both development and regeneration. The morphology of growth cone is a product of both intracellular signaling pathways and extracellular factors, and is closely linked with neuronal outgrowth. Studies of how growth cone morphology is changed by key regulatory proteins and by cell culture conditions are therefore important in elucidating the mechanisms of neurite regeneration.

In the first part of this thesis, we identified a single tyrosine residue (Y499) in *Aplysia* cortactin that is important for regulating filopodia formation in growth cone. Overexpression of the 499F phospho-deficient cortactin mutant decreased filopodia length and density, whereas overexpression of the 499E phospho-mimetic mutant increased filopodia length, regardless of the phosphorylation state of Y505 or Y509. Using a custom-made antibody against cortactin phosphorylated at Y499, we showed that phosphorylated cortactin is enriched in the peripheral domain, specifically along the leading edge. We found that treatment with the Src inhibitor PP2 decreased cortactin phosphorylation, while overexpression of Src2 increased cortactin phosphorylation. We demonstrated that the leading edge localization of phosphorylated cortactin is F-actin independent, and important in promoting filopodia formation. Finally, by interfering both with cortactin phosphorylation and Arp2/3 activation, we found that Arp2/3 complex acts downstream of cortactin to regulate filopodia density but not length. In conclusion, we have

characterized a tyrosine phosphorylation site in *Aplysia* cortactin that plays a major role in the Src/cortactin/Arp2/3 signaling pathway controlling filopodia formation.

In the second part of this thesis, we offer a comprehensive cellular analysis of the motile behavior of *Aplysia* growth cones on two-dimensional (2D) culture beyond the pausing state. We found that average growth cone size decreased with cell culture time whereas average growth rate increased. This inverse correlation of growth rate and growth cone size was due to the occurrence of large growth cones with a peripheral domain larger than 100 μm^2. The large pausing growth cones had central domains that were less consistently aligned with the direction of growth and could be converted into smaller, faster-growing growth cones by addition of a three-dimensional (3D) collagen gel. We conclude that the significant lateral expansion of lamellipodia and filopodia as observed during these culture conditions has a negative effect on neurite growth. Further, using the novel collagen gel and an easy-to-make microwell device, we developed a simple protocol for 3D culture of *Aplysia* bag cell neuron. We found that the morphology and growth pattern of bag cell growth cones in 3D culture closely resemble the ones of growth cones observed *in vivo*, and demonstrated the capability of our device for high-resolution imaging of cytoskeletal and signaling proteins as well as organelles. We expect that our microwell device will facilitate a wider adoption of 3D neuronal cultures to study the mechanisms of neurite regeneration.

CHAPTER 1. INTRODUCTION

1.1 *Aplysia californica* as a model system in neurobiology

1.1.1 Sea hare with a simple nervous system

Aplysia californica is the scientific name of a species of sea hare, native to the coast of the California state (Carefoot, 1987). *Aplysia* inhibits the intertidal region to eat red algae, which, in addition to being a food source, provides pigment to make this animal reddish and its protective ink purple (Kupfermann and Carew, 1974). *Aplysia* is hermaphroditic, has a life span of one year and an average bodyweight of 1 kg in the wild (Fig 1.1A) (Audesirk, 1979).

Though estimated to have only 20,000 neurons, *Aplysia* display remarkable ability to respond to external stimuli with altered behavior, making it a good model to study learning and memory (Pinsker et al., 1970, Moroz, 2011). Coupled with the big size of *Aplysia* neurons and easy access to its central nervous system, changes in animal behavior can be attributed to changes in connectivity of identified neurons and their subcellular molecular composition, thereby offering possibility for detailed analysis of neural activity (Brembs et al., 2002).

1.1.2 Bag cell neurons

Bag cell neurons reside in the abdominal ganglion of *Aplysia*, where ~400 cells form two clusters (Fig 1.1B). The physiological role of bag cell neurons is to secret egg laying hormone during mating season, which is sufficient to induce egg laying behavior of the animal (Conn and Kaczmarek, 1989, Hatcher and Sweedler, 2008). Befitting to this role, mature bag cell neurons are large (cell diameter 50 μm), contain large number of peptide-embedding vesicles, and do not form synapses with other neurons. Rather, the cell bodies of bag cell neurons are physically connected for concerted activity, and processes from bag cell neurons *in vivo* are specialized for hormone release, upon stimulation, directly to abdominal ganglion and into surrounding hemolymph (blood serum for invertebrate) (Kaczmarek et al., 1979, Kupfermann and Kandel, 1970, Nick et al., 1996b). Electrophysiological studies have found that depolarized bag cell neurons are capable of long lasting train of bursts up to 30 minutes, which correlated with sustained hormone release (Nick et al., 1996a, Wayne et al., 1998, White et al., 1998).

In vitro culture of isolated *Aplysia* bag cell neurons gained popularity with the advent of neuronal cell culture and video enhanced microscopy 30 years ago (Forscher and Smith, 1988, Dotti et al., 1988, Goldberg and Burmeister, 1986), which soon led to seminal discoveries about principles of neurite outgrowth (Winckler et al., 1999, Suter and Forscher, 1998, Suter et al., 1998, Thompson et al., 1996, Lin et al., 1996, Lin and Forscher, 1995). This is due to 1) the ability of cultured bag cell neurons to spontaneously regenerate neurites without induction; and 2) the formation of a wide and flat structure at neurite tip (neuronal growth cone) which is several times the size of growth cones from neurons of other origins. These advantages make cultured bag cell neurons a favored subject for neuro-regenerative studies, and a main target of investigation in this thesis.

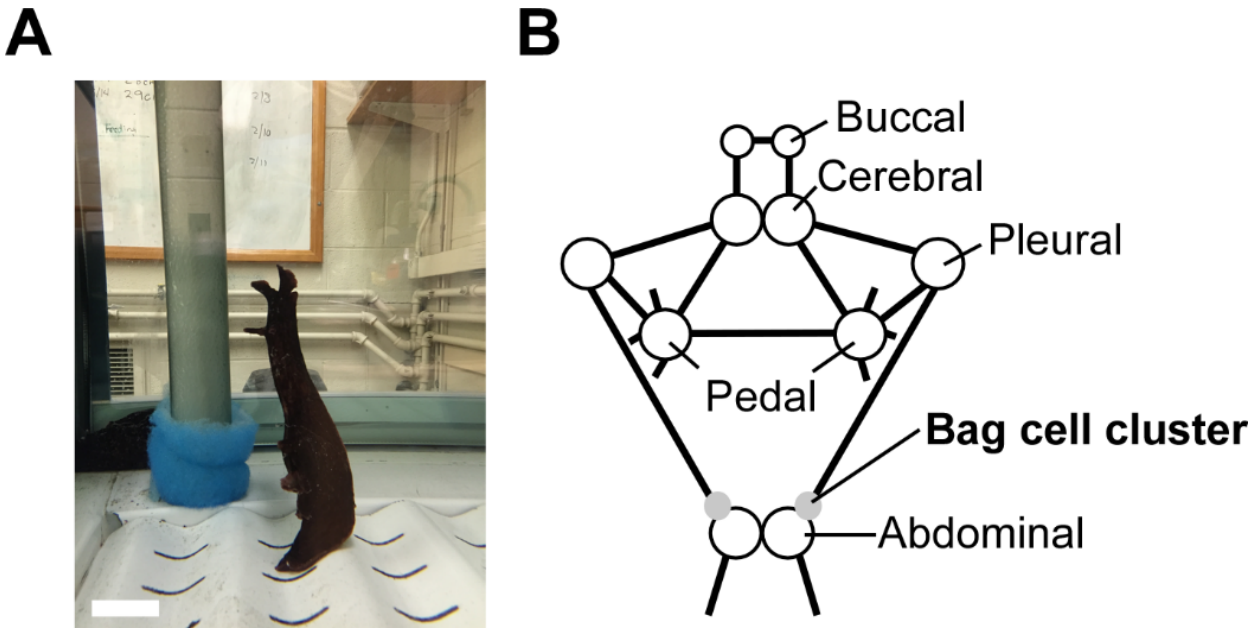

Figure 1.1. Anatomy of *Aplysia* central nervous system

A. Adult *Aplysia* in tank. B. Schematic of *Aplysia* central nervous system showing the connections between ganglions. Bag cell neurons in bag cell cluster were used in this study. Scale bar in A: 5cm. Panel B adapted from Biao Sun and Pei-San Tsai, 2011.

1.2 Neuronal growth cone

1.2.1 The neuronal growth cone is the motile end of neurites

Presence of a sensory and motile structure at the neurite tip during embryonic development was discovered by Santiago Ramon y Cajal, and the structure named growth cone (Fig 1.2). Subsequent observation of neurite elongation in different species verified the importance of the growth cone in directing the extension of axons and dendrites, in both development and disease (Goodhill et al., 2015, Vitriol and Zheng, 2012, Bovolenta and Mason, 1987). Neuronal growth cones are responsible for detecting guidance cues via soluble and substrate-bound molecules, making decisions about growth direction and rate, reorganizing force-generating components to power translocation, and are transformed into synaptic structures after establishment of correct connections (Kerstein et al., 2015, Hur et al., 2012, Lowery and Van Vactor, 2009). Proper wiring of a functional nervous system thus depends strongly on healthy growth cones, and growth cone defects in development often lead to severe neurological disorder (Engle, 2010). Importantly, the lack of neurite regeneration in the central nervous system (CNS) of human adults after injury remains a serious medical and social issue, and studies of neurons with higher regenerative potential, such as *Aplysia* bag cell neurons, are therefore needed for insights into neurite regeneration.

Figure 1.2. Drawing of growth cones in chicken embryo.

A, B and C are drawings of growth cones in 3 day old chicken embryo from the same type of neuron but at different positions. Note the morphological changes from flat (A) to club-like (C). The morphology of growth cone is strongly influenced by both intracellular and extracellular factors. Drawing by Santiago Ramon y Cajal, 1890.

1.2.2 Cytoskeletal organization in the neuronal growth cone

The motility of a growth cone is ultimately mediated by its two major components of cytoskeleton: microtubules and actin (Fig 1.3) (Omotade et al., 2017, Dent et al., 2011, Dent et al., 2003, Dent and Gertler, 2003, Bentley and O'Connor, 1994). Microtubules occupy the proximal region of the growth cone (central domain or C domain), while actin filaments make up the distal region (peripheral domain or P domain). The boundary of C domain and P domain is rich in membrane ruffles and called transitional zone (T zone). In contrast to C domain and T zone, which contain various organelles, P domain is considered a relatively "clean" region of membrane bound actin filaments, similar to the leading edge of migrating fibroblast (Xiong et al., 2009). The occasional invasion of microtubules into P domain is believed to be preferentially along bundled actin, although the presence of actin is not required for microtubule invasion (Burnette et al., 2007, Suter et al., 2004, Schaefer et al., 2002, Sabry et al., 1991). Both microtubule polymerization and translocation are involved in neurite elongation (Athamneh et al., 2017). Crosstalk in microtubule and actin regulation coordinates their functions for proper neurite outgrowth (Mahajan and Athale, 2012, Jang et al., 2010, Lee and Suter, 2008, Suter and Forscher, 2001, Rochlin et al., 1999, O'Connor and Bentley, 1993).

1.3 Actin in the neuronal growth cone

1.3.1 Actin and actin regulators

Actin is a highly conserved cytoskeletal protein that exists both in monomeric (globular actin or G-actin), and polymer forms (filamentous actin or F-actin) in all eukaryotic cells (Blanchoin et al., 2014, Dominguez and Holmes, 2011). Actin binds to ATP, which is slowly hydrolyzed during the polymerization process. Monomeric actin always binds with the same orientation, therefore creating a filament with preserved polarity. Specifically, the end with the ATP binding cleft is called "pointed" end (or minus end), with the other end called "barbed" end (or plus end). Although monomers could add to and come off from both ends, the critical G-actin concentration to reach equilibrium at barbed end is 1/5 that of the pointed end, and both polymerization and depolymerization happen faster at barbed end (Pollard, 1986). The polarity of F-actin is also important in directing the movement of molecular motors such as myosin along F-actin tracks (Houdusse and Sweeney, 2016).

In cells, actin is under the control of a wide variety of regulators, which substantially change actin behavior (Uribe and Jay, 2009). There are G-actin binding proteins such as profilin to alter monomer availability, cross-linking proteins such as fascin and actinin to facilitate the formation of filament bundles, severing proteins such as ADF/cofilin and gelsolin to break down F-actin into fragments and monomers, capping proteins to control the number of barbed ends, and formins that accelerate actin polymerization rate (Bamburg and Bernstein, 2010, Cao et al., 2016, DeWard et al., 2010, Jansen et al., 2011). These actin regulators are also under the control of multiple signaling molecules such as GTPase and calcium, as well as interacting or counteracting with each other, further adding to the complexity of actin regulation (Davidson and Wood, 2016).

Among various forms of actin structures, the formation of branches from existing F-actin is key to the generation of higher ordered architecture. This is enabled by a seven subunit protein complex called Arp2/3 complex that binds to the side of F-actin (mother filament) and initiates the formation of new F-actin (daughter filament) with a fixed angle of 70 degrees (Helgeson and Nolen, 2013, Uruno et al., 2001). Reiteration of this process leads to dendritic network of actin filaments which, when coupled with other actin regulators, provide force to propel cell movement (Mitchison and Cramer, 1996, Svitkina, 2018). Prior to branching, however, the Arp2/3 complex needs to be activated by one of the members from nucleating promoting factor (NPF) families, which contains N-WASP, cortactin, Abp1 and type 1 myosins (Olazabal and Machesky, 2001, Uruno et al., 2001, Suetsugu, 2013, Goley and Welch, 2006). Signaling pathways that control the state of NPFs are therefore crucial to the organization and dynamics of actin structures.

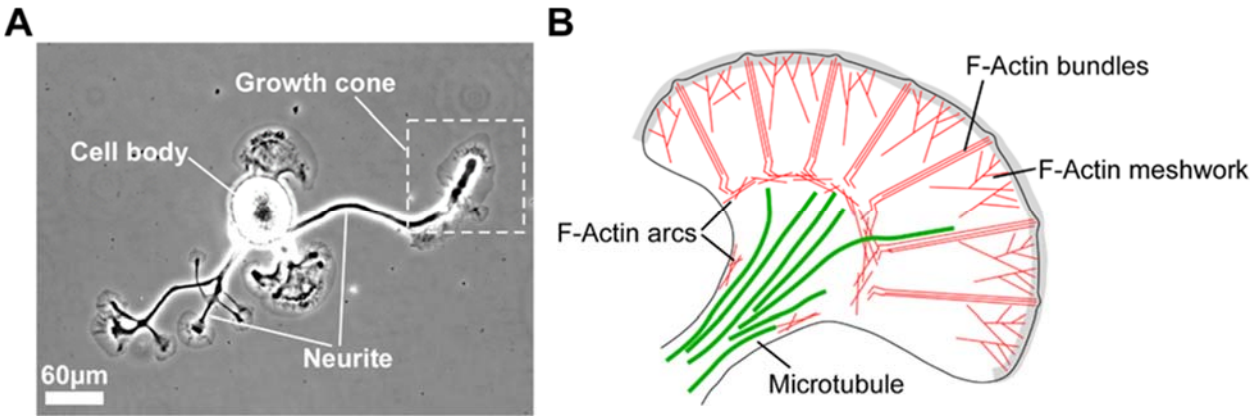

Figure 1.3. Cytoskeletal organization in neuronal growth cones

A. DIC image of a cultured *Aplysia* bag cell neuron. Neurites regenerate from the cell body. One growth cone is highlighted with dotted line. B. Schematic of bag cell neuron growth cone showing its cytoskeletal organization. Red lines represent F-actin, and green lines represent microtubules. Three F-actin structures can be found at growth cone: Bundled F-actin filaments and F-actin meshwork in P domain, and F-actin arcs in T zone and growth cone neck. Myosins locate on F-actin arcs and generates contractile force to power retrograde actin flow. F-actin bundles are buckled near T zone and depolymerized for G-actin recycling. Most microtubules are in C domain, but occasional invasion of microtubule into P domain could be observed. Shaded area denotes leading edge, where majority of F-actin barbed ends reside.

1.3.2 Actin organization in the neuronal growth cone

There are at least three different F-actin organizations in the neuronal growth cone: 1) bundled F-actin filaments with uniform polarity; 2) dendritic meshwork of F-actin filaments and 3) arcs of F-actin filaments with mixed polarity (Fig 1.3B) (Omotade et al., 2017, Schaefer et al., 2002, Burnette et al., 2007). F-actin bundles and dendritic F-actin meshwork are both found in the P domain and account for majority of the F-actin content in the growth cone. The leading edge of the growth cone, which is the narrow band immediately after the P domain edge, contains high density of barbed ends for F-actin formation (Lewis and Bridgman, 1992). In contrast, actin arcs locate in T zone and sides of growth cone neck, where they associate with myosin to generate contractile force for retrograde actin flow, and for constraining microtubule to consolidate newly formed neurite segment (Dent et al., 2011, Burnette et al., 2008, Lin et al., 1996, Lin and Forscher, 1995).

1.3.3 Actin dynamics in the neuronal growth cone

At steady state, the polymerization of F-actin at barbed end is balanced by the backward movement of bulk F-actin network in the P domain, resulting in an apparent pausing of the growth cone. The growth cone advances when polymerization rate exceeds retrograde flow rate and retracts when polymerization rate falls below retrograde flow rate (He et al., 2015). Control of actin polymerization/depolymerization rate at F-actin barbed end is the dominating factor in determining the net outcome of F-actin dynamics (Mallavarapu and Mitchison, 1999), and spatial asymmetry in actin dynamics underlies turning of growth cones either towards attractive cues or away from repulsive cues (Dent et al., 2011, Geraldo and Gordon-Weeks, 2009).

The constant retrograde flow of F-actin is powered by myosin II from the growth cone transitional zone. The actin retrograde flow rate can be reduced with inhibition of myosin activity, and can be increased after inhibition of Arp2/3 complex activity, possibly due to decrease in density of F-actin network in the P domain (Yang et al., 2012, Yang et al., 2013). F-actin bundles buckle when pulled close to T zone and are subsequently depolymerized for G-actin recycling (Lin et al., 1996). The availability of G-actin, and the competition between different F-actin structures for G-actin is probably involved in the generation and maintenance of F-actin network in the growth cone (Burke et al., 2014). The actin retrograde flow rate can be attenuated when adhesion complexes form between F-actin and extracellular substrate, which is a prerequisite for efficient cellular translocation (Hyland et al., 2014b, Mejean et al., 2013, Suter and Forscher, 1998). The entire F-actin structure in growth cone is under constant renewal at any given moment. On Poly-L-Lysine coated coverslips, the F-actin structure in the growth cone P domain within 10 μm from the leading edge is turned over in 2 minutes.

1.4 Filopodia

1.4.1 Anatomy of the filopodium

The filopodium (or filopodia for plural) refers to the slender membrane bound cellular protrusion about 200 nm in diameter, commonly found in growth cones, epithelial cells and fibroblasts (Jacquemet et al., 2015, Mattila and Lappalainen, 2008). The core of a filopodium is filled with 10-30 crosslinked F-actin filaments, with their barbed ends towards the extracellular space (Mogilner and Rubinstein, 2005). Bundled F-actin filaments likely contribute to the relatively high elastic modulus of filopodia, compared to the C domain and T zone of the neuronal growth cone (Xiong et al., 2009). A plethora of proteins can be found in filopodia. For example, actin polymerases like Ena/VASP and formin locate at the filopodium tip to regulate actin dynamics (Goncalves-Pimentel et al., 2011, Mellor, 2010). Src kinase locates at the filopodium tip, presumably through its interaction with lipid membrane, to regulate both actin dynamics and the formation of adhesion (He et al., 2015, Robles et al., 2005, Wu et al., 1996). Myosin X travels along actin tracks to transport cargos into the filopodium, and receptors for extracellular ligands are also concentrated in the filopodium (Gallo, 2013). Membrane curvature sensitive proteins such as BAR proteins are likely involved in the generation and maintenance of membrane protrusion,

and ring-like structures made of cortactin and dynamin are reported to bind filopodia with regular spacing, contributing to filopodia stability (Starnes et al., 2014, Yamada et al., 2013).

1.4.2 Function of filopodia

Filopodia protrude in front of growth cone to sample the environment. Analogous to extensible antennas, filopodia relay information from the environment to intra-filopodial space and more proximal regions of growth cone (McConnell et al., 2016, Davenport et al., 1993). The extension and retraction of filopodia are made possible by the regulation of actin polymerization/depolymerization activity, and the sensory role was supported by presence of multiple receptors in filopodia (Gallo, 2013). Due to the small volume of the filopodium, a small change in absolute number of signaling molecules could lead to a bigger change of concentration in filopodial space than elsewhere, possibly amplifying its sensory function (Davenport et al., 1993). Filopodia also form adhesions with substrate as well as other cells, and could exert pulling force thereafter (Bornschlogl, 2013, Chan and Odde, 2008, Robles et al., 2005, Wu et al., 1996). Lastly, during growth cone advancement, filopodia guide the invasion of microtubules and are precursors of future neurite (Burmeister et al., 1991, O'Connor and Bentley, 1993, Bentley and O'Connor, 1994, Schaefer et al., 2002, Zhou et al., 2002).

1.4.3 Mechanism of filopodia formation

Remodeling of both F-actin filaments and lipid membrane are important in filopodia formation, but only the former has been under intensive investigation. Two hypotheses regarding F-actin remodeling during filopodia formation have been proposed, each with support from experimental data and are not mutually exclusive (Fig 1.4). The first hypothesis, termed “convergent elongation model”, stresses the importance of Arp2/3 complex in initiating a cluster of F-actin filaments for subsequent bundling and elongation (Svitkina et al., 2003, Korobova and Svitkina, 2008). It states that daughter F-actin filaments generated from dendritic array first form a filopodium precursor close to leading edge, and collective elongation of this selective group of F-actin filaments leads to the filopodium elongation. The second hypothesis, termed “tip nucleation model”, claims that the initiation and elongation of a filopodium could be carried out directly through barbed end binding actin regulators such as formin and Ena/VASP proteins (Faix and Rottner, 2006, Mellor, 2010, Gallo, 2013). Although it is possible that filopodia form by more than one mechanism and

different cells utilize different strategies to construct filopodia, a defect in filopodia generation and neurite outgrowth has been demonstrated from neurons with knock-down of Arp2/3 complex, pointing to the involvement of Arp2/3 complex in formation of neuronal filopodia (Korobova and Svitkina, 2008). A detailed mechanism of filopodia formation and maintenance, including the sequential steps of filopodia initiation, elongation, merging and retraction is still missing.

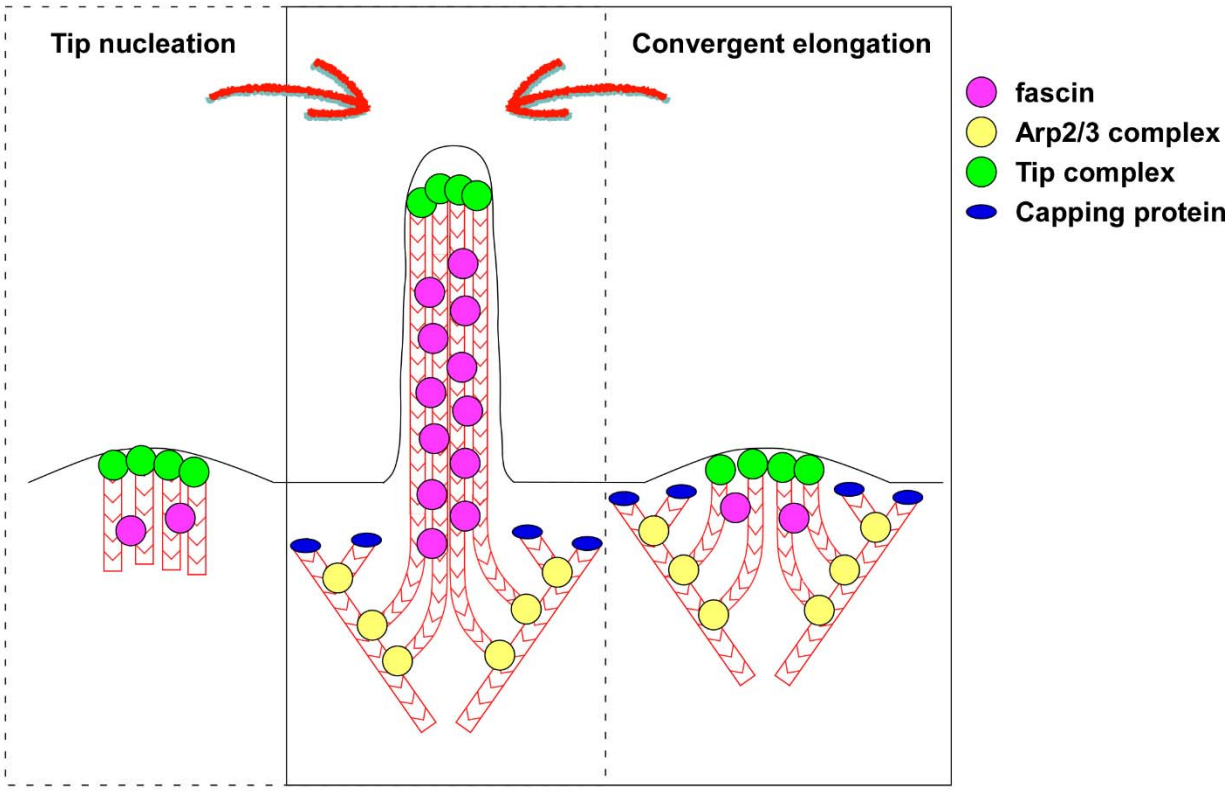

Figure 1.4. Two models of filopodia formation.

The dotted box represents "tip nucleation model". In this model, clustering of tip complex, which includes actin barbed end nucleating proteins Ena/VASP and formin, both initiate and elongate a filopodium. The solid line box represents "convergent elongation model", which suggests that a filopodium is initiated first by grouping of daughter filaments through Arp2/3 complex mediated F-actin branching. Both models recognize the importance of tip complex in filopodia elongation and the requirement of fascin for F-actin bundling.

1.5 Cortactin

1.5.1 Cortactin is an important actin regulator

Cortactin was first identified as a substrate of Src kinase and later found to possess multiple modules for actin regulation (Wu and Parsons, 1993, Schnoor et al., 2018). As shown in Fig. 1.5, the N-terminal acidic domain of cortactin binds and activates Arp2/3 complex, and the seven and half repeats bind F-actin. At the C-terminal, cortactin has an SH3 domain which mediates its interaction with many other proteins that are important in actin-related processes, such as N-WASP, dynamin, WIP and ZO-1 (Cosen-Binker and Kapus, 2006, MacGrath and Koleske, 2012). Bridging the F-actin binding repeats and SH3 domain is a proline-rich domain that could potentially bind its own SH3 domain, resulting in a closed conformation (Cowieson et al., 2008, Magalhaes et al., 2011).

Purified cortactin crosslinks F-actin filaments *in vitro* and weakly activates Arp2/3 complex to promote branching (Weed et al., 2000, Weaver et al., 2001). Cortactin also protects F-actin filaments from depolymerization (Weaver et al., 2001). However, with the addition of N-WASP and other accessory proteins, F-actin branching can be synergistically stimulated, partially due to the ability of cortactin to displace N-WASP from Arp2/3 complex, resulting in more efficient Arp2/3 complex activation (Kinley et al., 2003, Siton et al., 2011, Helgeson et al., 2014). In cells, cortactin can be found in essentially all actin-based structures, including filopodia, lamellipodia, cell adhesion complex, invadopodia, endocytic pit and podosome (Weed and Parsons, 2001, Ayala et al., 2008, Schnoor et al., 2018). Overexpression of cortactin has been found to promote cell migration, and duplication of cortactin gene has been implicated in cancer (Yin et al., 2017, Bryce et al., 2005, Lai et al., 2009).

In the nervous system, cortactin has high expression level and is concentrated in growth cones and dendritic spines (Hering and Sheng, 2003). Cortactin is important in activity-related reshaping of dendritic spine by altering actin architecture. In adhesion-mediated growth cone turning, cortactin has been found to accumulate at IgCAM sites (Decourt et al., 2009). As mentioned earlier, cortactin has been shown to help stabilize neuronal filopodia through its interaction with dynamin (Yamada et al., 2013). However, the function of cortactin in filopodia formation remains unclear.

1.5.2 Post-translational modifications of cortactin

Cortactin contains multiple sites for post-translational modification. Notably, acetylation of F-actin binding repeats decreases the ability of cortactin to bind F-actin filaments, and serine phosphorylation in proline-rich domain by ERK is important in changing the conformation of cortactin from closed to open (Martinez-Quiles et al., 2004, Zhang et al., 2007). After serine phosphorylation, the cortactin SH3 domain becomes available for binding of other proteins with proline-rich domains (Nieto-Pelegrin and Martinez-Quiles, 2009, Hoye et al., 2016). Interestingly, serine phosphorylation by ERK also induces cortactin ubiquitination and degradation in lung epithelial cells (Zhao et al., 2012).

Aplysia cortactin has three potential tyrosine residues in proline-rich domain for Src mediated phosphorylation (He et al., 2015). In other species, cortactin phosphorylation by Src occurs on multiple tyrosine residues, and cortactin phosphorylation has been found to reduce its F-actin cross-linking ability (Huang et al., 1997), while promoting actin assembly (Tehrani et al., 2007). A recent study from our lab regarding the role of cortactin in growth cone actin organization and dynamics has shed light on how actin behavior is influenced by cortactin tyrosine phosphorylation. Using high-resolution imaging of live neurons, we have shown that up-regulation of either Src2 (the tyrosine kinase that phosphorylates cortactin in *Aplysia*) or cortactin led to longer and denser actin-based filopodia in the peripheral domain of neuronal growth cones, as well as to an increase in the density of the actin-based lamellipodia network. Conversely, down-regulation of Src2, or the over-expression of a phosphorylation-defective triple tyrosine mutant (FFF) of cortactin, resulted in a shorter and looser filopodia arrangement, decreased density of lamellipodia, and more lateral movement of filopodia (He et al., 2015). Whether all three tyrosine residues are involved in the functionality of phosphorylated cortactin is unknown.

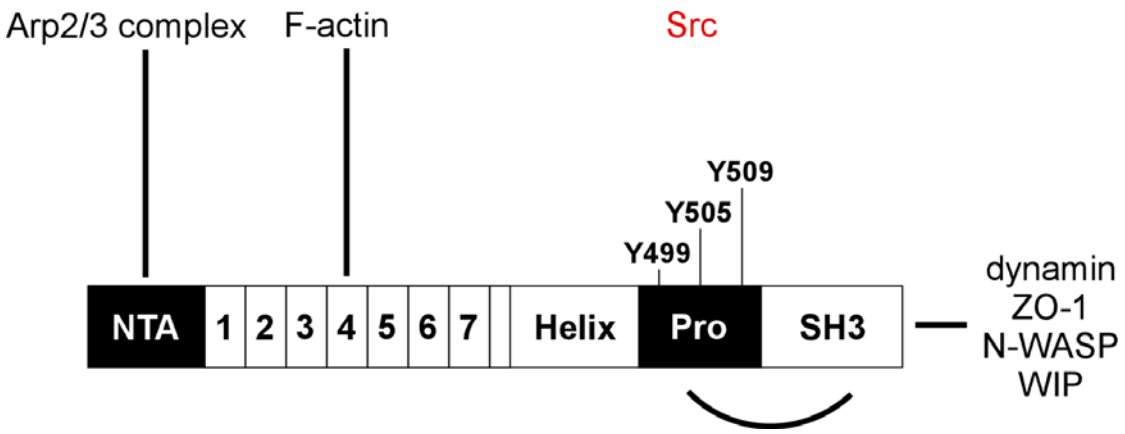

Figure 1.5. Schematic of *Aplysia* cortactin protein.

N-terminal Acidic (NTA) domain of cortactin weakly activates Arp2/3 complex; seven and half repeats binds to F-actin, with the fourth repeat shown to be necessary for this binding. SH3 domain mediates the interaction between cortactin and multiple proline-rich domain containing proteins. Proline-rich domain and SH3 domain from the same cortactin molecule can bind to each other, thus folding cortactin and rendering SH3 domain inaccessible for other proteins. There are three potential Src tyrosine phosphorylation sites in *Aplysia* cortactin, and identifying the functional tyrosine residue is the goal for first part of this thesis.

1.6 *In vitro* cell culture

1.6.1 Two-dimensional (2D) cell culture

Cell culture is a commonly used technique to study cellular activities under more controlled conditions than *in vivo* environment (Lee et al., 2008a, Zhao et al., 2009). At present, most cells are cultured on planar and rigid surfaces with substance coatings of varying degrees of biological relevance. Although much has been learned from 2D cell culture, the limitations are becoming increasingly clear as questions arise as to the transferability of knowledge gained from a highly artificial system. With more tools being created to facilitate direct observation and perturbation of biological processes *in vivo* (Chen et al., 2013, Chung and Deisseroth, 2013, Huisken et al., 2004), discrepancy in fundamental ways of cellular behavior between cells in their native environment and cells on 2D culture needs to be addressed. Notably, neurons on 2D culture have been shown to have substantially altered morphology (Lee et al., 2008b, Li et al., 2007), excitability (Desai et al., 2006, Lai et al., 2012), and gene expression profile (Li et al., 2007, Phillips and Otteson, 2011).

A more physiological culture system for neurons is therefore needed to ease concerns about 2D culture.

Aplysia bag cell neurons have traditionally been cultured on poly-lysine-coated coverslips, which lack topographical cues and extracellular matrix (ECM) proteins, while having un-physiological rigidity. The formation of large growth cones from bag cell neurons could be linked to this specific combination of culturing conditions, as the same type of cells cultured on hemolymph/laminin coated surface forms smaller and faster-growing neurite tips (Hyland et al., 2014a, Hyland et al., 2014b). It would be interesting to perform prolonged observation of the large growth cones, as almost every study focused exclusively on the pausing state, when neither net advancement nor clear retraction happened. Information about how growth cone enters and exits this pausing state would help complement our understanding of neurite outgrowth.

1.6.2 Three-dimensional (3D) cell culture

Alterations to traditional 2D culture methods are being developed as an effort to preserving the physiological behavior of cells while providing more freedom for experimental control. These include patterned substrates (Jang et al., 2010), natural and man-made polymers (Brannvall et al., 2007, Desai et al., 2006, Yan et al., 2017) as well as synthesized scaffolds (Ahmed et al., 2007, Guetta-Terrier et al., 2015, Lai et al., 2012, Lee et al., 2011). Recent developments in this direction have successfully generated *in vitro* organ-like structures, or organoids, in which multiple types of cell coordinate to perform functions of certain organs (Clevers, 2016, Johnson et al., 2016). Despite the clear advantages provided by these new culture methods and scientific breakthroughs made thereof, majority of labs still rely on 2D cell culture for most of their experiments. The slow dissemination of 3D cell culture methods could be due to requirement of special instruments or skills for device fabrication, cost consideration of expensive substrate, or the narrow application of certain protocols. A versatile 3D cell culture system that is affordable would therefore greatly facilitate the adoption of 3D culture, and help accelerate acquisition of biologically relevant knowledge.

1.7 Summary

Neuronal growth cones are known to have a wide spectrum of morphology *in vivo* ever since they were first discovered, and research into the mechanisms of morphological changes holds the key to understanding neurite motility and guidance. The growth cone morphology is an output of both intracellular signaling and extracellular environment, which converge on regulation of actin and microtubule cytoskeletons to alter the growth cone behavior. Being a substrate of Src kinase and an actin regulator, cortactin is in a unique position to translate extracellular cues into intracellular remodeling of actin filaments, functioning as a signaling hub to direct growth cone morphological changes. Investigations into how cortactin phosphorylation affects its function on actin-based structure, in this case filopodia, are needed to better elucidate actin-regulating pathways in growth cone (see Chapter 3).

Morphologies of neuronal growth cones *in vitro* are subject to cell culture conditions, which need to be carefully examined before certain morphology can be chosen as "representative". This has not been done for *Aplysia* bag cell neuron. We try to provide a more complete survey of growth cone morphologies from cultured bag cell neurons on poly-lysine coated coverslips, where they are most commonly plated on, and correlate the growth cone size with growth cone motility (see Chapter 4). We also developed 3D culture protocol to better understand how cell culture conditions change the growth cone morphology and dynamics in more physiologically relevant settings (see Chapter 5).

CHAPTER 2. MATERIALS AND METHODS

2.1 2D Cell culture

Aplysia bag cell neurons were collected from Dispase-digested abdominal ganglion of 150-200 g *Aplysia californica* (Marinus Scientific, Long Beach, CA) and plated on 20 µg/ml poly-L-lysine (70–150 kDa; Sigma-Aldrich, St. Louis, MO) coated coverslip as described previously (Grzywa et al., 2006). Culture media were made by adding artificial seawater (ASW) into commercially available L15 media (Invitrogen, Life Technologies, Grand Island, NY). Final solution (L15-ASW) contains 400 mM NaCl, 9 mM $CaCl_2$, 27 mM $MgSO_4$, 28 mM $MgCl_2$, 4 mM L-glutamine, 50 µg/ml gentamicin, 5 mM HEPES, pH 7.9, 950-1000 mOsm. For better solubility of inhibitors, Low Ionic Strength ASW (LIS-ASW) was used in drug treatments, which contains 100 mM NaCl, 10 mM KCl, 5 mM $MgCl_2$, 5 mM $CaCl_2$, 15 mM HEPES and 60g/L Glycine, pH 7.9, 950-1000 mOsm.

2.2 2D-3D transition culture

Cells were cultured on PLL-coated coverslips for 24 h to allow for the formation of growth cones, and then an imaging chamber was assembled (Suter, 2011). Liquid 2 mg/ml type I rat tail collagen (Corning, Corning, NY,) based gel mixture (containing 25% *Aplysia* hemolymph and 20 µg/mL PLL) was introduced into the chamber on top of the cells and allowed to solidify at 37°C for 1 h. The imaging chamber was placed back into dishes with L15-ASW for continued cell culture at RT, until chambers were mounted for imaging. Cells cultured in this setup maintain a healthy morphology for at least 10 days.

2.3 3D cell culture

A simple device for 3D neuronal cell culture was developed by attaching a punched plastic chip (0.020 inch thickness, Yellow, SHSP-200, Small Parts, Inc., Miami Lakes, FL) to a standard #1.5 coverslip using waterproof double-sided tape (3M 442KW double-sided film tape, S-18740, Uline, Pleasant Prairie, WI) (Fig. 5.1A). The cylindrical space created thereby has a volume of 16 µl and can be used as a chamber for 3D neuronal culture. To prepare liquid gel for 3D culture (for example

with a final volume of 400 μL), mix 40 μL 200 μg/mL PLL with 60 μL 5X ASW, 100 μL Hemolymph and 200 μL Type I collagen (From rat tail, typical concentration 4mg/mL) and adjust pH to 7.0. As shown in Fig. 5.1D, after the liquid gel mixture with neurons was loaded into the microwell and inverted during the gelling phase, gravitational force pulled neurons close to gel surface until further movement was balanced by the surface tension of the gel. This procedure typically positioned neurons within 50 μm of the gel surface, and this proximity was maintained after gel solidification, when the microwell was flipped again and medium added. Positioning of bag cell neuron is achieved within 5 min after inverting, but a typical gelling time of 50 min was chosen to ensure complete gel solidification. The distance between cell soma and gel surface is far enough to allow neurite regeneration in 3D with most regenerated neurites being close enough to the gel surface to be imaged with high-resolution objectives.

2.4 mRNA mediated protein overexpression

mRNAs for overexpression of *Aplysia* proteins were made from the mMESSAGE mMACHINE T7 Ultra *in vitro* transcription kit (Ambion, Life Technologies, Grand Island, NY) similar to our previous study (He et al., 2015). A typical final concentration of 0.5 mg/ml mRNA was mixed with Dextran (3kD Texas red dextran, fixable, Thermo Fisher Scientific) and delivered into soma through cell injection, shortly (about 4 h) after cell plating. Cells were given an additional 24 hours for adequate protein expression and growth cone formation. NP2 micromanipulator and FemtoJet microinjection system (Eppendorf, Hauppauge, NY) were used together with Nikon TE2000-U Eclipse inverted microscope to find cells. Immunostaining of growth cone with cortactin antibody (clone 4F11, 05-180, mouse monoclonal anti-cortactin (p80/85) antibody, Millipore, Billerica, MA) was used to ensure selection of growth cones with at least 1.5 fold increase in protein production for subsequent analysis of growth cone phenotypes created by different mutants. List of all cortactin mutants used in Chapter 3 can be found in Table 1.

Table 1. List of cortactin mutants

Name	Activity
Cort Y499F Y505F Y509F (FFF)	Triple phosphorylation deficient
Cort Y499F Y505 Y509 (499F)	Single phosphorylation deficient
Cort Y499 Y505F Y509 (505F)	Single phosphorylation deficient
Cort Y499 Y505 Y509F (509F)	Single phosphorylation deficient
Cort Y499E Y505 Y509 (499E)	Single phosphorylation mimetic
Cort Y499E Y505E Y509E (EEE)	Triple phosphorylation mimetic
Cort Y499E Y505F Y509F (EFF)	Single phosphorylation mimetic Double phosphorylation deficient
Cort Y499F Y505E Y509E (FEE)	Single phosphorylation deficient Double phosphorylation mimetic

2.5 Immunocytochemistry

Growth cones were fixed with 3.7% formaldehyde in ASW plus 400 mM sucrose for 15 min at room temperature, before permeabilization with fixation solution plus 0.05% saponin for 10 min. After several washing with phosphate-buffered saline (PBS)/0.005% saponin, samples were blocked with 5% BSA in PBS/Saponin for 1 hour at room temperature. Primary antibody was diluted in blocking buffer and incubated with samples for 2 h at room temperature. 4F11 antibody was typically used at 2 μg/mL, p-cort at 4 μg/mL, and n-cort at 8 μg/mL. To stain microtubules, the primary antibody (mouse monoclonal anti-alpha-tubulin, clone B-5-1-2, Sigma) was diluted to 10 μg/ml in blocking solution and incubated for 1 h at room temperature. Goat anti-rabbit Alexa-568 and Goat anti-mouse Alexa-647 conjugated secondary antibodies (A-11011 and A-21235, Thermo Scientific, Waltham, MA) were diluted in PBS/Saponin, typically with 1:500 dilution, and incubated with samples for 1 h at room temperature. For peptide blocking, 5 μg peptide was used

for every microgram of antibody, and was added into primary antibody solution during sample incubation. Alexa-488 Phalloidin (A12379, Thermo Scientific, Waltham, MA) diluted with PBS/0.005% saponin to a final concentration of 66 nM was used to incubate samples at room temperature for 30 minutes to label F-actin. Phalloidin labeling was done before antibody labeling. To label mitochondria in live neurons, TMRM (Tetramethylrhodamine, Methyl Ester, Perchlorate, T668, Thermo Fisher Scientific) was added to culture medium to a final concentration of 100 nM for 30 min before imaging.

2.6 Conventional microscopy

Coverslips with cells were assembled into imaging chambers as described previously (Suter, 2011). Samples were imaged on Nikon TE2000 E2 inverted microscope (Nikon, Melville, NY) with 60x oil immersion objective plus additional 1.5x magnification. X-cite 120 metal halide lamp (EXFO, Quebec, QC, Canada) and corresponding filter sets (Chroma Technology, Bellows Falls, VT) were used for fluorescence imaging. Digital acquisition was supported by an Andor iXon 888 Ultra electron-multiplying charge-coupled device (EMCCD) camera under the control of MetaMorph 7.8 software (Molecular Devices, Sunnyvale, CA). Time lapse series were acquired at 30 s intervals for 3.5 h (Figure 4.4A); 60 s intervals for 3 h (Figure 4.4B); 120 s intervals for 13 h (Figure 4.5A), and at 30 s intervals for 3 h (Figure 4.6G).

2.7 Super-resolution imaging

For super-resolution microscopy, raw data were recorded on a custom-built single molecule switching nanoscopy setup based around an Olympus IX-73 microscope stand (IX-73, Olympus America Inc., Waltham, MA) with a 100x/1.35 NA silicone oil-immersion objective lens (FV-U2B714, Olympus America Inc.), a 405 nm (DL-405-100, CrystaLaser, Reno, NV) for activation and a 642 nm laser (2RU-VFL-P-2000-642-B1R, MPB Communications Inc.) for excitation. The filter turret contained a quad bandpass (Di03-R405/488/561/635-t1 and FF01-446/523/600/677, Semrock Inc.). A Deformable Mirror (Multi-3.5, Boston Micromachines, Cambridge, MA) removed optical aberrations following the procedure described previously. Fluorescence passed through an additional bandpass filter (FF01-731/137-25, Semrock Inc.) placed just before the camera. The fluorescence signal was recorded on a sCMOS Orca-Flash4.0v3 (Hamamatsu, Tokyo,

Japan). The overall system magnification was ~54x, resulting in an effective pixel size of 120 nm. Molecules were localized using previously described algorithms (Huang et al., 2013, Huang et al., 2016). Image acquisition was done by Dr. Michael J Mlodzianoski; reconstruction was done by Dr. Michael J Mlodzianoski and Dr. Donghan Ma. Samples were prepared by Yuan Ren at Suter lab.

2.8 Growth cone morphological analysis

Morphological analysis in Chapter 3 was conducted at growth cone peripheral domain (P domain), where filopodia are regularly spaced and point to leading edge radially. Filopodial density is defined as the average number of filopodia per unit length of leading edge. Filopodial length is calculated by measuring the distance between filopodia tip (protruding outside of lamellipodia) and filopodia base (usually close to central domain and visible in both DIC and fluorescence images with F-actin or cortactin staining). Ratiometric images were constructed by using the Ratio Plus plugin in ImageJ (NIH, Pasadena, MD). Fluorescence intensity in growth cone P domain was quantified after background subtraction using MetaMorph 7.8 (Molecular Devices, Sunnyvale CA).

In chapter 4, in order to determine individual neurite growth rates, the displacement of a neurite tip over a three hour interval (3.5 h for Figure 4.2) was measured and divided by the time. P domain size was measured and used to correlate with the growth rate of an individual growth cone. To account for different shape and domain organization of big and small growth cones, only the P domain directly in front of C domain was included. Specifically, the center of the C domain was determined, which served as the origin of a Cartesian coordinate system superimposed on the growth cone with the y-axis in the direction of growth cone advance. Only the area of the P domain that was in front of the x-axis was included in the size measurements.

2.9 Western blot

Aplysia central nervous system (CNS) lysate was prepared by homogenizing whole CNS tissue from adult *Aplysia* with Omnimixer (Omni International, Kennesaw, Georgia) in lysis buffer (50 mM Tris-HCl, 150 mM NaCl, 2 mM EGTA, 2 mM EDTA,1% Triton X-100, 0.5 mM Pefabloc SC Plus (Roche, Indianapolis, IN), 1% protease inhibitor cocktail (Sigma, St. Louis, MO), 1 mM Na_3VO_4, 10 mM NaF, and 20 mM beta glycerophosphate, pH 7.5) and centrifuged at 10,000 g for

30 min at 4 degree. Only supernatant was collected. In the PP2 treatment group, a final concentration of 25 μM PP2 (Sigma) was added during homogenization process. Lysates were separated through standard SDS-PAGE with 7.5% gel, before transferred onto PVDF membrane. Blocking was with 10% FBS in PBS containing 4 mM Na_3VO_4 and 50 mM beta-glycerophosphate for 1 h at room temperature. For primary antibody incubation, 1:250 diluted p-cort or n-cort antibody was added into 0.05% PBST containing 5% FBS, 4mM Na_3VO_4, 50 mM beta-glycerophosphate, along with 1:500 diluted 4F11. Incubation was carried out overnight at 4 degree. After washing with 0.1% PBST, membrane was incubated with 1:5000 Goat anti-Rabbit 680 for p-cort or n-cort, together with 1:5000 Goat anti-Mouse 800 for cortactin 4F11 antibody in 0.05% PBST, 5% FBS, 0.01% SDS, 4 mM Na_3VO_4 and 50 mM beta-glycerophosphate for 1 h at room temperature. Following extensive washing of membrane with 0.1% PBST, signals were acquired on Odyssey imaging system (LI-COR, Biosciences, Lincoln, NE). For peptide blocking experiments, 5 μg peptide was used for every microgram of antibody during primary antibody incubation with membrane.

CHAPTER 3. A SINGLE TYROSINE PHOSPHORYLATION SITE IN CORTACTIN IS CRITICAL FOR FILOPODIA FORMATION IN NEURONAL GROWTH CONES

3.1 Synopsis

In this chapter, we investigate how tyrosine phosphorylation of cortactin by Src2 kinase promotes filopodia formation in *Aplysia* bag cell neuron growth cones. We identify the functionally important tyrosine residue (Y499) that mediates the effect of phosphorylated cortactin in filopodia formation, and demonstrate that phosphorylated cortactin localizes at the growth cone leading edge and filopodia tips in an F-actin independent fashion. We also show that Arp2/3 complex acts downstream of phosphorylated cortactin to regulate filopodia density but not length.

3.2 Results

3.2.1 Phosphorylation state of *Aplysia* cortactin Y499 residue dictates the effect of cortactin on filopodia formation

From our previous data, we have found that overexpression of phosphorylation-dead mutant of cortactin (FFF) in growth cone led to a decrease in both filopodia length and density (He et al., 2015). Here, we identified the functional tyrosine residue(s) that mediate the effect of phosphorylated cortactin on filopodia formation. *Aplysia* cortactin has three putative tyrosine phosphorylation sites Y499, Y505, and Y509 in the proline-rich region, which do not align well with any of the better characterized tyrosines in vertebrate cortactin. In order to identify which of these three tyrosines is the key residue for Src-mediated phosphorylation, we created single tyrosine Y to F mutants. We then expressed these single tyrosine cortactin mutants in cultured *Aplysia* bag cell neurons and analyzed filopodia phenotypes in order to find the single phosphorylation defective cortactin mutant(s) that phenocopies the triple phosphorylation defective cortactin mutant previously described. Therefore, we compared filopodial density and length for each growth cone, after overexpressing single tyrosine phosphorylation defective cortactin mutants in cultured *Aplysia* neurons, along with triple tyrosine phosphorylation defective cortactin and wildtype cortactin. The leading edge of the peripheral (P) domain of growth cone was shown for each group (boxed region in Fig. 3.1A), in both Differential Interference Contrast

(DIC) (Fig. 3.1B-H) and fluorescent channel revealing total cortactin protein following immunostaining (Fig. 3.1B'-H'). Among all three single mutations, only 499F overexpression faithfully recapitulated the reduced filopodial density and length phenotype caused by the triple tyrosine mutant FFF (Fig. 3.1B-K, B'-H'). These results suggests that Y499 is the critical phosphorylation site in cortactin regulating growth cone filopodia formation. Wildtype cortactin overexpression increased filopodial length but not density compared to dextran injection controls (Fig. 3.1J-K), indicating that filopodial density but not length is at its maximum under control conditions.

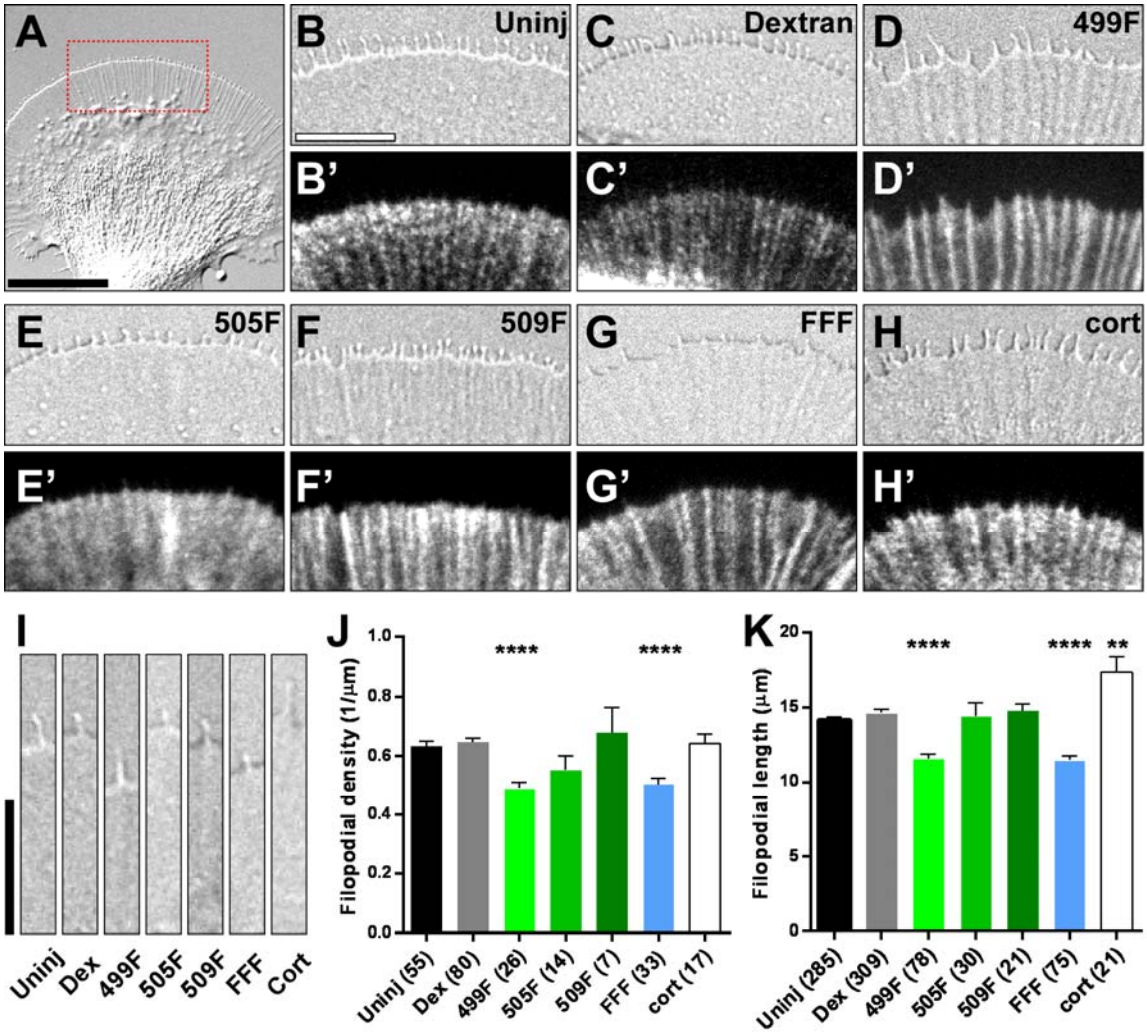

Figure 3.1. Growth cone filopodial density and length are reduced by overexpressing cortactin 499F mutant.

Growth cones were formed by neurons injected with fluorescent dextran only or in combination with mRNAs encoding different cortactin mutants. A. Example of *Aplysia* growth cone. Filopodia organization in boxed region is quantified. B-H. DIC images of filopodia at growth cone leading edge. B'-H'. Immunostaining of total cortactin with 4F11 antibody. Overexpressed cortactin localizes along filopodia. I. Filopodium from each group was selected for length comparison. The bottom of image corresponds to filopodium base. J. 499F and FFF cortactin mutants significantly reduced filopodial density compared to controls. Numbers in parentheses indicate numbers of growth cones analyzed. K. 499F and FFF cortactin mutants significantly reduced filopodial length, while overexpression of wildtype cortactin increased filopodial length. Numbers in parentheses indicate numbers of filopodia analyzed. Data is presented as mean ± SEM. **: $P < 0.01$. ****: $P < 0.0001$. Dunnett's multiple comparison. Scale bar in A: 20 μm; Scale bar in B: 10 μm; Scale bar in I: 10 μm.

As a complementary approach, we mutated cortactin Y499 site to glutamic acid, thus creating a phospho-mimetic 499E mutant. After overexpression of either the 499E or EEE (triple phospho-mimetic mutant), filopodial density was not changed (Fig. 3.2A) while an increase in filopodial length was observed (Fig. 3.2B). This indicates that a phospho-mimetic residue at the cortactin Y499 site alone can lead to a similar filopodia length phenotype as a triple phospho-mimetic mutant EEE, again suggesting that the Y499 is the critical tyrosine phosphorylation site on cortactin with respect to filopodia length regulation.

To further confirm that cortactin Y499 is the critical phosphorylation site regulating filopodial density and length, two more mutants were generated. In the FEE mutant, the Y499 site was mutated to phenylalanine and the Y505 and Y509 sites to phospho-mimetic glutamic acid. Similarly, in the EFF mutant, the Y499 was mutated to glutamic acid and the Y505 and Y509 sites to phenylalanine. The goal of creating these constructs was to test the hypothesis that Y499 is the only critical tyrosine residue in *Aplysia* cortactin that plays a role in filopodia formation. As shown in Fig. 3.2C and D, overexpression of the FEE mutant decreased filopodial density and filopodial length, again pheno-copying the FFF mutant. Overexpression of the EFF mutant led to increased filopodial length without further increasing filopodial density, which is a similar phenotype induced by overexpression of EEE (Fig. 3.2A and B). Since control growth cones already have a high density of filopodia, increasing cortactin activation by cortactin EEE expression may not further increase filopodia density. Similarly, overexpression of wildtype cortactin increased filopodial length but not density (Fig. 3.1I and J). Altogether, these cell biological results indicate

that Y499 is the only critical tyrosine residue in *Aplysia* cortactin that mediates the function of phosphorylated cortactin with respect to filopodia formation.

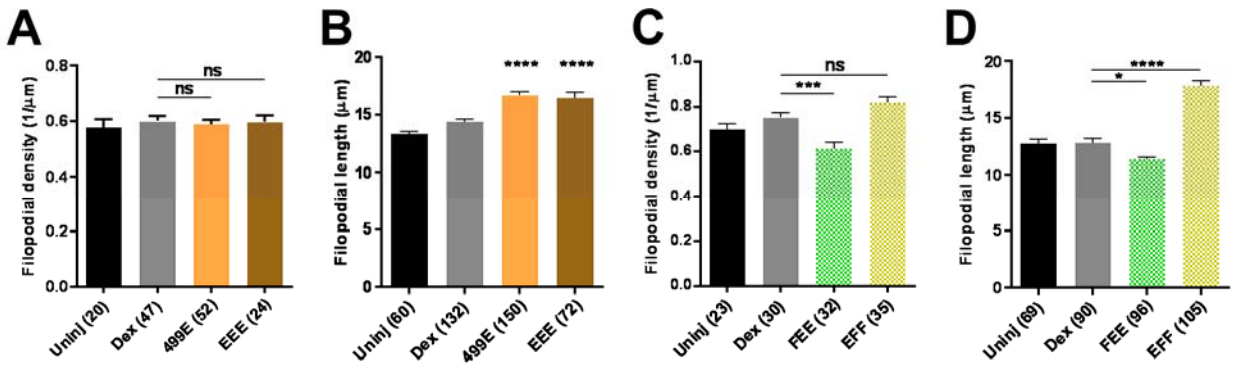

Figure 3.2. Cortactin Y499 is the only phosphorylation site relevant for regulating filopodia formation.

A. Filopodial density was not changed after either 499E or EEE cortactin mutant overexpression. B. Filopodial length is increased by expressing the phospho-mimetic 499E cortactin mutant. 499E and EEE significantly increased the filopodia length to comparable levels compared to control. Data presented as mean ± SEM. Numbers in parenthesis indicate numbers of filopodia analyzed. ****: $P < 0.0001$. Dunnett's multiple comparison. C. FEE mutant significantly decreased filopodia density compared to control. Numbers in parenthesis indicate numbers of growth cones analyzed. D EFF mutant significantly increased filopodial length, while FEE significantly decreased filopodia length. This suggests that the phosphorylation state of cortactin Y499 dictates the function of cortactin in filopodia length and formation. Data is presented as mean ± SEM. Numbers in parenthesis indicate numbers of filopodia analyzed. *: $P < 0.05$. ***: $P < 0.001$. ****: $P < 0.0001$. Dunnett's multiple comparison.

3.2.2 Phosphorylated cortactin is enriched at the growth cone leading edge

To further investigate the function of cortactin tyrosine phosphorylation at Y499, we made a polyclonal phospho-specific peptide antibodies against cortactin-pY499 (p-cort) and one against the same non-phosphorylated peptide (n-cort). First, we verified the specificity of both antibodies using Western blotting of *Aplysia* CNS lysate and purified cortactin protein (Fig. 3.3). Native cortactin is commonly shown to exist as p80/85 doublets, where the mobility shift of p85 comes from heavy post-translational modification (van Damme et al., 1997, Wu and Parsons, 1993). When using *Aplysia* CNS lysate as substrate, p-cort antibody could recognize phosphorylation

signals from both p80 and p85 bands (Fig. 3.3A and B), while n-cort antibody only shows one band corresponding to the p80 position (Fig. 3.3C). The phosphorylation signal from p-cort antibody can be reduced by inhibition of Src kinase activity with PP2 (Fig. 3.3A), and removed after adding p-cort peptide into primary antibody solution during membrane incubation (Fig. 3.3B). Likewise, the n-cort signal was removed after adding n-cort peptide into primary antibody incubation (Fig. 3.3C). This shows that p-cort and n-cort antibodies have good specificity towards native phosphorylated and un-phosphorylated *Aplysia* cortactin respectively. Both p-cort and n-cort antibodies recognized purified *Aplysia* cortactin from bacterial expression as well (Fig. 3.3D). Inclusion of p-cort or n-cort peptides for respective antibodies during immunostaining of growth cone greatly reduced fluorescence intensity in their corresponding channel, without affecting the staining pattern of either total cortactin or actin (Fig 3.4, compare the signal intensity between C and G, and between K and O). Taken altogether, we have obtained two reliable antibodies that can be used to probe the phosphorylation state of *Aplysia* cortactin.

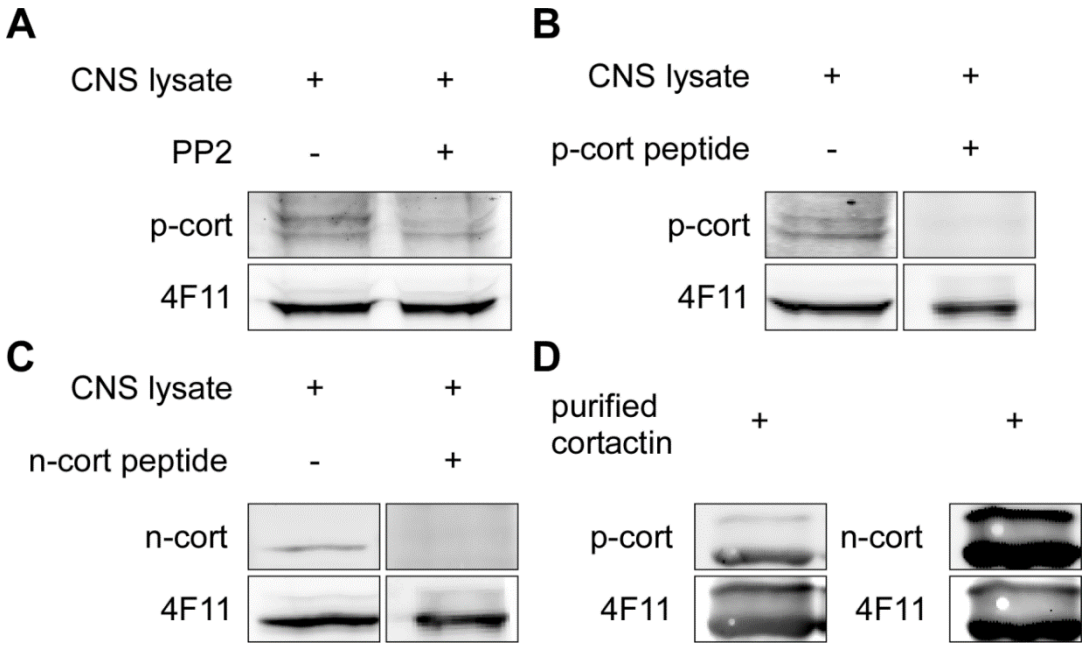

Figure 3.3. Verification of p-cort and n-cort antibody specificity through Western blot.

A. p-cort antibody detects a doublet band at 100 kD in *Aplysia* CNS lysate. The upper band was reduced after pre-incubation of lysate with PP2, suggesting that p-cort antibody recognizes a Src-dependent epitope. B. Two p-cort protein bands can be detected from *Aplysia* CNS lysate but not after pre-incubation of the antibody with phosphorylated cortactin peptide (p-cort peptide). C. n-cort signal can be detected from *Aplysia* CNS lysate but not after pre-incubation of antibody with

un-phosphorylated cortactin peptide (n-cort peptide), suggesting a good specificity of n-cort antibody against un-phosphorylated cortactin. D. Both p-cort and n-cort antibodies detected two bands in bacterially expressed and purified *Aplysia* cortactin.

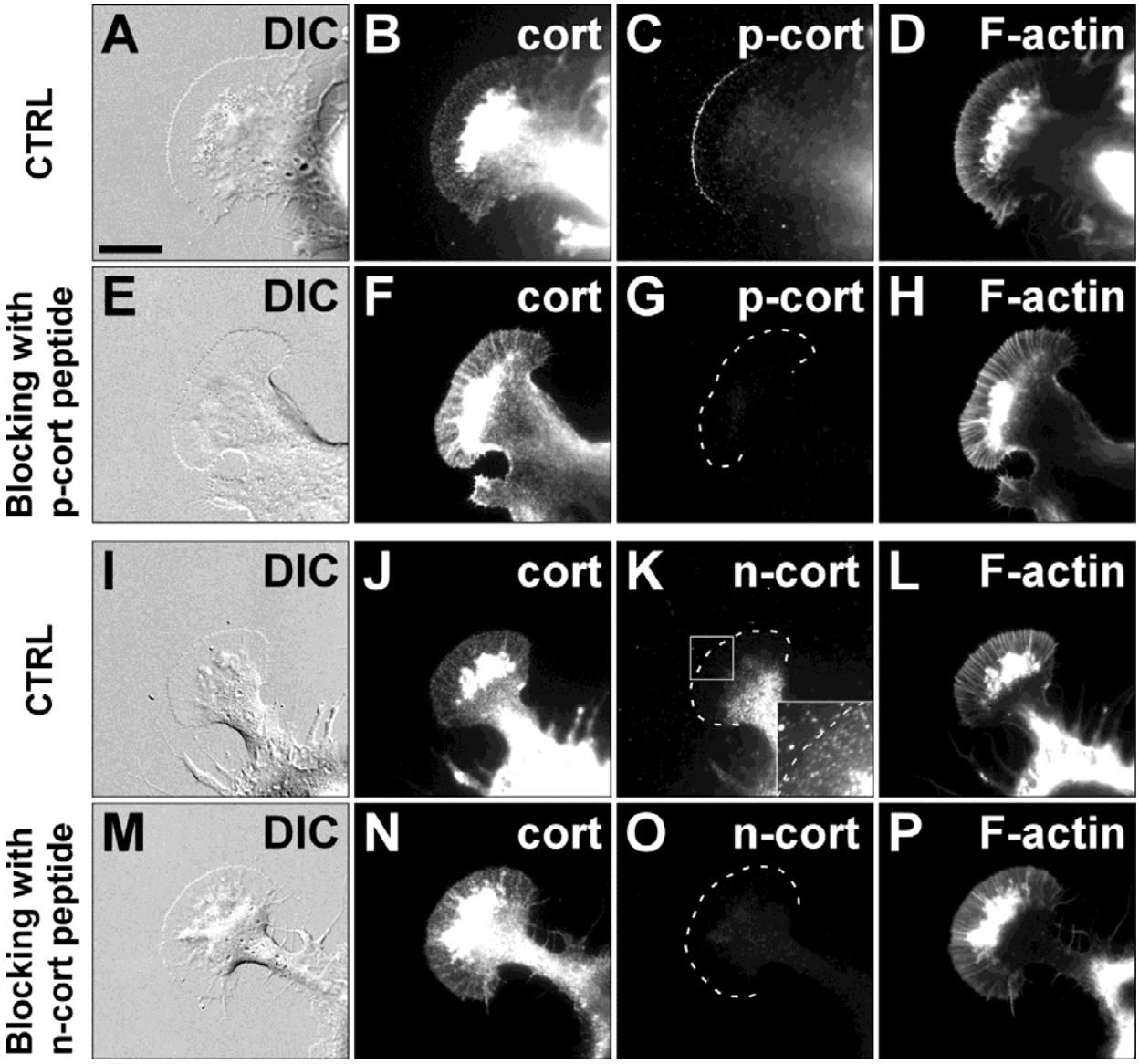

Figure 3.4. Verification of p-cort and n-cort antibody specificity through cellular immunostaining.

A-D. Control growth cone stained for total cortactin (with 4F11 antibody), phosphorylated cortactin (with p-cort antibody) and F-actin (with Phalloidin-Alexa-488). E-H. Immunostaining of growth cone with p-cort peptide added during primary antibody incubation. Fluorescent signal was reduced only in p-cort channel. Dashed line in G shows P domain edge. I-L. Control growth cone stained for total cortactin (with 4F11 antibody), un-phosphorylated cortactin (with n-cort

antibody) and F-actin (with Phalloidin-Alexa-488). M-P. Immunostaining of growth cone with n-cort peptide added during primary antibody incubation. Fluorescent signal was reduced only in n-cort channel. Dashed line in K and O shows P domain edge. Inlet in K shows a magnified region of growth cone edge with enhanced exposure. Note that no apparent pattern can be observed in P domain. Images in each channel were acquired and displayed with the same settings. See discussion for more details. Scale bar in A: 20 μm.

In control growth cones, p-cort staining showed a striking preferential localization along leading edge, quite different from the pattern of total cortactin as detected by the monoclonal antibody 4F11, which was relatively more homogenous in P domain and enriched along filopodia shafts (Fig. 3.5A-C; Fig. 3.1B'-H'). By calculating the ratiometric value of phosphorylated cortactin over total cortactin for each pixel, we were able to visualize that the leading edge exhibits the highest level of cortactin phosphorylation in the growth cone (Fig. 3.5D). This leading edge enrichment of phosphorylated cortactin, however, can be effectively removed when growth cones were treated with 25 μM Src2 inhibitor PP2 for 15 minutes (Fig. 3.5E-H). This significant reduction in cortactin phosphorylation was due to the loss of p-cort signal, while the fluorescent intensity of total cortactin remained constant (Fig. 3.5I-K). Super-resolution imaging of growth cone with p-cort antibody also confirmed the localization of phosphorylated cortactin along growth cone leading edge and at filopodia tip (Fig. 3.6A and B). Importantly, phosphorylated cortactin signal was much weaker inside lamellipodia and absent along filopodia shaft, suggesting a tight spatial regulation of cortactin phosphorylation. The hot spots of p-cort signal away from leading edge may reflect active endocytic sites, which have been shown to involve cortactin tyrosine phosphorylation (Cao et al., 2010, Zhu et al., 2005). In conclusion, cortactin phosphorylated by Src2 is highly enriched at the leading edge.

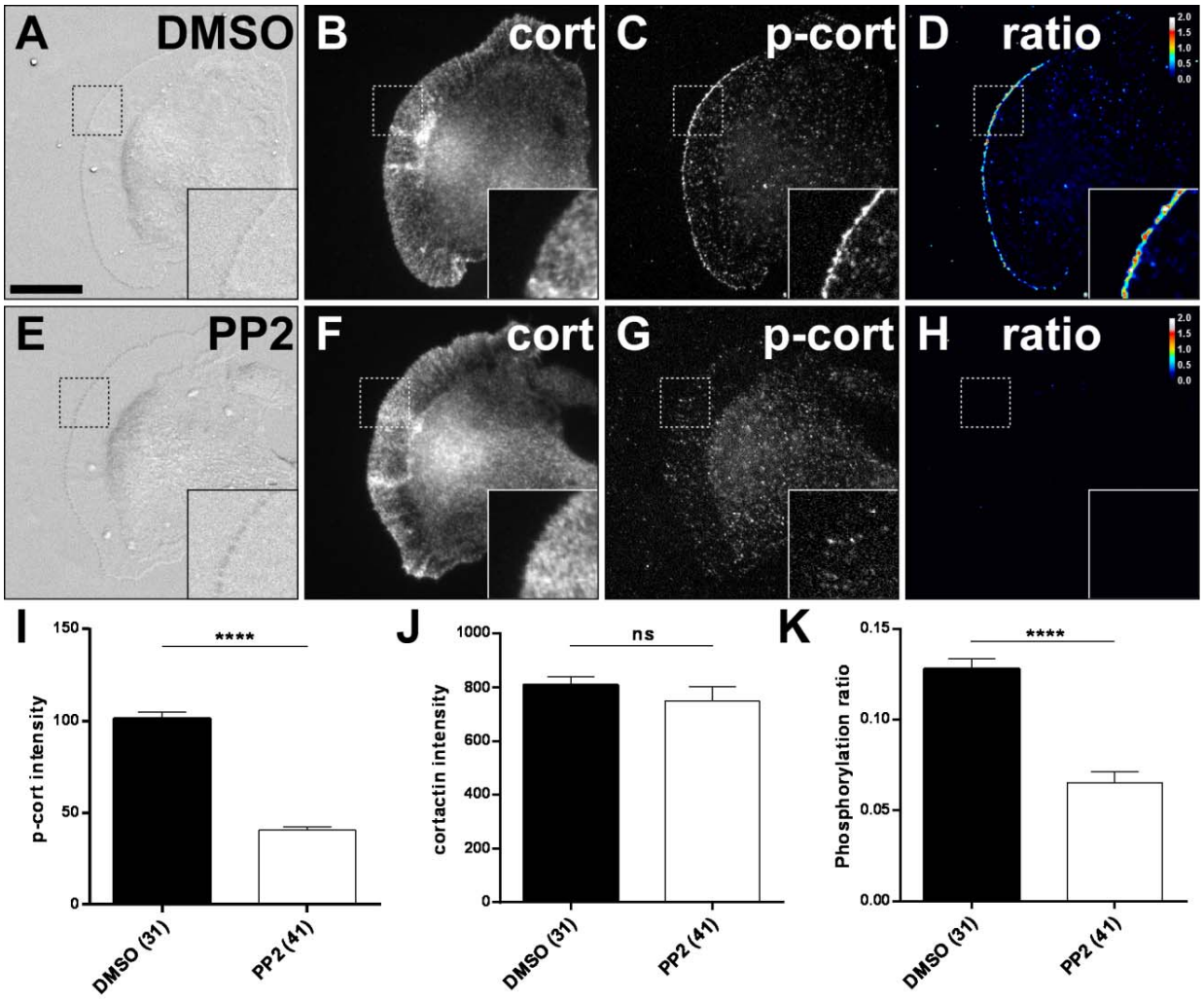

Figure 3.5. Phosphorylated cortactin is enriched at the growth cone leading edge.

A-D. Images of growth cones treated with 0.1% DMSO. E-H. Images of growth cones treated with 25 μM Src2 inhibitor PP2 for 15 minutes. Immunostaining with both p-cortactin antibody and total cortactin antibody (4F11) was used to determine the level of cortactin phosphorylation. A, E. DIC image; B, F. Immunostaining of total cortactin; C, G. Immunostaining of phosphorylated cortactin. D, H. cortactin phosphorylation ratio (background corrected p-cortactin/total cortactin) represented as ratiometric image. Enlargements of boxed regions are shown as insets. PP2 treatment removed p-cortactin signals from the leading edge. I-K. Quantification of p-cortactin intensity, total cortactin intensity and cortactin phosphorylation ratio. PP2 treatment reduced p-cortactin ratio without affecting total cortactin level. Data is presented as mean ± SEM. Numbers in parenthesis indicate numbers of growth cones analyzed. **: $P < 0.01$. ****: $P < 0.0001$. Unpaired t-test. Scale bar: 20 μm.

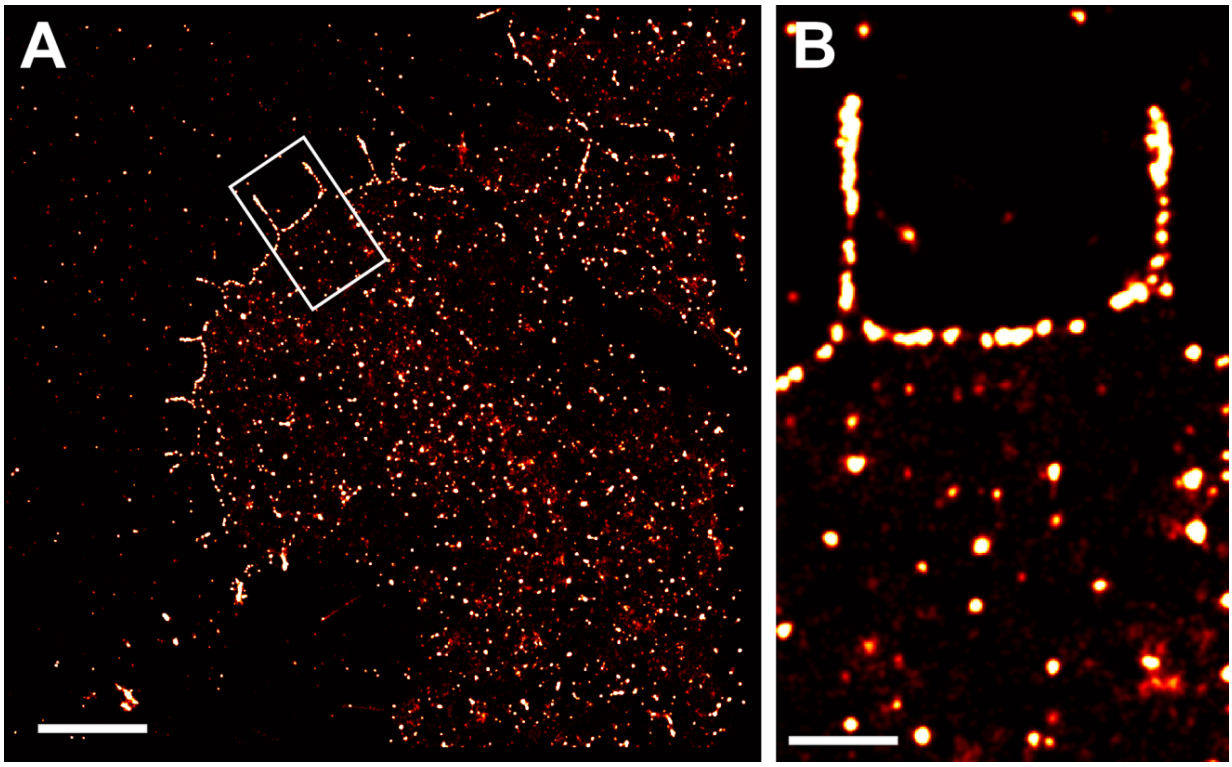

Figure 3.6. Super-resolution imaging of phosphorylated cortactin in growth cone.

A. dSTORM image of growth cone with p-cort antibody staining. Phosphorylated cortactin signal is sporadic within growth cone but concentrated along leading edge and filopodia. B. Magnified image of boxed region in A. Phosphorylated cortactin is enriched along leading edge and filopodia tip, and absent from filopodia shaft. Scale bar in A: 4 μm; Scale bar in B: 1 μm.

3.2.3 Src2 phosphorylates cortactin at Y499 in growth cones

Aplysia expresses two Src tyrosine kinases referred to as Src1 and Src2 (Wu et al., 2008). By overexpressing different Src2 and cortactin constructs, we have recently provided functional evidence that Src2 phosphorylates cortactin and thereby promotes filopodia formation and lamellipodia protrusion via the actin cytoskeleton (He et al., 2015). Here, we went on to investigate whether Src2 phosphorylate cortactin in cultured *Aplysia* neurons and growth cones by overexpressing Src2 protein in neuronal growth cones. Each growth cone was immunostained for both total cortactin and p-cort to generate ratiometric image of cortactin phosphorylation (Fig. 3.7A-H), and the ratios of cortactin phosphorylation in growth cone P domain were compared

between cells injected with TE buffer only (CTRL) or Src2 mRNA (Src2) (Fig. 3.7I). Overexpression of Src2 led to a modest but significant increase of cortactin phosphorylation ratio in growth cone (Fig. 3.7I), without changing the preferential localization of phosphorylated cortactin along growth cone leading edge and near filopodia tip (Fig. 3.7G and H). In contrast, overexpression of wildtype cortactin, but not triple tyrosine phosphorylation defective mutant FFF, led to an increase in the fluorescent intensity of p-cort in growth cone (Fig. 3.7J). Since our p-cort antibody was made to recognize phosphorylated cortactin at Y499, these results suggest that cortactin is indeed phosphorylated by Src2 at Y499 in growth cones. Interestingly, both overexpression of wildtype cortactin and triple phosphorylation defective mutant cortactin resulted in a reduction of cortactin phosphorylation ratio (Fig. 3.7J-L), implying that cortactin phosphorylation is tightly regulated possibly by a limited pool of active Src2.

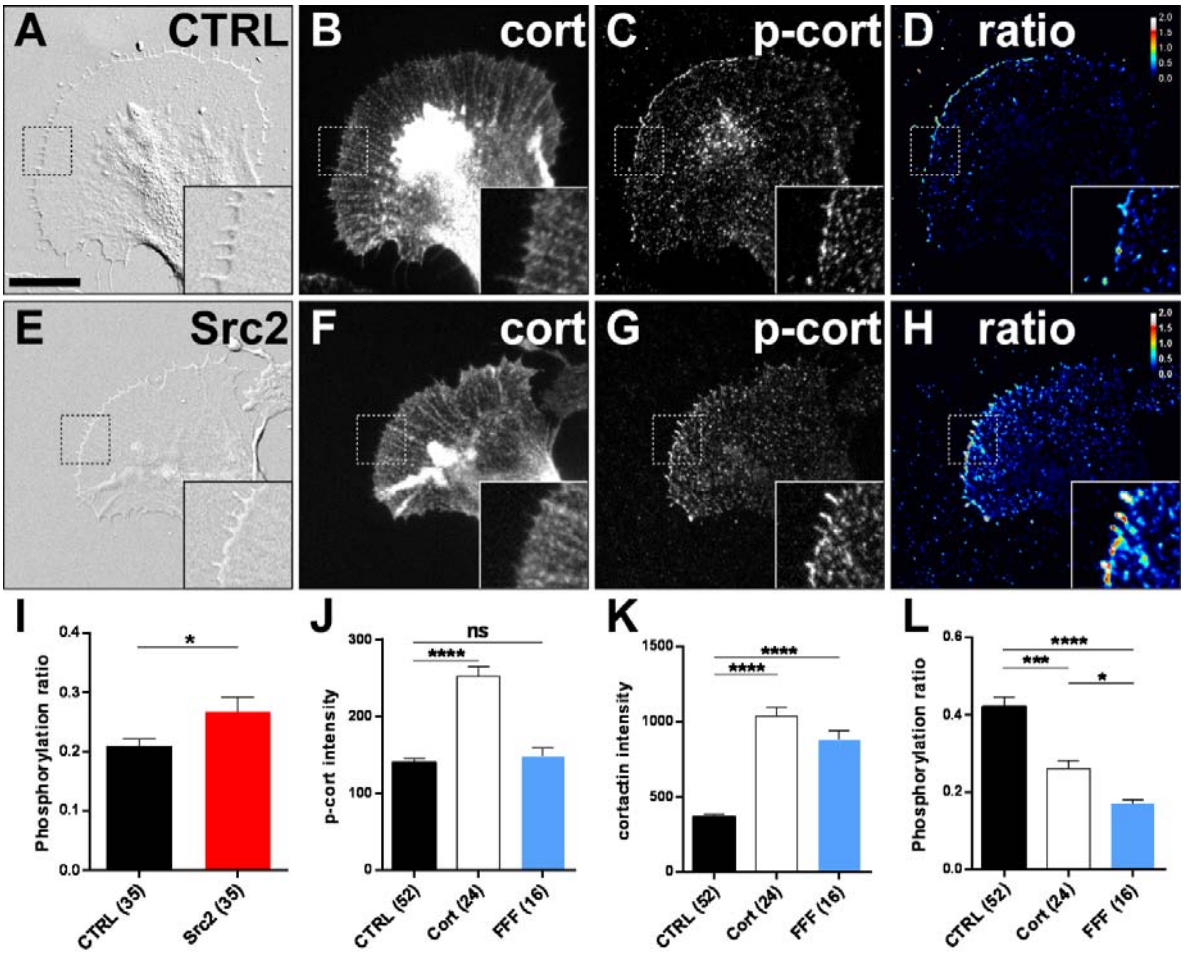

Figure 3.7. Src2 phosphorylates cortactin at Y499 in *Aplysia* neurons.

A-D. Growth cone with injection of TE buffer alone. E-F. Growth cone that overexpresses Src2. A, E. DIC image. B, F. Immunostaining of total cortactin. C, G. Immunostaining of phosphorylated cortactin. D, H. cortactin phosphorylation ratio. Enlargements of boxed regions are shown as inlets. Phosphorylated cortactin localizes at leading edge and filopodia tips. I. Cortactin phosphorylation ratio is increased by Src2 overexpression following microinjection with Src2 mRNA compared to cells that were injected with TE buffer only. J-L. Overexpression of wildtype cortactin led to increased cortactin phosphorylation level, whereas overexpression of cortFFF did not. Overexpression of both wildtype cortactin and cortFFF reduced p-cortactin ratio. Data is presented as mean ± SEM. Numbers in parenthesis indicate numbers of growth cones analyzed. *: $P<0.05$; ****: $P < 0.0001$. Dunnett's multiple comparison. Scale bar in A: 20 μm.

3.2.4 Phosphorylated cortactin is part of a membrane-associated complex that promotes filopodia formation

Next, we tested whether the leading edge localization of phosphorylated cortactin is F-actin-dependent. To address this question, we treated the growth cones with Cytochalasin B and Latrunculin A, both of which have been used to reversibly induce F-actin disassembly in *Aplysia* bag cell neuron growth cones (Burnette et al., 2007, Prager-Khoutorsky and Spira, 2009). Here, we apply both drugs in a time-controlled manner to study the potential change in p-cort signal following F-actin disruption. Fig. 3.8A-D shows a complete set of drug treatments, where growth cones were fixed and stained after treatment with either LIS-ASW plus 0.1% DMSO (Fig. 3.8A-A''') for 2 minutes, 500 nM Cytochalasin B for 2 minutes (Fig. 3.8B-B'''), 500 nM Cytochalasin B for 5 minutes (Fig. 3.8C-C'''), or 2 minutes washout with LIS-ASW after 500 nM Cytochalasin B for 5 minutes (Fig. 3.8D-D'''). Filopodia disappeared in a progressive fashion with Cytochalasin B treatment and regenerated within 2 minutes after drug removal (Fig. 3.8A-D), concurrent with the gradual loss and reappearance of F-actin signal in the P domain (Fig. 3.8A'-D'). Interestingly, the p-cort signal persisted at the leading edge throughout treatments (Fig. 3.8A''-D''), again displaying a different behavior than total cortactin (Fig. 3.8A'''-D'''). Due to the existence of a narrow Cytochalasin B-resistant F-actin band at the leading edge, we can't fully exclude the possibility that this phosphorylated cortactin is anchored through an interaction with F-actin. To better determine whether the localization is truly F-actin dependent, we treated growth cones with 1uM Latrunculin A for 2 minutes (Fig. 3.8E-E''') and 5 minutes (Fig. 3.8F-F'''), before probing the localization of F-actin, p-cort and total cortactin. Similar to the Cytochalasin B treatment, clearing of filopodia and F-actin with Latrunculin A was still progressing at 2 minutes (Fig. 3.8E,

E’) and became complete by 5 minutes (Fig. 3.8F, F’). By the end of Latrunculin A treatment, both phosphorylated (Fig. 3.8F’’) and total cortactin (Fig. 3.8F’’’) were still visible at the leading edge, whereas no F-actin signal was detectable (Fig. 3.8F’). These results strongly suggest that the localization of phosphorylated cortactin at the leading edge is independent of F-actin, possibly through its interaction with other membrane-associated proteins.

Because inhibition of Src activity reduced cortactin phosphorylation (Fig. 3.3 and 3.5), we added PP2 to the actin drug washout solution to test the importance of cortactin phosphorylation during filopodia regeneration. Growth cones were either fixed after 1 minute washout with LIS-ASW plus 0.1% DMSO following 500nM Cytochalasin B treatment (Fig. 3.8G-G’’’), or after 1 minute washout with LIS-ASW plus 25 uM PP2 following 500 nM Cytochalasin B plus 25 uM PP2 treatment (Fig. 3.8H-H’’’). In agreement with previous results, the p-cort band remained at leading edge at the absence of PP2 (Fig. 3.8G’’); however, it was completely removed when Src was inhibited with PP2 (Fig. 3.8H’’). Meanwhile, the reappearing F-actin band behind the leading edge, which indicates the regenerating F-actin network and filopodial bundles, became narrower in PP2-treated growth cones (Fig. 3.8G’ and H’), suggesting that actin remodeling is Src-dependent. Therefore, the leading edge localization of phosphorylated cortactin seems to be critical for promoting filopodia formation in neuronal growth cones.

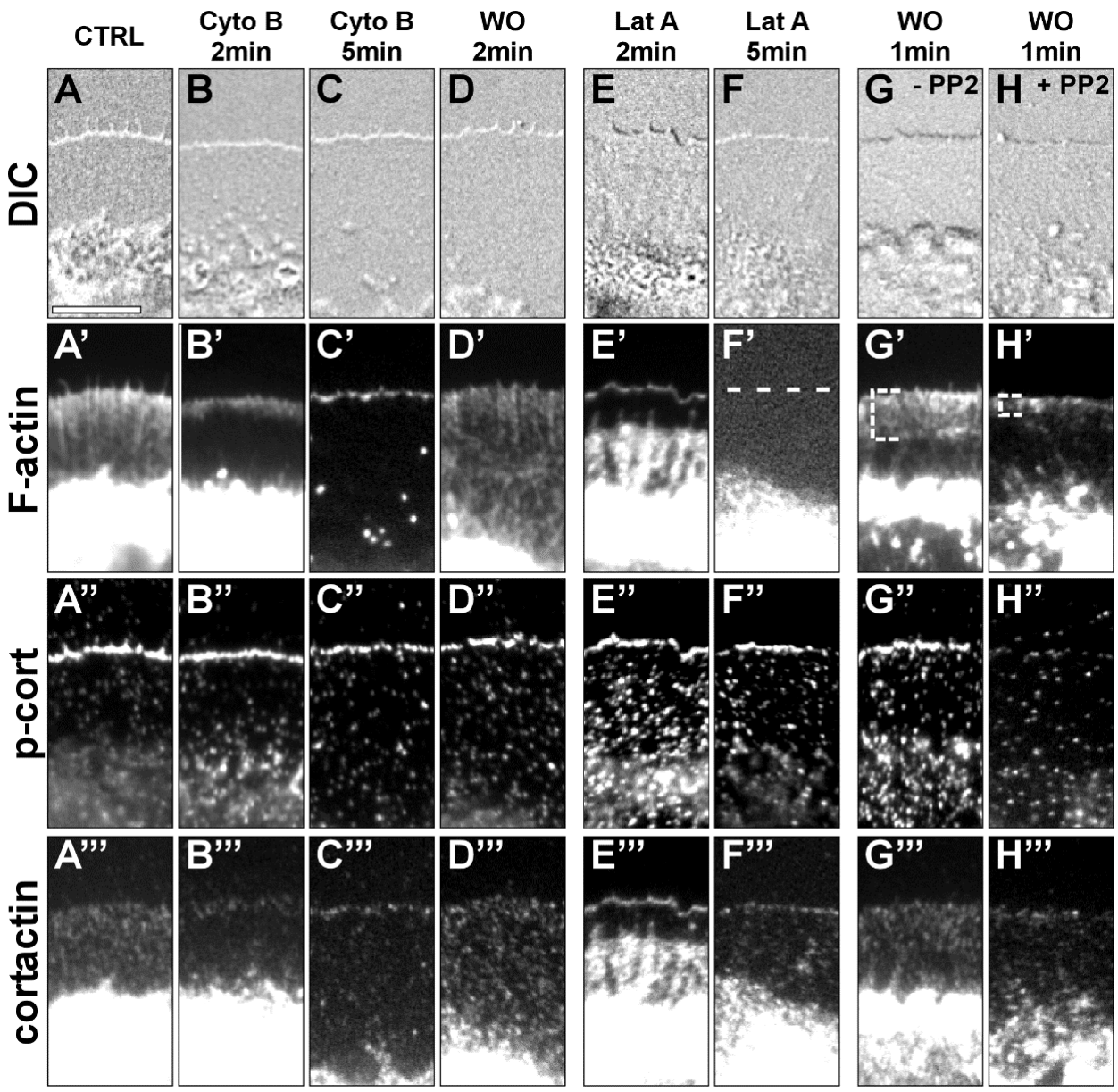

Figure 3.8. Phosphorylated cortactin is part of a membrane-associated complex that promotes filopodia formation.

Localization of F-actin, p-cortactin and total cortactin at growth cone P domain after treatment with LIS-ASW (CTRL, A-A'''), 500 nM Cytochalasin B (Cyto B) for 2 minutes (B-B'''), 500 nM Cyto B for 5 minutes (C-C'''), 2 minutes washout with LIS-ASW after 500 nM Cyto B for 5 minutes (D-D'''), 1 uM Latrunculin A (Lat A) for 2 minutes (E-E'''), 1 uM Lat A for 5 minutes (F-F'''), 1 minute washout with LIS-ASW after 500 nM Cyto B for 5 minutes (G-G'''), 1 minute washout with LIS-ASW plus 25 uM PP2 after 500 nM Cyto B plus 25 uM PP2 for 5 minutes (H-H'''). A-D: Filopodia disappear after 5 min Cyto B treatment and regenerate in 2 min after washout (WO). E-F: Lat A treatment for 5 minutes completely eliminated F-actin from P domain, but did not remove p-cortactin signal at P domain edge. G-H: regeneration of filopodia after Cyto

B treatment was inhibited by PP2, concurrent with a loss of p-cortactin signal from leading edge, suggesting that phosphorylated cortactin at the leading edge promotes filopodia formation. Dash line in F' denotes P domain edge; brackets in G' and H' indicate regenerated filopodia. Scale bar: 5 μm.

3.2.5 Arp2/3 complex acts downstream of cortactin to regulate filopodia density but not length

Due to the importance of Arp2/3 complex in actin organization and dynamics, and the known role of cortactin in Arp2/3 complex activation, we investigated whether Arp2/3 complex activation acts downstream of phosphorylated cortactin to regulate filopodia formation. To that end, we expressed cortactin NTA domain as dominant negative Arp2/3 inhibitor, or the cortactin FFF mutant as dominant negative construct for cortactin tyrosine phosphorylation in cultured *Aplysia* bag cell neurons by microinjection of mRNA. As shown in Fig. 3.9A, both NTA and cortactin FFF overexpression decreased filopodial density. However, no further decrease in filopodial density was detected when NTA was co-expressed together with cortactin FFF, suggesting that preventing cortactin-mediated activation of Arp2/3 complex in the background of cortactin that cannot be phosphorylated by Src tyrosine kinase can't further decrease filopodial density. These results suggest Src-phosphorylated cortactin and activated Arp2/3 complex likely function in the same pathway to regulate filopodial density. On the other hand, NTA expression did not decrease filopodial length, whereas cortactin FFF expression did in agreement with our previous findings (Fig. 3.9B). These findings suggest that Src-mediated phosphorylation of cortactin regulates filopodial length through a pathway that does not involve the Arp2/3 complex, which is consistent with an expected role of the Arp2/3 complex in actin assembly regulation in lamellipodial network but not at filopodial tips.

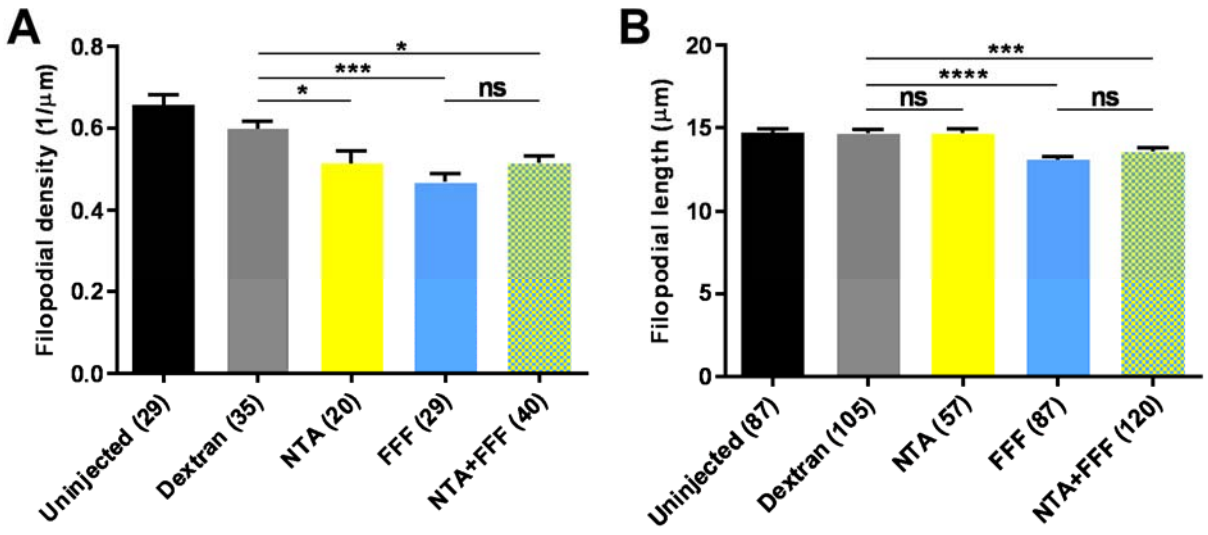

Figure 3.9. Cortactin to Arp2/3 signaling controls filopodial density but not length.

A. Whereas individual NTA and FFF overexpression significantly reduced filopodia density, the co-expression of NTA and FFF did not lead to further reduction of filopodia density, suggesting that cortactin and Arp2/3 are in the same signaling pathway with respect to filopodia formation/stability. Data is presented as mean ± SEM. Numbers in parenthesis indicate numbers of growth cones analyzed. ***: $P < 0.001$. *: $P < 0.05$. Dunnett's multiple comparison. B. Only FFF but not NTA overexpression decreased filopodia length. This suggests that cortactin phosphorylation but not Arp2/3 plays a role in controlling the length of filopodia. Data is presented as mean ± SEM. Numbers in parenthesis indicate numbers of filopodia analyzed. ****: $P < 0.0001$. ***: $P < 0.001$. Dunnett's multiple comparison.

3.3 Discussion

Src is a non-receptor tyrosine kinase that is involved in a number of cellular activities such as cell division, migration, proliferation, adhesion, and cell survival (Aleshin and Finn, 2010, Parsons and Parsons, 2004, Robles et al., 2005, Roskoski, 2004). Src functions by phosphorylating certain substrate proteins after being activated near the cell membrane (Liu et al., 1999). In neuronal growth cones, Src has been found to be important in transducing signals from receptors such as apCAM and EphA to actin during growth and guidance (Knoll and Drescher, 2004, Suter and Forscher, 2001). The phosphorylation of cortactin by Src is critical for the role of cortactin in actin regulation *in vitro* or in non-neural cells (Cao et al., 2010, Navratil et al., 2014, Nieto-Pelegrin and Martinez-Quiles, 2009, Radhakrishnan et al., 2014). However, the effect of cortactin

phosphorylation by Src in neuronal growth cones has only recently been demonstrated by work from our group (He et al., 2015). Src2 is one of two Src tyrosine kinases identified in *Aplysia* (Wu et al., 2008). Using high-resolution imaging of live neurons, we have shown that up-regulation of either Src2 or cortactin led to longer and denser actin-based filopodia in the peripheral domain of *Aplysia* growth cones, as well as to an increase in the density of the actin-based lamellipodia network. Conversely, down-regulation of Src2, or the over-expression of a phosphorylation-defective triple tyrosine mutant (FFF) of cortactin, resulted in a shorter and looser filopodia arrangement, decreased density of lamellipodia, and more lateral movement of filopodia (He et al., 2015). In our current study, we were able to pinpoint to Y499 in *Aplysia* cortactin proline-rich domain as the functional tyrosine residue that mediates the effect of phosphorylated cortactin on filopodia formation, as cortactin 499F phenocopied cortactin FFF in reducing filopodial density and length (Fig. 3.1J and K), and 499E increased filopodial length to comparable level as EEE (Fig. 3.2B). Moreover, overexpression of cortactin FEE mutant reduced filopodial density and length, whereas overexpression of cortactin EFF mutant increased filopodial length (Fig. 3.2C and D). These results suggest that cortactin Y499 is the only relevant tyrosine residue whose phosphorylation state dictates the function of cortactin on filopodia formation. Furthermore, our data with p-cort antibody demonstrated that Src2 phosphorylated cortactin at Y499 *in vivo* (Fig. 3.3 and 3.7). Therefore, we have characterized a key phosphorylation site on cortactin, which serves as an important switch in communicating Src kinase activation to actin reorganization in neuronal growth cone.

Murine cortactin has been shown to be phosphorylated at Y421, Y466 and Y482 by Src family kinase, where the phosphorylation of Y466 and Y482 happens in a progressive manner after the initial phosphorylation of Y421 (Head et al., 2003, Nieto-Pelegrin and Martinez-Quiles, 2009). Functional analysis found that phosphorylation of Y421 and Y466, but not Y482, is important in generating free actin barbed ends in invadopodia formation (Oser et al., 2010). Recent study with cancer cells proposed that a pool of constitutively phosphorylated cortactin Y421 becomes further phosphorylated at Y470 (human equivalent of mouse Y466), which is sufficient for the redistribution of cortactin to cell adhesion site (Hoye et al., 2016). For *Aplysia* cortactin, a sole phosphorylation/de-phosphorylation event at Y499 seems to be responsible for the altered behavior of cortactin on actin remodeling, at least in the context of filopodia formation (Fig. 3.2C

and D). We believe Y499 in *Aplysia* cortactin is functionally equivalent to Y421 in mouse and human cortactin, based on their position as the first tyrosine in proline-rich domain, although a considerable discrepancy in primary sequence of their proline-rich domains makes alignment dubious. The multiple tyrosine phosphorylation events and subsequent divergence in activities of differently phosphorylated cortactin could be a product of evolution to fine tune cortactin functions. On the other hand, a simple phosphorylation regime for *Aplysia* cortactin by Src2 may make it a desirable system for future functional and structural studies concerning Src and cortactin.

The leading edge localization of phosphorylated cortactin (Fig. 3.3, 3.6 and 3.8) is in agreement with the leading edge localization of active Src2 (He et al., 2015, Robles et al., 2005), as well as with the role of cortactin in promoting filopodia formation from sub-membrane region. Other key actin regulators, including N-WASP, formin, Ena/VASP and Arp2/3 complex are also localized at leading edge to control actin organization and dynamics, with which phosphorylated cortactin may interact to control the density and length of filopodia (Buck et al., 2017, Faix and Rottner, 2006, Mellor, 2010, Small et al., 2002). Cortactin phosphorylation may also be regulated by these actin binding proteins (Nieto-Pelegrin and Martinez-Quiles, 2009, Weidmann et al., 2016), as well as by the structural integrity of F-actin itself (Abedi and Zachary, 1998, Di Ciano et al., 2002, Fan et al., 2004). Indeed, cortactin phosphorylation at growth cone leading edge seems to be under tight spatial control, as the phosphorylation ratio quickly drops to background level just a few micrometers away from growth cone leading edge (Fig. 3.3D and 3.7D, H). Cortactin phosphorylation signal is quickly lost with short time inhibition of Src2 activity (15 minutes in Fig. 3.3H and K; 6 minutes in Fig. 3.8H''), along with the disappearance of p-cort band from growth cone P domain edge. This implies a fast de-phosphorylation mechanism for cortactin that works in concert with Src2 to control cortactin phosphorylation level temporally. Investigating which phosphatase is involved in reversing cortactin phosphorylation would be a good further direction (Weidmann et al., 2016). Once phosphorylated, however, cortactin becomes stably anchored at leading edge to promote filopodia formation (Fig. 3.8).

From in vitro studies, tyrosine phosphorylation of cortactin has been shown to promote actin assembly and branching, while reducing its F-actin crosslinking ability (Huang et al., 1997, Tehrani et al., 2007). This seems to be consistent with our data, where phosphorylated cortactin localizes only at the "birth place" of filopodia, where enhanced actin assembly and branching

increases length and number of filopodia, and un-phosphorylated cortactin binds along F-actin bundles to potentially stabilize filopodia (Fig. 3.1B'-H'; Fig. 3.3B and C; Fig. 3.7B and C). Un-phosphorylated cortactin is thought to exist in a "closed" conformation with an intramolecular interaction between its proline-rich domain and SH3 domain (Cowieson et al., 2008, Evans et al., 2012, Schnoor et al., 2018). Phosphorylation of serine residues by ERK is proposed to release this self-interaction and "open" cortactin, thereby making SH3 domain available for binding of other proteins such as N-WASP; in contrast, phosphorylation of tyrosine residues by Src inhibits N-WASP binding and activation (Lua and Low, 2005, Schnoor et al., 2018). Whether Src phosphorylated cortactin exist in closed or open conformation *in vivo* is unknown. Our data suggest that majority of cortactin without tyrosine phosphorylation maintains a closed conformation where the un-phosphorylated tyrosine residue is embedded, as our n-cort antibody detected cortactin signal from denatured protein through Western blot (Fig. 3.4C and D), but failed to detect signal in growth cone P domain or along filopodia shaft, where majority of cortactin is hypothesized to be in un-phosphorylated state (compare Fig. 3.3B and C with Fig. 3.5K). Therefore, Src mediated cortactin phosphorylation may be a subsequent step of ERK mediated unfolding of cortactin molecule, and helps to maintain an open conformation. Although the direct interaction between Src phosphorylated cortactin and N-WASP is decreased, tyrosine phosphorylated cortactin could bind WIP with its SH3 domain to indirectly synergize with N-WASP to promote actin branching, as well as recruit SH2 containing adaptor proteins such as Nck to activate N-WASP (Kinley et al., 2003, Lua and Low, 2005, Martinez-Quiles et al., 2001, Tehrani et al., 2007). The availability of cortactin SH3 domain could also recruit other proline-rich domain containing proteins such as Dynamin to form special structures along filopodia, which may also help localize phosphorylated cortactin at P domain edge even at the absence of F-actin (Fig. 3.8F-F'''').

Although traditionally viewed as a nucleation promoting factor (NPF), at least some of cortactin's function can be exerted independent of its NTA domain, highlighting the scaffolding role of cortactin in actin remodeling (Ayala et al., 2008, Lai et al., 2009, Magalhaes et al., 2011, Olazabal and Machesky, 2001). We found that double inhibition of cortactin phosphorylation and Arp2/3 complex activation did not further decrease filopodia density compared with single inhibition of either cortactin phosphorylation or Arp2/3 complex activation, suggesting cortactin acts through Arp2/3 complex to regulate filopodia density (Fig. 3.9A). Phosphorylated cortactin could either

synergize with N-WASP through the aforementioned mechanisms to promote actin branching, or accelerate the release of cofilin to create more barbed ends to serve as precursors of filopodia (Helgeson and Nolen, 2013, Magalhaes et al., 2011, Oser et al., 2010, Oser et al., 2009). In contrast, inhibition of Arp2/3 complex activation alone had no effect on filopodia length, pointing to the possibility that cortactin utilizes other binding partners to control filopodia length (Fig. 3.9B). Considering that filopodia elongation is governed mainly by actin regulators at the plus end of actin bundles, phosphorylated cortactin may recruit formin to promote actin polymerization, as has recently shown in the formation of invadopodia (Ren et al., 2018). The exact mechanism of cortactin dependent filopodia formation and maintenance awaits further exploration.

A schematic regarding the multifaceted functions of cortactin during filopodia formation is shown in Fig. 3.10. One filopodium is highlighted and separated into three regions: filopodium tip, leading edge and filopodium shaft. Density of filopodia is controlled mainly by F-actin branching frequency at the leading edge. Length of the filopodium is controlled by the tip complex, which determines the assembly/disassembly state of F-actin filaments. The stability of filopodia is controlled by multiple bundling proteins along the filopodium shaft. Tyrosine phosphorylated cortactin enhances F-actin branching at leading edge, probably directly through activation of Arp2/3 complex, and indirectly by forming protein complexes with other NPFs such as N-WASP, resulting in increased number of filopodia. At the filopodium tip, tyrosine phosphorylated cortactin could promote F-actin assembly, possibly through its interaction with actin polymerases such as Ena/Vasp. At the filopodium shaft, cortactin phosphorylation is dispensable for bundling of F-actin filaments.

A

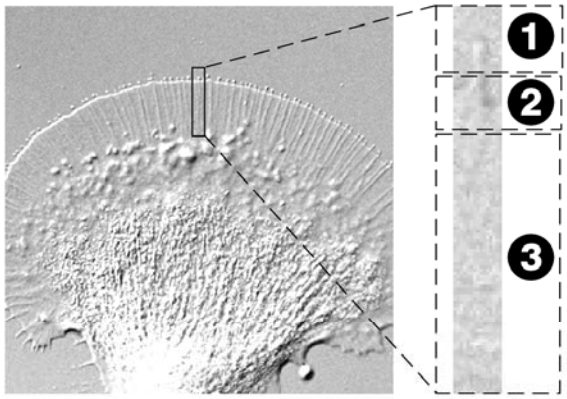

B

Position	Process	Major cortactin species	Cortactin binding partners
1	F-actin assembly/disassembly	p-cort	Ena/Vasp ?
2	F-actin branching	p-cort	Arp2/3 complex N-WASP Lipid membrane ?
3	F-actin bundling	n-cort	F-actin Dynamin

Figure 3.10. Schematic of functions of cortactin in filopodia formation

A. One growth cone filopodium is highlighted and separated into three regions: filopodium tip, leading edge and filopodium shaft, corresponding to regulation of filopodia length, density and stability. B. Cortactin has different localizations and regulates different aspects of filopodia formation, depending on the phosphorylation state and binding partners.

CHAPTER 4. MORPHOLOGICAL CHANGES OF NEURONAL GROWTH CONES IN CELL CULTURE

4.1 Synopsis

In this chapter, we provide a comprehensive description of the morphological changes of *Aplysia* bag cell neuron growth cones on PLL coated coverslip, and found an inverse correlation between growth cones size and growth cone motility, especially for large growth cones (P domain size > 100 μm^2). We also demonstrate that changes in cell culture conditions can induce *in vivo* like growth cone morphologies.

Results from this chapter have been published under the title "Increase in growth cone size correlates with decrease in neurite growth rate" in Neural plasticity, vol. 2016, Article ID 3497901, 13 pages, 2016. doi:10.1155/2016/3497901.

4.2 Results

4.2.1 *Aplysia* growth cones become smaller with time in culture

Previous studies on *Aplysia* bag cell neuronal growth cones have mainly focused on large fan-shaped specimens cultured for one or two days on PLL substrates (He et al., 2015, Lee et al., 2008a, Schaefer et al., 2002, Schaefer et al., 2008, Suter et al., 1998). Such growth cones not only exhibit a distinct organization of cytoplasmic domains but also a highly organized actin and microtubule cytoskeleton with well-characterized dynamic properties. However, the vast majority of these growth cones do not significantly translocate during a typical observation time of 30 to 60 min. Here, we compared the size of growth cones from cultured bag cell neuron on PLL-coated coverslips at different times in culture. At 18 h after plating, multiple large growth cones with a diameter between 50 and 100 μm appeared around the cell body. These growth cones share a stereotypic organization, with a flat P domain and organelle-rich C domain separated by the T zone that features extensive membrane ruffles (Figure 4.1A). By 78 h, growth cones moved further away from the cell body and were considerably smaller in size. The smaller growth cones had fewer filopodia and a less obvious T zone (Figure 4.1A). The portion of the filopodia extending beyond the leading edge became proportionally longer compared to the portion of the filopodia

embedded in the lamellipodia (arrow in lower right image). Statistical analysis revealed a wide distribution of P domain size at both time points (note the log scale), as well as a significant drop of the average P domain size at 78 h when compared to the 18 h time point (Figure 4.1B).

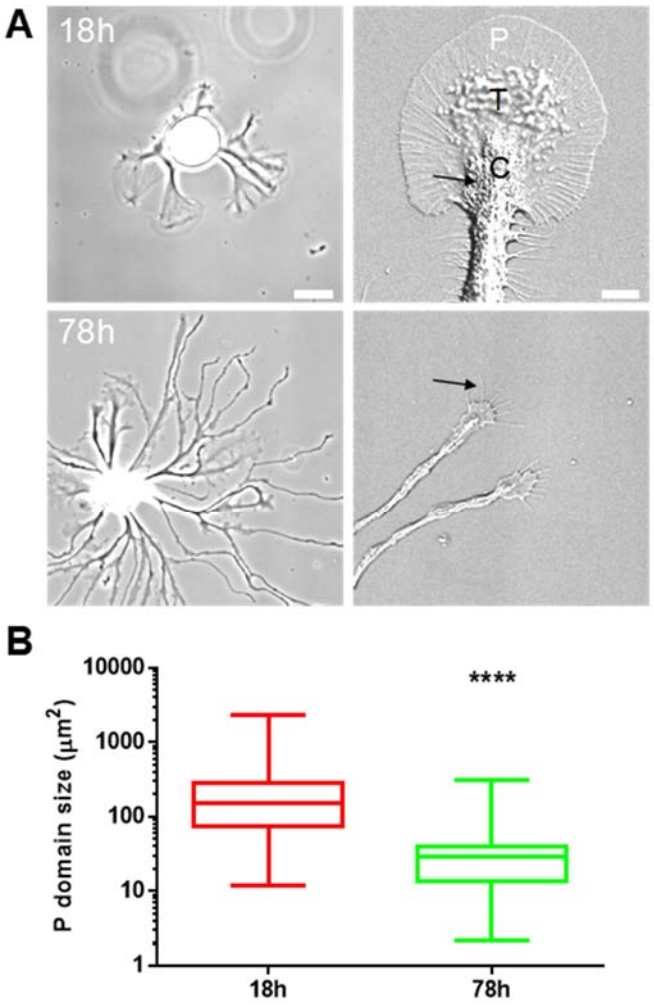

Figure 4.1. Growth cone size decreases between 18 and 78 h in cell culture.

A. Representative differential interference contrast (DIC) images of *Aplysia* bag cell neurons at 18 h (upper panels) and 78 h after cell plating (lower panels). Left panels show lower magnification and right panels show higher magnification. P and C domain and T zone are indicated in upper right image. Arrows points to vesicles in the C domain in upper right image and to filopodium in lower right image. B. Statistical comparison of P domain size between 18 h and 78 h, shown in log scale. Average P domain size ± SEM at 18 h is 242.1 ± 39.1 μm^2 (n=74); average P domain size at 78 h is 37.7 ± 7.5 μm^2 (n=45). Data are pooled from 3 independent experiments. Box: 25th and 75th percentile plus median line; whisker: min and max. ****=P<0.0001. Mann-Whitney test. Scale bar on the left: 60 µm; scale bar on the right: 10 µm.

4.2.2 Large growth cones tend to have lower growth rates

In order to test if growth cone size has an impact on growth rate, we took images of individual growth cones on the second day of plating, at 3.5 h interval (at 53 h and 56.5 h after plating). As can be seen from Figure 4.2A, the large growth cone exhibited minimal advancement within 3.5 h, while the two smaller growth cones translocated 45 and 50 μm, respectively, over the same period of time. A plot of growth cone advance rate vs. P domain size indicated a non-linear correlation, with the highest growth rate at around 50 μm^2 and a decline of growth rate for growth cones with P domain larger than 100 μm^2 (Figure 4.2B). Growth cones with P domains smaller than 100μm^2 did not show a clear correlation between size and advance rate (inset in Figure 4.2B). Growth cones with P domains larger than 200μm^2 were less abundant and usually had growth rates of less than 2μm/h. In conclusion, our results show that large growth cones tend to grow slowly, whereas small growth cones do not have a clear correlation between size and advance rate.

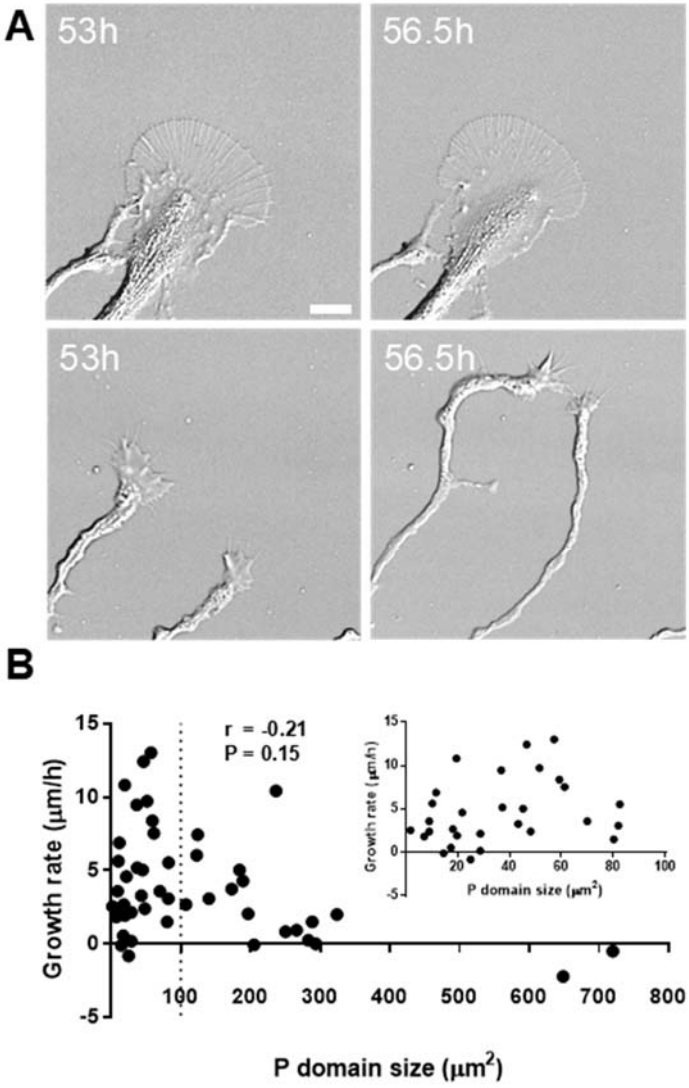

Figure 4.2. Correlation between P domain size and growth rate.

A. DIC images of examples of a large growth cone (upper panels) and two small growth cones (lower panels) imaged at 53 h (left) and 56.5 h (right), respectively. B. Plot of growth rate against P domain size for individual growth cones (n=47). Spearman correlation coefficient and P value for all growth cones included are shown. Inset shows the data for growth cones with P domain smaller than 100 μm^2. Data is representative of two independent experiments. Scale bar: 10 μm.

4.2.3 Neurite growth rate increases with time in culture as growth cone size decreases

Prompted by the findings that growth cone size decreases with increased cell culture time, and that larger growth cones exhibit lower growth rates, we set out to test whether an increase in growth rate can be observed at later time points of cell culture. To this end, images of individual growth cones were taken at 3 h intervals at 24, 48, and 72 h after cell plating (Figure 4.3A). As predicted, we observed a significant decrease in average P domain size, concomitant with a significant increase in average growth rate with time in culture (Figure 4.3B and C). Plots of growth rate vs. P domain size for individual growth cones, however, showed a non-linear correlation (Figure 4.3D) in agreement with data shown in Figure 4.2B. These plots revealed that the P domain size is a poor predictor of growth rate for individual growth cones with P domain size smaller than 50μm^2; however, it becomes a better predictor for larger growth cones, since 100 % of growth cones with P domain size larger than 100 μm^2 have small growth rate (less than 2 μm/h). In summary, the decreased percentage of large growth cones at later time points of cell culture accounts for the increase in average neurite growth rate with time in culture. At later times in culture, the majority of neurite outgrowth was carried out by smaller growth cones with P domain size of less than 50 μm^2.

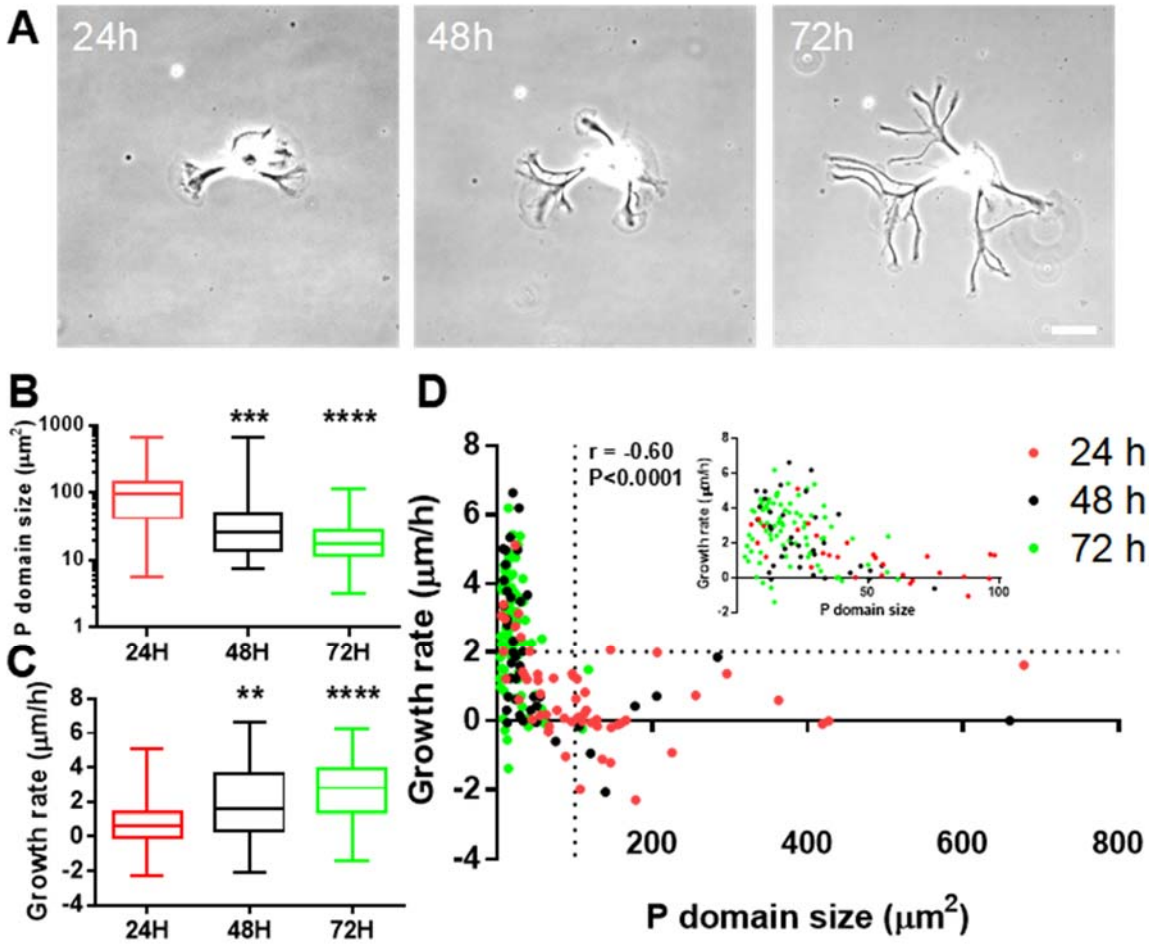

Figure 4.3. Neurite growth rates increases with decreasing growth cone size and time in culture.

A. A cultured bag cell neuron was followed at 3 time points after plating (24 h, 48 h, and 72 h). At each time point, the displacement of growth cones over a 3 h time interval was used to calculate the growth rate. B. Statistical comparison of P domain size at 24 h, 48 h, and 72 h after plating, respectively. Average P domain size ± SEM for 24 h is 120.4 ± 16.2 μm^2; for 48 h is 61.0 ± 16.8 μm^2; for 72 h is 22.8 ± 2.2 μm^2. C. Statistical comparison of growth rate. Average growth rate ± SEM for 24 h is 0.8 ± 0.2 µm/h; for 48 h is1.9±0.3 µm/h; for 72 h is 2.6 ± 0.2 µm/h. D. Plot of growth rate and P domain size for individual growth cones at different time points. Growth cones from different time points are shown in different color (red: 24 h, n=56; black: 48 h, n=43; green: 72 h, n=80). Spearman correlation coefficient and P value are shown for data pooled from three time points. Inset shows the plot only for growth cones with P domain smaller than 100 μm^2. Plot is representative of two independent experiments. Box: 25th and 75th percentile plus median line; whisker: min and max. **=P<0.01; ***=P<0.001; ****=P<0.0001. Dunn's test. Scale bar: 50 µm.

4.2.4 Large and small growth cones show different C domain and T zone dynamics

In order to identify other differences between large and small growth cones besides size that might explain their different growth rates, we used high-resolution live cell imaging over the time course of 3 h to study their motile behavior. In agreement with previous findings (Figure 4.2), growth cones with P domains larger than 100 μm^2 rarely showed net advancement (Figure 4.4A). These large, fan-shaped growth cones exhibited swaying of the C domain that terminates at membrane ruffles – also referred to as intrapodia - in the T zone and a gradual decrease in the extent of membrane ruffles in the T zone over time. In contrast to the large growth cones, small, motile growth cones advanced by protruding lamellipodia between newly formed filopodia, while avoiding the formation of a large fan-shaped P domain (Figure 4.4A, small growth cone on the right; Figure 4.4B). Furthermore, in smaller growth cones, the C domain followed more consistently the base of filopodia and maintained its directionality better than in large growth cones (Figure 4.4b). We measured the angle between the mean orientation of the C domain boundary and the direction of growth cone advancement as an indicator for the persistency of the C domain advancement and engorgement (Figure 4.4C). We found that large, pausing growth cones frequently showed swaying of the mean C domain orientation along with splitting of the C domain, suggesting that persistent C domain advance could be more challenging for large growth cones (Figure 4.4C). On the other hand, small advancing growth cones exhibited a more persistent orientation of the C domain. After spending a significant amount of time (typically more than 3 h) in the pausing state, a large growth cone either completely retracted or retracted some of its P domain to form smaller growth cones. In this way, large growth cones gave rise to new neurites through branching from their original P domains (Figure 4.4D). In summary, the persistent advance of the C domain is more common in small growth cones and may contribute to the faster growth of small growth cones when compared to large fan-shaped growth cones.

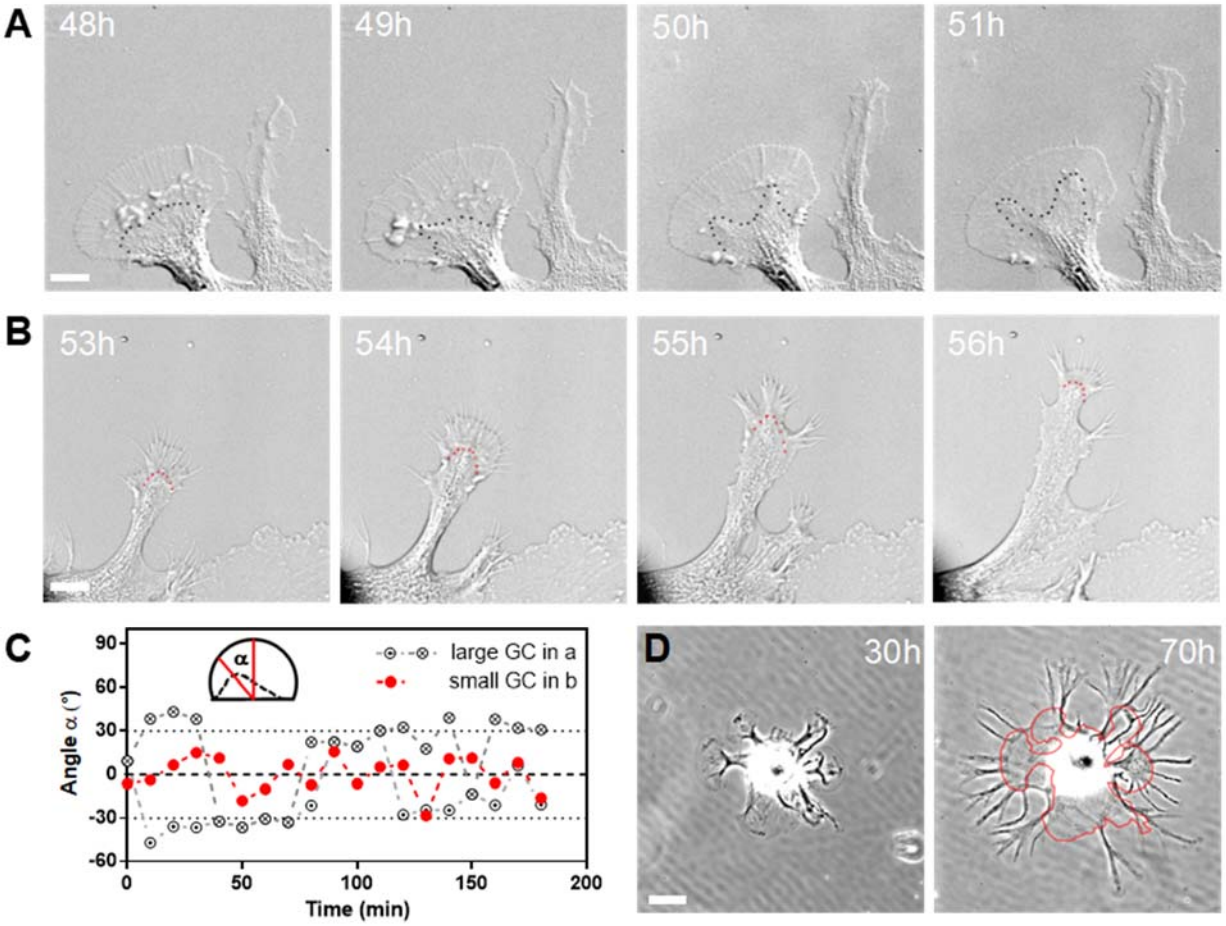

Figure 4.4. Large and small growth cones show different motile behavior.

A. DIC Time-lapse imaging of a large, fan-shaped growth cone on the left revealed minimal net advancement during 3 h, whereas the small growth cone on the right translocated over a distance of 9 µm during the same time period. The C domain boundary is marked with a black dotted line. Note the splitting of C domain at the 50 h time point. B. DIC Time series of a small growth cone that showed significant translocation within 3 h. P domain protrusion is followed by advancement of the C domain (boundary marked with red dotted line). C. Angle between the direction of the C domain and the direction of growth cone advancement, measured at 10min intervals. A diagram of C domain with -45 degree relative to the direction of growth cone advance is shown as an inset. The small growth cone shown in B exhibited little fluctuation of the angle, whereas the large growth cone shown in A showed swaying of the C domain manifested by larger fluctuations of the angle (crossed circles) or splitting of the C domain (crossed and dotted circles). D. Images of the same cultured bag cell neuron taken 40 h apart. Outline of growth cones at 30 h is overlaid to the image taken at 70 h. Note the formation of new neurites by branching from edges of P domain. Scale bars in A and B: 10µm; scale bar in D: 60 µm.

4.2.5 The cessation of growth cone motility correlates with formation of flat P domain and T zone

Next, we went on to characterize the cellular events that lead to the formation of large growth cones, which is shown in Figure 4.5A. In this example, two growth cones (GC1 and GC2, indicated at 2 h time point) formed within 2 h of cell plating from a proximal neurite that remained following dissection of the ganglion (Figure 5.5A; time point 0 h is immediately after cell plating). The nascent growth cones advanced both by protrusion of filopodia and "veil-like" lamellipodia in-between filopodia. The growth rate fluctuated and was as high as 15 µm /h. The expansion of lamellipodial veils eventually connected all filopodia, which formed a uniform array of spikes in the fan-shaped P domain of the large growth cone 1 (GC1) at the 7 h time point. The flattening of both P domain and T zone coincided with the loss of growth cone motility in both the large GC1 and the small GC2 (red and black arrow in Fig 5.5B). By 7 h after plating, both growth cones reached the pausing state and resembled the larger growth cone shown in Figure 4.4A. Whereas the large GC1 never exited this pausing state and became completely retracted within the next 10 h (data not shown), the smaller GC2 started to protrude again after formation of membrane ruffles both along the leading edge and in the T zone around 9 h and by elongation of filopodia from the P domain edge between 9 and 10 h (Figure 5.5C). Thus, the formation of flat P domain and T zone seems to be a hallmark of large, pausing growth cones. Furthermore, these observations suggest that local changes in actin and membrane dynamics need to occur in order to exit this pausing state.

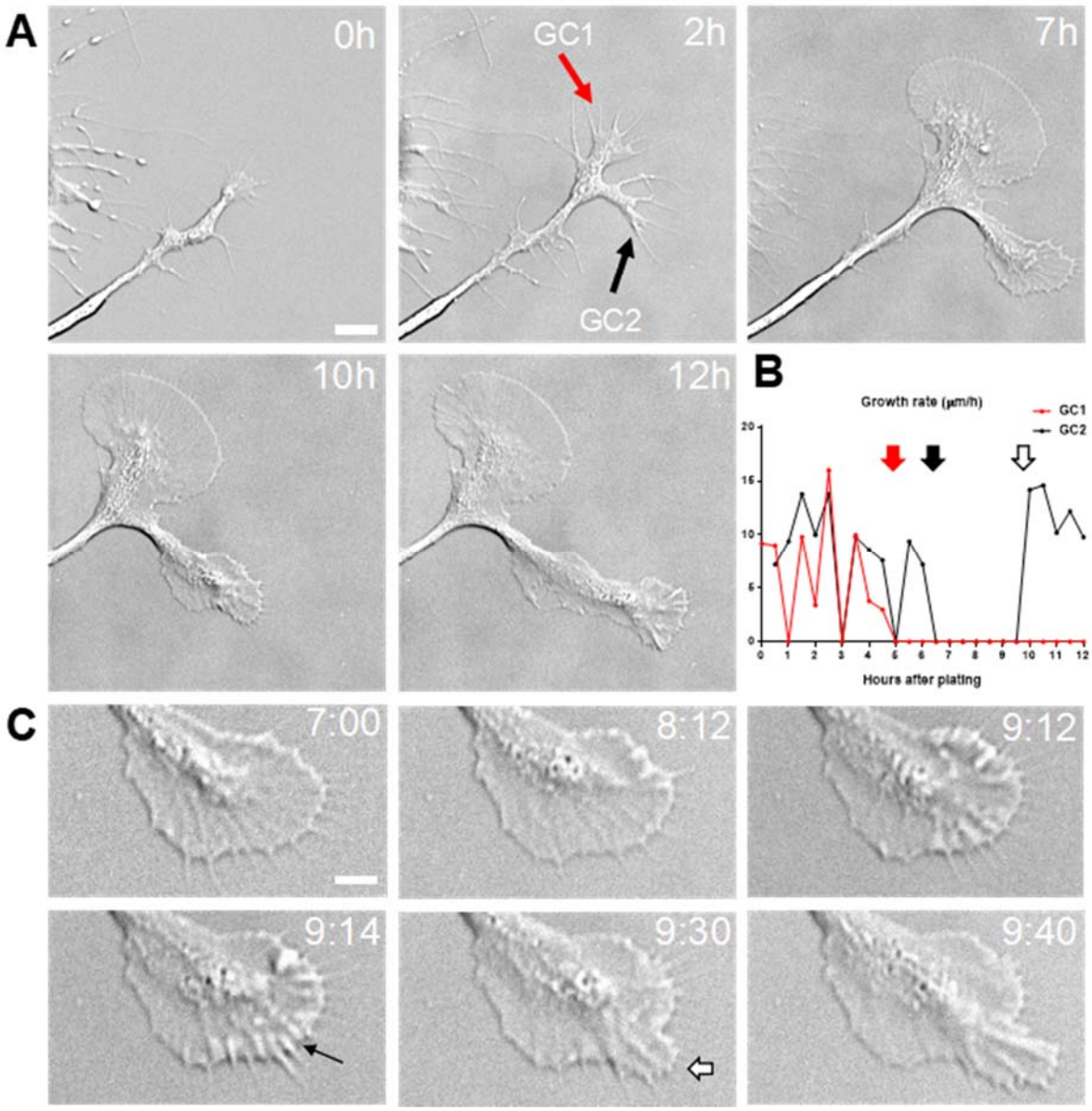

Figure 4.5. A flat P domain and T zone is indicative of immotile behavior.

A. DIC time-lapse series of two growth cones followed for 12 h immediately after cell plating. Both growth cone 1 (GC1) and growth cone 2 (GC2) lost motility after generating flat P domain and T zone, whereas GC2 regained motility at 10 h after a three hour pausing phase. B. Plot of growth rate of GC1 and GC2, calculated at 30 min interval. Red and black arrows indicate the formation of flat P domain for GC1 and GC2, respectively. White arrow indicates when GC2 resumed protrusion of the P domain after pausing. C. Time-lapse series of GC2 between 7 h and 9 h 40 min demonstrating the initial pausing followed by the recovery of the motile protruding state. Note the formation of membrane ruffles along the leading edge, which precedes P domain protrusion (black arrow at 9 h 14 min time point). White arrow at 9 h 30 min time point indicates protrusion of filopodia and lamellipodia. Scale bar in a: 10 µm; scale bar in C: 20 µm.

4.2.6 Collagen I-based gel promotes faster outgrowth of bag cell neuronal growth cones

Our results so far suggested that the formation of large, fan-shaped growth cones after 1 day in culture was caused by a significant expansion of filopodia and lamellipodia, which are promoted by the two-dimensional (2D) PLL substrate. In an attempt to rescue large growth cones from this pausing state, we provided them with an additional substrate support from the dorsal side. In doing so, we designed an anisotropic three-dimensional (3D) collagen culture system. After growth cones had formed on PLL-coated coverslips, a layer of a collagen I-based gel containing 25% *Aplysia* hemolymph and 20 µg/mL PLL was introduced on top of the neurons, and the cells were cultured for an additional 24 h (Figure 4.6A). This 2D-3D transition in culture environment had a clear impact on the morphology of growth cones, and promoted neurite outgrowth when compared to growth on 2D PLL substrates (Figure 4.6B). Figure 4.6C shows a large growth cone on PLL before and after introduction of the collagen gel. Compared with the growth cone on plain PLL substrates, growth cones in 3D culture were consistently smaller and had less distinct domain separation (Figures 4.6C and D). Average total growth cone size before gel application was 1238 ± 178µm^2 (n=37) and after gel application was 70 ± 24µm^2 (n=25; Figure 4.6E). Time lapse imaging of growth cones dynamics advancing at the 2D-3D interface revealed mean growth rates of 13.4 µm^2/h (Figures 4.6F and G). Addition of hemolymph to the collagen gel was critical to convert the large pausing growth cones to smaller advancing growth cones. However, we do not believe that the changes observed were solely due to hemolymph, since growth cones cultured on planar surfaces coated with PLL and hemolymph result in a morphological phenotype that is midway between growth cones grown on PLL and at the 2D-3D interface. The neurites formed after gel addition were more rounded and smooth, a sign of neurite consolidation (Figures 4.6D and G). This rounded neurites induced by the addition of 3D collagen gel were more similar to the pre-existing neurite following dissection of the abdominal ganglion (Figure 4.5A) and different from the more spread neurites generated on the plain PLL substrates (Figure 4.4). Therefore, application of the collagen gel promoted neurite outgrowth of bag cell neurons, possibly by providing substrate support on the dorsal side of the growth cone and triggering smaller growth cones.

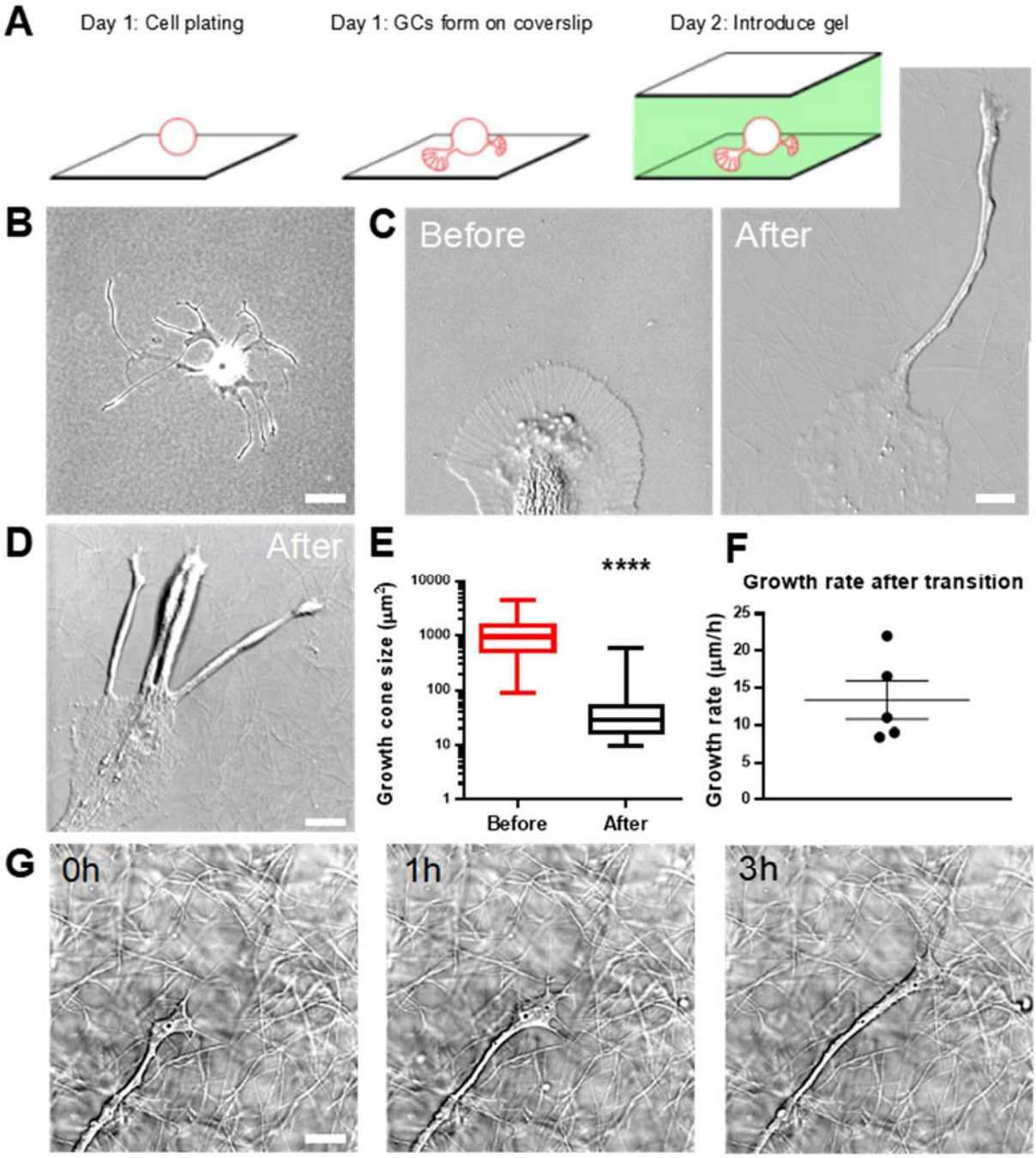

Figure 4.6. Collagen I gel rescues the motile behavior of bag cell neuronal growth cones.

Figure 4.6. Collagen I gel rescues the motile behavior of bag cell neuronal growth cones.

A. Schematic depicting the time frame of the 2D-3D culture system. B. Low magnification phase contrast image of a bag cell neuron cultured for 30 h in 3D culture system. Small growth cones appeared at the ends of long neurites. C. High magnification DIC images of a growth cone before and after addition of the collagen gel. A rounded neurite developed from the leading edge of original P domain within 24 h. D. Another example of a single growth cone that generated multiple neurites after introduction of the 3D culture system. E. Statistical analysis of growth cone size before and after gel application. Average growth cone size ± SEM before gel application is 1238 ± 177.9μm^2 (n=37); average growth cone size after gel application is 70.3 ± 24.2μm^2 (n=25). Box: 25th and 75th percentile; whisker: min and max. ****=P<0.0001. Mann-Whitney test. F. Growth rate of neurites after transition, measured from time lapse of individual growth cones as in G. Average growth rate is 13.4 ± 2.6μm/h calculated from 5 growth cones in three independent experiments. G. Time-lapse series of a growth cone advancing at the interface of 2D and 3D culture. Compared with the large growth cones in 2D cultures, this growth cone has a more compact morphology and advances at higher growth rates (10-20 μm/h). Scale bar in B: 60 μm; scale bar in C, D and G: 10 μm.

4.3 Discussion

4.3.1 Stages of neurite outgrowth of cultured *Aplysia* bag cell neurons

Growth cones formed by *Aplysia* bag cell neuron cultured on PLL-coated solid surfaces have proven to be an excellent model system for the past 30 years, as it enabled seminal discoveries regarding the nature of F-actin retrograde flow (Lin et al., 1996, Lin and Forscher, 1995), substrate-cytoskeleton coupling (Mejean et al., 2013, Suter et al., 1998, Suter and Forscher, 1998), microtubule and actin dynamics (He et al., 2015, Lee et al., 2008a, Schaefer et al., 2002, Schaefer et al., 2008), and cellular mechanotransduction (Athamneh et al., 2015, Athamneh and Suter, 2015, Hyland et al., 2014b, Mejean et al., 2013). Common features of the growth cones analyzed in the aforementioned studies are large size (typically with P domains larger than 100μm^2), fan shape, and clear domain distinction, the combination of which provides unique advantages especially for high-resolution measurements of cytoskeletal dynamics and cellular mechanics. While being a well-defined system, these large growth cones represent only one type among the diverse growth cone morphologies observed *in vitro* and *in vivo*. It is therefore necessary to investigate the motile behavior of bag cell growth cones beyond the typically reported shape to better compare findings made with different growth cone model systems. We believe that the basic mechanisms of how cytoskeletal dynamics is harnessed for growth cone motility and advance are highly conserved

across different species and growth conditions. What varies among different growth cone systems, growth states and conditions is the relative contribution of individual processes to net outgrowth, such as 1. actin assembly and recycling, 2. myosin activity, 3. adhesion and clutching, 4. membrane delivery and recycling. Thus, the large, fan-shape *Aplysia* growth cone can be considered a transient "pausing growth cone", in which actin assembly and retrograde flow rates are well balanced (He et al., 2015). It can exit this pausing stage through a new stimulus such as an adhesion protein-coated bead or needle (Athamneh et al., 2015, Suter et al., 1998), by branching or introduction of a collagen gel (this study) as further discussed below.

To achieve a more comprehensive assessment of the motile behavior of cultured bag cell growth cones, we analyzed the morphology and motility of bag cell growth cones on PLL-coated coverslip at different time points in culture in an unbiased manner with respect to growth cone morphology and size and describe how the large growth cones develop over time. During the first 24 h after plating, multiple large, fan-shaped growth cones formed with P domains larger than 100 μm^2. These growth cones formed from pre-existing neurites or *de novo* from the cell body. The large P domain was induced by multiple lamellipodial veils protruding and connecting an increasing number of filopodia (Figure 4.5A). The formation of these large growth cone took about 3-5 h, and they typically spent a significant amount of time (more than 3 h) in the pausing state (Figure 4.4A). Large growth cones then typically branched into neurites with growth cones of smaller size between 24 and 72 h after plating (Figures 4.1, 4.3, and 4.4D). None of the neurites was morphologically distinct from others indicating that an axon cannot be distinguished from dendrites in bag cell neurites, which is not surprising considering that these cells primarily have neurosecretory function. Although a simple linear correlation between P domain size and growth rate for individual growth cones could not be established for all observed growth cones, a lower growth rate (smaller than 2μm/h) was usually found for large growth cones (P domain size more than 100μm^2), which is in agreement with previous study where instantaneous growth rates of large growth cones were measured (Figure 4.2B) (Hyland et al., 2014a). Small growth cones can advance as fast of 10μm/h on PLL substrates in the absence of any additional growth promoting factors (Figure 4.2A), suggesting the lower growth rate seen for large growth cones is likely due to the significant growth cone enlargement. When neurite outgrowth was promoted by either adding hemolymph or plating on coverslips coated with hemolymph/laminin, a reduction in growth

cone size could be readily observed (Burmeister et al., 1991, Hyland et al., 2014a). Bag cell neurons plated on laminin/hemolymph-coated silicone gel also displayed smaller size and faster growth rate (Hyland et al., 2014b). Thus, a smaller size seems to be a pre-requisite for fast growth in the case of *Aplysia* bag cell neuronal growth cones, whereas the large growth cones conventionally used for imaging cytoskeletal dynamics are representative of a pausing state. Because of this, one should therefore be careful when directly comparing absolute numbers such as retrograde flow rates gained from pausing *Aplysia* bag cell neuronal growth cones with faster-growing growth cones derived from other species, or when extrapolating to growth cones *in vivo*. It will be interesting to investigate whether actin assembly and retrograde flow rates are different between large, pausing and small, advancing growth cones, in order to better understand the causal relationship between growth cone size and advance rate. A definite causal relationship between size and growth rate, however, could only be established if we would find a substrate-independent way to directly enlarge the size of fast moving *Aplysia* bag cell neuron growth cones.

4.3.2 Large and small growth cones have different C domain dynamics and ruffling activity

Whereas the dynamics of large *Aplysia* bag cell growth cone has been extensively studied on shorter time scales, we have complemented this knowledge here with live cell imaging on longer time scales. Two cellular features were discovered when large growth cones developed from small growth cones: 1) the C domain frequently changed its direction when large growth cones were in a pausing state and sometimes split into two domains; 2) T zone ruffles appeared soon after the formation of a large growth cone, and then gradually disappeared (Figure 4.4A). Efficient engorgement of the C domain into the area where the P domain was previously located is an important step during the formation of axons (Goldberg and Burmeister, 1986). Swaying of the C domain as observed in large growth cones (Figure 4.4) may indicate a decision-making phase before final engorgement occurs in a particular direction. The varying angle between C domain orientation and the direction of growth in large growth cones (Figure 4.4C) could be caused by the symmetrically expanding P domain and the fact that there are not enough microtubules and vesicles to fill the expanding C domain evenly. When the symmetry in the P domain was broken by disruption of actin bundles, large growth cones could be re-oriented (Zhou et al., 2002). Splitting of the C domain was usually followed by branching of growth cones. It appears that large growth cones can only exit the pausing state by branching into smaller ones, or they completely

retract. Branching happened either spontaneously (Figure 4.4) or by applying a collagen gel (Figure 4.6D). A similar branching pattern was observed after treatment of Helisoma growth cones with conditioning factors (Williams and Cohan, 1994). In contrast, in fast growing small growth cones, the P domain was biased towards the direction of a small number of filopodia, and C domain maintained better alignment with the direction of growth (Figure 4.4B and C). Interestingly, in small growth cones, ruffles in the P=domain were often generated towards the direction of advancement along the leading edge, preceding the formation of filopodia from P domain (Figure 4.4B and 5C); whereas in large growth cones, ruffles were usually confined to the T zone and eventually disappeared (Figure 4.4A). Whether the ruffles along the leading edge of small growth cones and in the T zone of large growth cones have the same function with respect to motility is unclear at this point. We speculate that the initial ruffling activity in the T zone of large growth cones may indicate an attempt of the growth cone to grow vertically as opposed to expand horizontally.

4.3.3 Rescue of growth cone translocation through 3D collagen gel

In vivo data suggests a correlation between growth cone morphology and motility: rapidly growing retinal ganglion cell growth cones in the optic nerve are smaller and have simple shape, whereas at decision making positions such as the optic chiasm, growth cones adopt a more elaborate fan-shape with filopodial and lamellipodial extensions, and grow at a significantly reduced rate (Holt, 1989, Mason and Wang, 1997). The large growth cones from *Aplysia* bag cell neurons cultured on PLL may behave similarly to the second group, searching for chemical and physical cues that are scarce under the current culture conditions. For *Aplysia* bag cell neuron, this pausing state usually takes a long time (typically longer than 3 h) and redirecting its growth has been difficult. Physical interaction with either an *Aplysia* cell adhesion molecule (apCAM)-coated bead or microneedle could lead to reorientation of C domain and increased advance rate (Athamneh et al., 2015, Suter et al., 1998). However, since the microneedle was kept in the same position in these experiments, increased neurite growth rate did not persist once the C domain reached the microneedle. Through application of collagen I-based gel containing hemolymph on top of the growth cones, we were able to create and maintain a topographical cue that could reliably rescue the forward translocation of large growth cones (Figure 4.6). Growth cones found in this culture environment had smaller size, faster growth rate, and a dramatically different morphology that was reminiscent of growth

cone on patterned substrate (Jang et al., 2010). The neurons in this 2D-3D transition setup are not completely independent from the planar PLL-surface as indicated by the fact that neurites tend to remain close to the cover glass surface. To our knowledge, this 3D collagen gel is the only culture method that can induce well-consolidated neurites from *Aplysia* bag cell neurons. We believe the growth cones formed in this 2D-3D transition setup may be more similar to the growth cones in living animals with respect to morphology and motility. The relative contributions of individual processes of cytoskeletal and membrane dynamics may differ between the 2D and 3D environments resulting in the observed differences in morphology and motility. The effect of this collagen gel-based approach may be attributable to the presence of micron scale topographical cue that can be sensed and responded to by the growth cone. By creating and maintaining this local difference, individual growth cones maintain a rapidly advancing state similar to retinal ganglion cell growth cones in the optical tract. Although technically challenging, it will be interesting to quantitatively analyze motility, cytoskeletal dynamics, and force production of bag cell growth cones in 3D and compare with existing 2D data to better understand the machinery that powers growth cone advancement *in vivo*.

CHAPTER 5. A LOW-COST MICROWELL DEVICE FOR HIGH RESOLUTION IMAGING OF NEURITE OUTGROWTH IN 3D

5.1 Synopsis

In this chapter, we offer a simple protocol for three-dimensional culture of *Aplysia* bag cell neurons and showcase the compatibility of our protocol with high-resolution imaging of neurite outgrowth.

Results from this chapter have been published under the title of "A low-cost microwell device for high-resolution imaging of neurite outgrowth in 3D." in Journal of neural engineering 15, no. 3 (2018): 035001.

5.2 Results

5.2.1 Device design and workflow

Design of our 3D culture device is shown in Fig. 5.1 and described in Chapter 2.3. In contrast to many current 3D culture methods, our setup eliminated the contact between soma and coverslip during cell culture, which has been shown to not only bias neurite outgrowth towards coverslip surface but also change gene expression patterns. The short distance between neurons and culture media also makes it easy to apply cell-permeable molecules and inject cells as shown below. To induce neurite outgrowth, we created a novel collagen-based gel mixture, which contains 20 μg/ml PLL and 25% *Aplysia* hemolymph. PLL helped to maintain the mechanical strength of collagen gel in high salt media, whereas hemolymph was found to be critical for stimulating neurite regeneration, possibly due to the presence of endogenous growth promoting factors. Both PLL and hemolymph were added at their minimum effective concentration to promote robust outgrowth at highest possible rates.

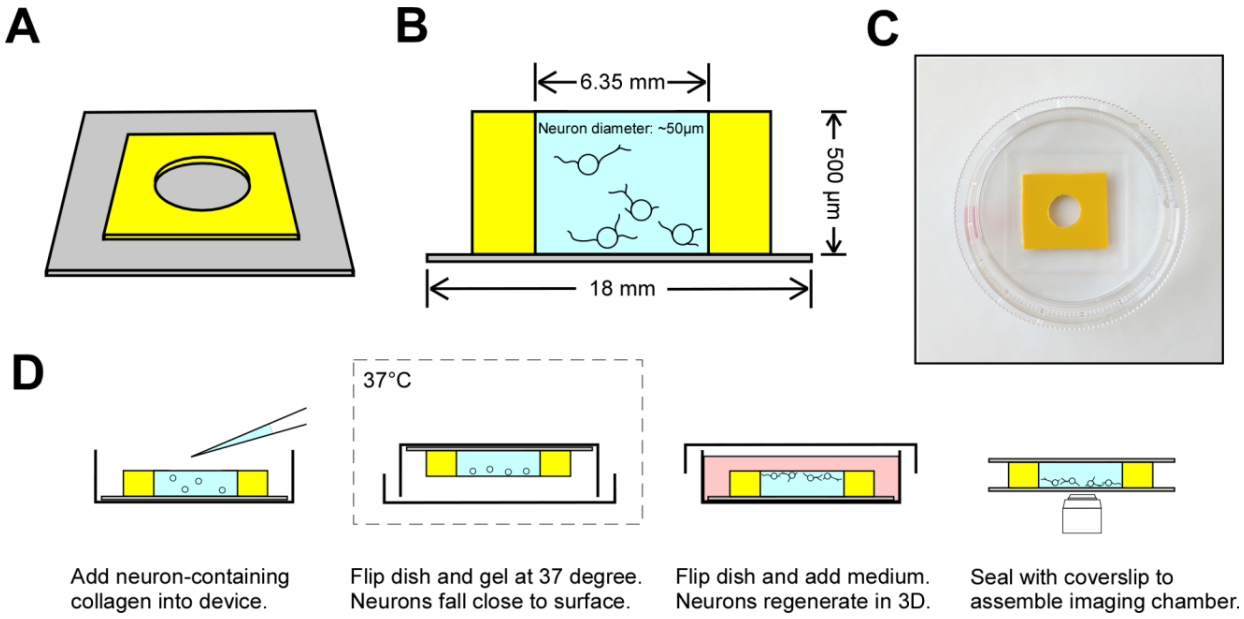

Figure 5.1. Design of 3D culture device.

A. Schematic showing top view of the microwell device mounted on a coverslip. B. Side view of microwell filled with neuron-containing collagen gel. The height is exaggerated in this drawing for illustrative purpose. C. Picture of a glass coverslip with an attached microwell in an empty Petri dish. D. Schematic demonstrating the work flow of neuronal culture and imaging using the 3D culture device.

5.2.2 Neurite outgrowth in 3D

Bag cell neurons exhibited robust neurite regeneration in the 3D gel. As shown in Fig. 5.2A, multiple neurites developed from the identified neuron between 24 and 30 h after neurons had been embedded (Fig. 5.2A). Contrary to the growth pattern on a coverslip, neurite outgrowth was no longer confined to a planar surface. The three-dimensional exploration of the gel space was evidenced by the neurite tips growing out of the plane of focus between 26 and 30 h (Fig. 5.2A). We could observe a variety of complex behaviors of neurite growth, including elongation, retraction, and branching. In contrast to the flattened cell bodies commonly seen in 2D cultures, the cell body of a bag cell neuron retained its spherical shape (Fig. 5.2B), again suggesting the isotropic property of the culture environment. The growth in 3D was very clear when a neurite branching point was imaged, where almost all daughter neurites became out of focus, whereas the

mother neurite remained in focus (Fig. 5.2C). To directly show the growth of a neurite in 3D at high magnification, a neuronal growth cone at a neurite tip was identified and imaged for 4 h (Fig. 5.2D). During this time period, we saw a net advancement of more than 20 μm with an average growth rate of 5.2 μm/h. The average advance rate of 22 growth cones in our 3D culture system was 5.6 ± 0.6 μm/h (±SEM), which is similar to growth rates of bag cell neurons cultured on PLL-coated 2D glass coverslips. As shown in Fig. 5.2D, the neuronal growth cones in this 3D culture system are significantly smaller, more compact, and club-shape when compared to the large, fan-shaped growth cones developed by these neurons, when plated on PLL-coated 2D glass coverslips. The average growth cone diameter in this 3D culture system is 6.4 ± 0.4 μm (±SEM; n=34) compared to the large, fan-shaped growth cones in 2D that span 50-100 μm and more. The smaller size is likely due to the fact that the growth cones have less space to expand in the 3D gel and face an almost isotropic environment in all dimensions. In chapter 4, we have shown that smaller growth cones tend to grow faster than large fan-shaped cones. Smaller, club-shaped growth cones are more commonly observed *in vivo* and in 3D cultures; thus, our findings on bag cell neurite outgrowth in 3D is consistent with previous reports. Taken together, our novel gel mixture supports neurite regeneration of *Aplysia* bag cell neurons in 3D, which can be readily imaged at different magnifications using our microwell device.

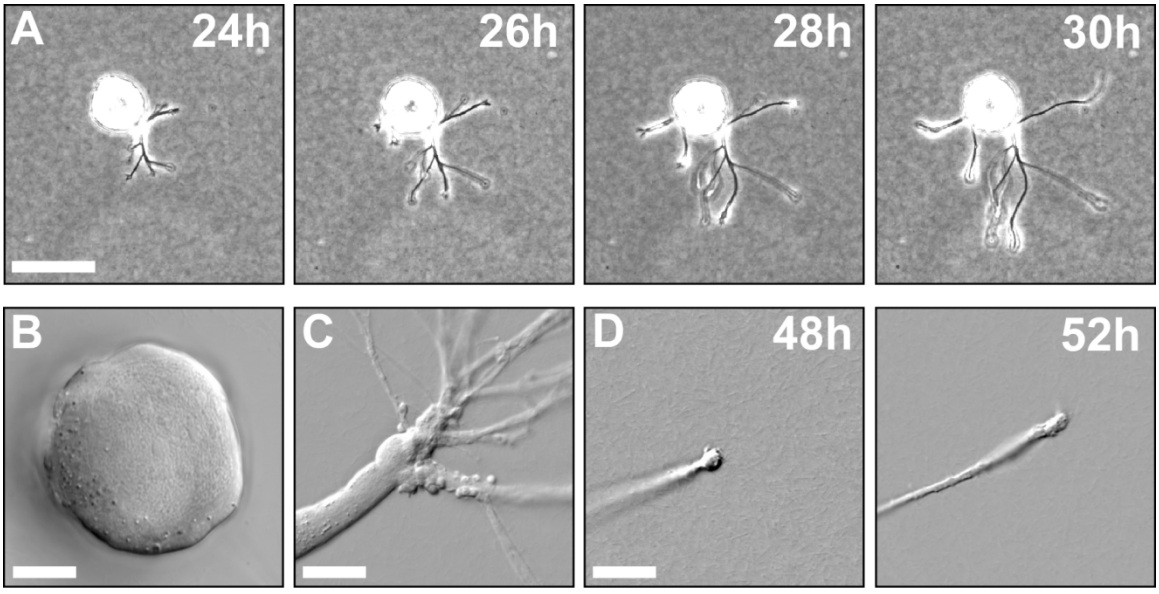

Figure 5.2. Neurite outgrowth in a 3D collagen gel.

A. Snapshots of a bag cell neuron regenerating neurites in 3D. Note the extension of neurites in multiple directions. B. The cell body of a bag cell neuron in the gel retains spherical shape. C. A neurite branching point with the mother neurite remaining in focus. Note the abundant daughter neurites growing in different directions. D. A neuronal growth cone growing at an average rate of 5.2 μm/h was imaged for 4 h. Scale bars: 50 μm (A); 20 μm (B-D).

In addition to transmitted live cell imaging, the porous nature and optical clarity of collagen gel allows fluorescent labeling of molecules of interest after chemical fixation. To demonstrate the compatibility of our device with fluorescent imaging, we identified specific neurons with nascent neurite outgrowth 24 h after embedding (Fig. 5.3A inset), and fixed them 24 h later. Significant neurite outgrowth can be seen in Fig. 5.3A, which is reminiscent of the *in vivo* morphology of mature *Aplysia* bag cell neurons. The location of F-actin and microtubule cytoskeleton fits well with their known role in neurite regeneration, F-actin being concentrated in the tip of the neurite whereas microtubules being prominent along the length of the neurites (Fig. 5.3B). Similarly, the distribution of F-actin and microtubules in the growth cone in 3D seems to follow the same principle as in growth cones in 2D cultures, with F-actin enriched in the growth cone periphery followed by microtubules in the neurite shaft (Fig. 5.3C). Fig. 5.3D shows another example of a neuronal growth cone at higher magnification, where bundles of microtubules terminate at hotspots of F-actin. This distribution of the growth cone cytoskeleton is similar as previously reported for spiral ganglion neurons growing in 3D matrigel culture. It is also consistent with earlier *in vivo* observations of pioneer growth cones in developing grasshopper embryos, which showed that microtubules follow F-actin accumulation in filopodia, as well as with *in vitro* findings demonstrating that microtubules preferentially grow along filopodial bundles of actin filaments in the growth cone periphery. Because of the preservation of both morphology and antigenicity of cytoskeletal proteins after fixation in 3D, our microwell can serve as a reliable tool to study localization of molecules during neurite regeneration.

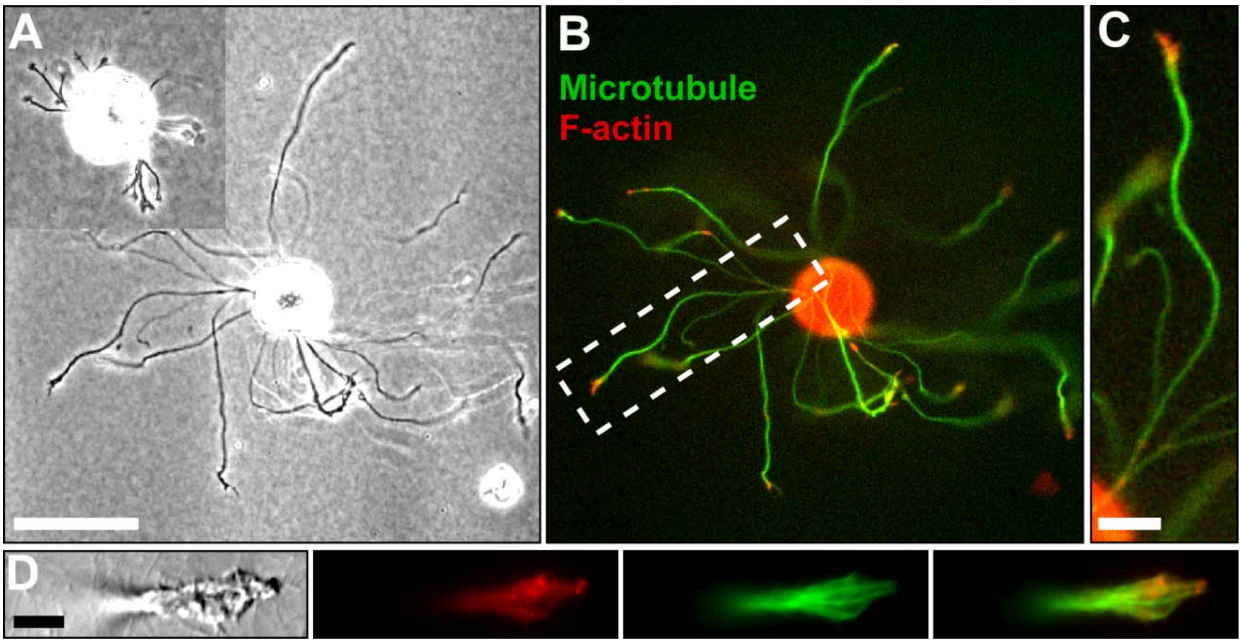

Figure 5.3. Cytoskeletal labeling of fixed neurons.

A. DIC image of a bag cell neuron embedded in the collagen gel showing robust neurite outgrowth at 48 h after plating. Inset shows the same cell with nascent neurites 24 h earlier at the same scale. Scale bar: 50 μm. B. Fluorescent cytoskeletal staining of the neuron shown in A. Microtubules were stained with a primary tubulin and fluorescent secondary antibody (green), whereas F-actin was stained with Alexa-488 phalloidin (red). C. Enlarged boxed region in B showing the localization of microtubules and F-actin along neurite and within the neuronal growth cone. Yellow indicates co-localization of microtubules and F-actin in growth cone neck. Scale bar: 12.5 μm. D. A club-shaped neuronal growth cone at higher magnification in 3D culture system. Bundles of microtubules terminate at hotspots of F-actin. Scale bar: 5 μm.

5.2.3 High-resolution fluorescent live cell imaging in 3D

A major benefit of our microwell is its compatibility with high-resolution live cell imaging of fluorescently labeled proteins and organelles of interest, which is in increasing demand in cell biological research. We have demonstrated this capability of our system with two live cell imaging probes as shown in Figs. 5.4 and 5.5. In the first approach (Fig. 5.4A), we added cell-permeable dye TMRM (tetramethylrhodamine methyl ester) into the cell culture media, which readily diffuses into embedded neurons and specifically labels healthy mitochondria with intact membrane

potential. As shown in Fig. 5.4B, a dense population of mitochondria were successfully labeled along the neurite shaft and in the neuronal growth cone. We magnified the boxed region in Fig. 5.4B and assembled a time-lapse montage showing the dynamics of mitochondria in a developing neurite. Whereas the majority of mitochondria were docked during this period (the solid oval in Fig. 5.4C marks a stationary mitochondrion), transportation of mitochondria in both directions was evident. The average rate of anterogradely transported mitochondria is 0.5 ± 0.1 μm/s (±SEM; n=5; dashed oval in Fig. 5.4C), which is in good agreement with established values of fast axonal transport of mitochondria. Both the high labeling efficiency and intensity as well as the transportation rate indicate the presence of active mitochondria and speak to the healthiness of regenerating neurites. Furthermore, this experiment demonstrated the feasibility of using small membrane-permeable molecules for live cell fluorescent imaging.

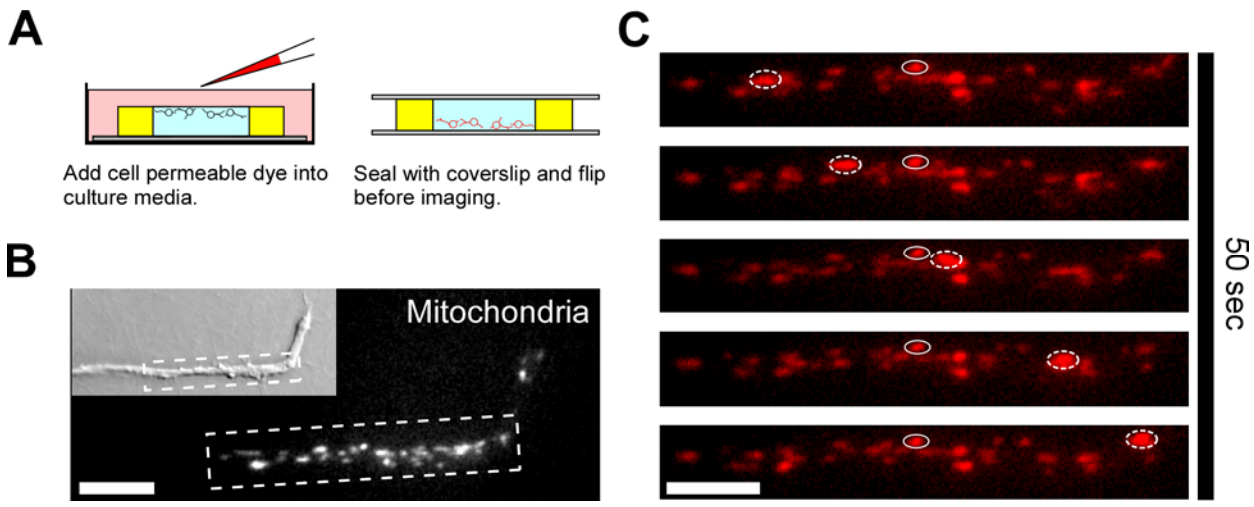

Figure 5.4. Live cell imaging of neurons in 3D using a mitochondrial dye.

A. Workflow of live cell imaging. TMRM was used to label healthy mitochondria. B. A segment of a neurite with dense mitochondria. The neuronal growth cone is advancing towards the upper-right direction. The DIC image in the inset is shown at half the magnification. Scale bar: 10 μm. C. Time-lapse montage of the neurite region boxed in panel B. Solid oval indicates a docked mitochondrion, whereas the dashed oval points to an anterogradely moving mitochondrion (mean rate 0.8 μm/s). Scale bar: 20 μm.

A second approach to introduce intracellular labeling of live cells is through ectopic expression of fluorescent proteins. In the case of embedded bag cell neurons, we can achieve this by injecting mRNA encoding fluorescent proteins into the cell bodies (Fig. 5.5A). This is possible because of the large soma size of *Aplysia* bag cell neurons and the short distance between neurons and gel surface. As an example, we microinjected in vitro transcribed mRNA of a phosphotyrosine (pY) biosensor along with Texas Red dextran as a cytosolic injection/volume marker into embedded neurons. This *Aplysia*-specific pY biosensor was adapted from a previously developed vertebrate pY biosensor and contains two SH2 domains derived from *Aplysia* Src1 tyrosine kinase linked to EGFP. We initially validated this biosensor by expressing it in bag cell neurons cultured in 2D. We found a typical punctate distribution of pY signals in the growth cone including increased signal at the tips of filopodia (data not shown), which is in agreement with previous studies conducted on 2D neuronal cultures that showed enriched tyrosine phosphorylation at filopodia tips including Src-mediated phosphorylation promoting filopodia extension. Microinjection of pY biosensor mRNA into neuronal cell bodies did not prevent the regeneration of neurites in 3D (Fig. 5.5B). The fluorescent signals from both ectopically expressed protein (Fig. 5.5C) and fluorescent injection/volume marker (Fig. 5.5D) could be observed in the neurite regenerating in the 3D gel. Most importantly, we found that the pY biosensor showed preferential localization to the tip of dynamic filopodia (Fig. 5.5C and E) as found in 2D neuronal cultures. The pY distribution was distinct from the relative flat signal profile of fluorescent dextran along the length of filopodia (Fig. 5.5D and F). In summary, these results demonstrate that we can use cell injection to express genetically encoded fluorescent proteins in neurons cultured in 3D, and perform multi-channel, high-resolution live cell imaging of regenerating neuronal growth cones.

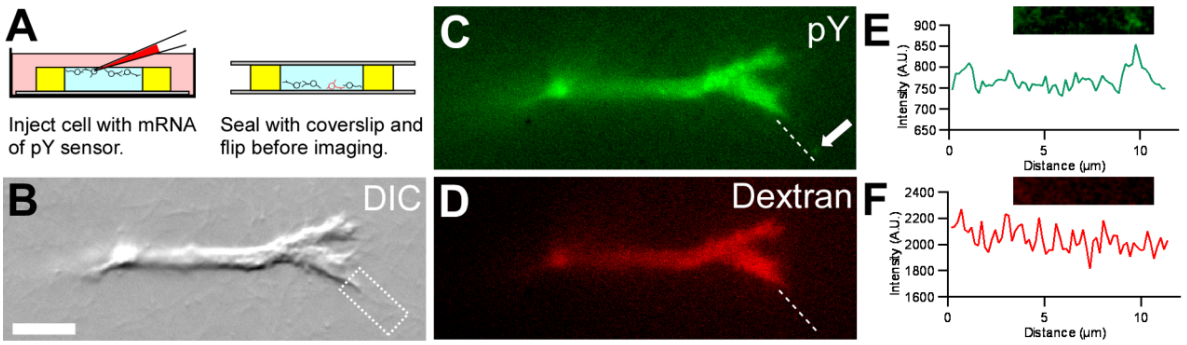

Figure 5.5. Live cell imaging of pY biosensor.

A. Workflow of live cell imaging. In vitro transcribed mRNA of pY biosensor was injected into the neuronal cell body together with Texas Red dextran as a volume marker. B. DIC image of a distal neurite branching into two growth cones in 3D. Scale bar: 5 μm. C. pY signal of the growth cone shown in B. The arrow indicates a bright spot of phosphotyrosine signal at the tip of the filopodium. D. Texas Red dextran signal of the growth cone shown in B. No bright spot can be seen at the tip of the filopodium. E. Fluorescent line scan of the pY signal along the filopodium next to the dotted line shown in C. The peak signal corresponds to filopodium tip. F Fluorescent line scan of dextran signal at the same location. No bright spot was detected at tip of the filopodium.

5.2.4 Super-resolution imaging of neuronal growth cones in 3D cultures

Recent developments in sub-diffraction-limited imaging techniques have resulted in discoveries of previously hidden cellular structures such as actin rings in neuronal processes, and offered exciting new insights into the structural organization of macromolecular complexes especially in the cell membrane such as synapses. To demonstrate the compatibility of our microwell device with super-resolution imaging, we immunostained microtubules and performed direct Stochastic Optical Reconstruction Microscopy (dSTORM) imaging of microtubules in distal neurites of bag cell neurons near the neuronal growth cone in 3D. As a contrast to the diffraction-limited image of microtubules (Fig. 5.6A), the reconstructed super-resolution image of the same sample revealed bundles of microtubules near the neck of the growth cone with significantly improved resolution (Fig. 5.6B). The axial positions of individual localized molecules within the microtubules and microtubule bundles in this example are indicated by colors and span a depth of 1 μm. Taken together, our simple microwell showed good performance when conducting super-resolution imaging of neuronal growth cones in 3D.

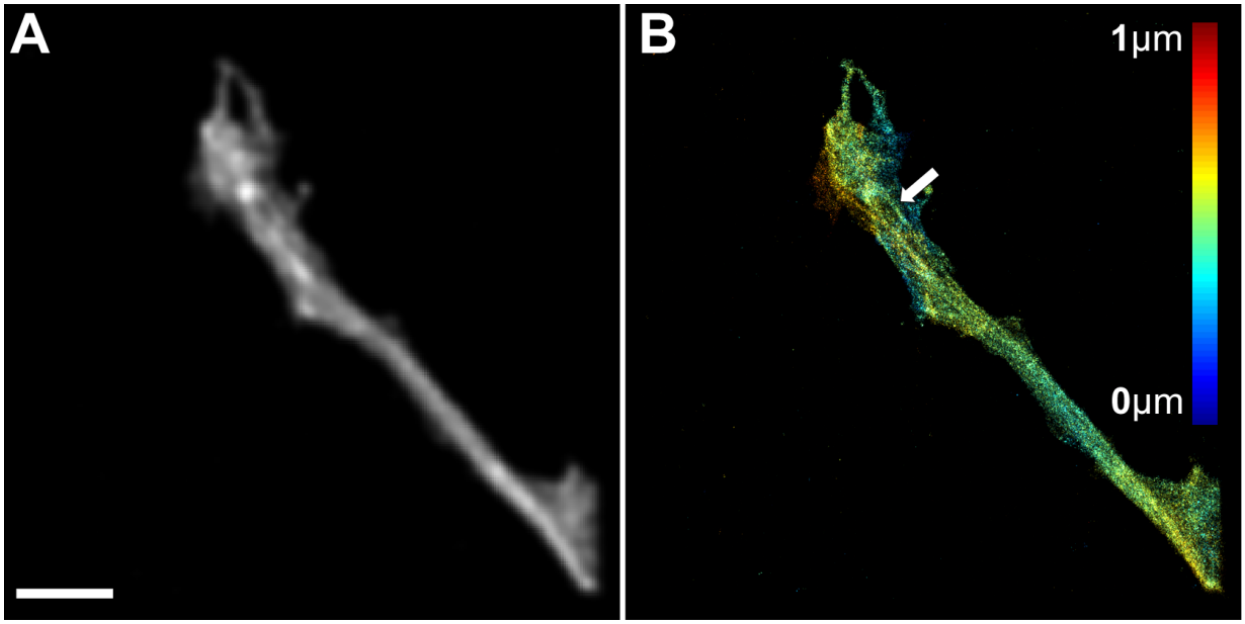

Figure 5.6. Super-resolution imaging of microtubules in distal neurite and neuronal growth cone in 3D cultures.

A. Diffraction-limited wide field fluorescent image of stained microtubules in the growth cone and distal neurite of a bag cell neuron cultured in 3D. Scale bar: 5 µm. B. The same growth cone shown after reconstruction of 0.47 million molecules using single molecule switching nanoscopy. Arrow points to a microtubule bundle within the growth cone neck. Color encodes the axial position of labeled alpha-tubulin molecules. The growth cone was located about 5 µm from the cover glass surface.

5.3 Discussion.

5.3.1 Cost-effective fabrication of a 3D neuronal cell culture device

In recent years, the supporting device for in vitro neurite regeneration has expanded from protein-coated glass coverslips to compliant materials, patterned substrates, and biocompatible gels (Ahmed et al., 2007, Brannvall et al., 2007, Georges et al., 2006, Hyland et al., 2014b, Luo and Shoichet, 2004). This trend in creating a more physiologically relevant environment for neurons is a logical step going beyond the limitations of the traditionally used flat and rigid cell culture surfaces. However, for many laboratories such scientific reasoning is often countered by high costs of device fabrication or challenging device assembly. The motive of our work here is to build an

affordable and simple microwell device to assist researchers overcome some of these barriers to 3D neuronal cell cultures. To that end, we used commonly available lab and office supplies, including standard glass coverslip, hole puncher, double-sided tape and plastic shims. The cost of our microwell is estimated to be significantly lower than most other 3D culture devices, and its assembly requires no special instrument or training. In our present study, a small amount (16 µl) of gel was sufficient to support 3D neurite outgrowth. Due to its straightforward design, we expect that individual labs will be able to easily modify microwell parameters such as size and thickness to meet their needs. In summary, the affordability and simple design of our microwell will make 3D neuronal cell culture conducive to a wider audience.

5.3.2 Proper positioning of neurons facilitates neurite outgrowth and imaging

We engineered a workflow with our microwell to optimize positioning of neurons in gel, for both sustained 3D neurite outgrowth and efficient imaging with both low- and high-power objectives. During neurite regeneration, the neuronal soma and all growing neurites interact only with collagen gel fibers and are not influenced by the gel-device interface. The uniform arrangement of neurons during embedding and the small cell-to-cell microenvironment variability increases data reproducibility and helps identifying suitable cells for imaging. We demonstrated how our microwell can be used to track neurite outgrowth from a single neuron at low magnification (Fig. 5.2A; Fig. 5.3A, B and C), and high magnification (Fig. 5.2B, C and D; Fig. 5.3D). Due to the proximity of the neurons to the gel surface, we were able to apply a cell permeable fluorescent dye or inject cells with mRNA for fluorescent protein expression. We performed high-resolution, live cell imaging of organelle transport along the neurite (Fig. 5.4) as well as monitoring signaling events at the growth cone (Fig. 5.5). Finally, we tested the compatibility of our 3D culture microwell with super-resolution imaging and were able to resolve bundles of microtubules in the growth cone (Fig. 5.6). All images and videos were acquired without making any modification to existing microscope platforms. Therefore, our microwell is a versatile tool for 3D neuronal cell culture, and can be adopted quickly to other cell culture systems and imaging set-ups.

5.3.3 Morphology and dynamics of *Aplysia* growth cones in 3D culture

We used a novel mixture of collagen to promote regeneration of *Aplysia* bag cell neurons in 3D, which has been used to successfully convert 2D cultured bag cell neuron growth cone into *in vivo*-

like morphology (Fig. 4.6). In comparison to outgrowth in 2D, neurites grow at similar rate but towards different directions in 3D, resulting in a growth cone morphologies that are not fan-shaped as observed in 2D cultures but more similar to growth cones observed *in vivo* in other species, such as zebrafish (Hutson and Chien, 2002). At this point, it is difficult to determine the exact relative contribution of molecular versus dimensional signals to neurite growth in our gel system; however, the fact that growth cone size and advance rate could be altered by adding the gel on top of neurons cultured on PLL-coated coverslips suggests that the 3D environment supports neurite regeneration (Fig. 4.6). The regenerated neurites are healthy, harboring rapid transport of mitochondria along the neurite (Fig. 5.4), and display dynamic activity at the growth cone (Fig. 5.2D; Fig. 5.5). In agreement with previous studies, the basic organization of actin and microtubule cytoskeleton are consistent between 2D and 3D cultured *Aplysia* bag cell neurons (Fig. 5.3; Fig. 6), as well as the enrichment of pY signaling at filopodia tips in the growth cone (Fig. 5.5) (Suter, 2011, Suter and Forscher, 2001). This suggests that the central motility and signaling machinery is maintained under these different environmental conditions, which in turn result in distinct growth cone morphologies. Our system will enable future studies to further explore the exact underlying cellular and molecular mechanisms of growth cone advancement in 3D.

CHAPTER 6. FUTURE PERSPECTIVES

6.1 Verification of cortactin phosphorylation *in vitro*

Much is known about how cortactin regulates F-actin organization in a purified system, either by itself or with the help of other actin-regulating proteins. Cortactin used in these experiments are often of mouse or human origin, and the functions of cortactin from lower species are unexplored (Helgeson and Nolen, 2013, Helgeson et al., 2014, Schnoor et al., 2018). In our case, we have demonstrated how changes in the phosphorylation state of a single tyrosine in *Aplysia* cortactin alters its function towards actin remodeling in neuronal growth cone, but the exact mechanism could be better elucidated when combined with *in vitro* data.

We hypothesize that *Aplysia* Src2 protein phosphorylates *Aplysia* cortactin at Y499 *in vitro*. To test this hypothesis, we will purify *Aplysia* Src2 and dominant negative Src2 (DNSrc2, with mutation in kinase domain resulting in loss of kinase activity) proteins from bacterial expression system, and purify a series of *Aplysia* cortactin proteins from bacterial expression system. The cortactin mutation series will include Y499F505F509, F499Y505F509 and F499F505Y509, in which only one of the three tyrosine residues could be phosphorylated, as well as F499F505F509, in which all three tyrosine residues are unphosphorylatable (negative control). We will perform kinase assay to look for the tyrosine residue that could be phosphorylated by Src2 *in vitro*, and we expect to see phosphorylation signal only with the combination of Src2 and cortactin Y499F505F509.

We can also test if tyrosine phosphorylated cortactin could promote F-actin assembly *in vitro*, by synergizing with other F-actin polymerases such as Ena/Vasp. We will compare F-actin assembly rate from pure G-actin, pure G-actin plus p-cortactin, pure G-actin plus Ena/Vasp, and pure G-actin plus p-cortactin plus Ena/Vasp. We predict a highest F-actin assembly rate from pure G-actin plus p-cortactin plus Ena/Vasp group, which is higher than the sum of F-actin assembly rate from groups with only p-cortactin or only Ena/Vasp. Such synergy will be consistent with the *in vivo* data that p-cortactin overexpression promotes filopodia elongation in an Arp2/3 independent manner at filopodia tips.

Because cortactin proteins from mouse and human have multiple tyrosine residues that could be phosphorylated by Src kinase, and our data for *Aplysia* cortactin suggests that only one tyrosine residue is phosphorylated by *Aplysia* Src2 *in vivo*, it will be interesting to compare the crystal structures of *Aplysia* cortactin with cortactins of other species to gain insights into the evolutionary divergence of cortactin proteins. Moreover, because the three tyrosine residues from *Aplysia* cortactin are very close (Y499, Y505, Y509), a high-resolution structure of *Aplysia* cortactin is needed to better understand the substrate selection mechanism of Src family kinases. Structural investigations could be performed by collaboration with one of the many structural biology labs at Purdue.

6.2 Interaction between dynamin and cortactin in filopodia formation

Among the many binding partners of cortactin, dynamin might be an overlooked candidate in filopodia formation and maintenance. Dynamin is a GTPase commonly associated with vesicle pinching during endocytosis, as it's capable of using GTP hydrolysis to change lipid membrane curvature (Ferguson and De Camilli, 2012). Although dynamin has been shown to be able to bind cortactin for a long time, and implicated in re-organizing F-actin structure in cell lines and during endocytosis, the mechanism remain unclear (Krueger et al., 2003, Zhu et al., 2005). Studies have also found that dynamin could directly bind to F-actin and promote bundle formation *in vitro* (Gu et al., 2010), and most interestingly, together with cortactin, they form large ring structures on F-actin bundles (Yamada et al., 2013, Yamada et al., 2016). In purified system, the ring structure could be in either closed or open state, determined by the hydrolysis state of GTP (Yamada et al., 2013). Observation of dynamin ring along filopodia in neuronal growth cone has been reported, and shown to be important in filopodia stabilization (He et al., 2015, Yamada et al., 2013).

We hypothesize that a ring structure, similar to those shown in mature filopodia, may also be important during filopodia formation to help bundle F-actin filaments in filopodia precursor, and that cortactin phosphorylation is needed for generation of ring structure between cortactin and dynamin. This hypothesis highlights the Arp2/3 complex-independent, indirect function of cortactin in actin regulation. We could look for existence of this hypothesized ring structure by super-resolution imaging of growth cone with nascent filopodia (during filopodia formation after drug treatment, as shown in Fig. 3.8), using either cortactin and dynamin antibodies.

6.3 Screening for proteins involved in filopodia initiation with bag cell neuron

Aplysia bag cell neuron growth cone has been a good model system for studies of cytoskeletal dynamics (He et al., 2015, Suter et al., 2004). Combing our drug induced filopodia regeneration assay with high resolution live cell imaging, we could now look closer into the initiation stage of filopodia formation, and better test models about mechanisms of filopodia initiation. Specifically, at least for bag cell neuron growth cones, there seems to be an F-actin independent, membrane associated complex at leading edge that's resistant to actin depolymerization, of which phosphorylated cortactin is a member. Further screening of proteins in this region, for example with antibody based immunofluorescence, will surely reveal more candidates involved in the early stage of filopodia formation, and uncover mechanisms for actin regulation. Furthermore, with introduction of fluorescently labeled actin, the dynamics of actin during filopodia initiation can be directly observed and analyzed through speckle microscopy.

6.4 Role of cortactin in apCAM-actin coupling and force transduction

Thanks to the large size of *Aplysia* growth cone on coverslip, we could use either coated beads or needles to physically interact with the growth cone (Athamneh et al., 2015, Suter et al., 1998, Suter and Forscher, 1998). This perturbation of growth cone, termed Restrained bead interaction or RBI assay, can be coupled with high resolution imaging of actin or microtubule dynamics to gain detailed information about cytoskeletal remodeling relevant to growth cone turning (Decourt et al., 2009, Suter et al., 2004). Application of RBI assay also include direct measurement of force generated by growth cone (Athamneh et al., 2015, Athamneh and Suter, 2015). Transmission of traction force between apCAM coated bead and growth cone cytoskeleton has been found to be regulated by Src kinase activity (Suter and Forscher, 2001, Suter et al., 2004). It's possible that cortactin functions downstream of Src to mediate this force transduction, and defects in cortactin phosphorylation would lead to decoupling of Src activation and actin reorganization (Decourt et al., 2009). To test this hypothesis, growth cones with an overexpression of phosphorylation deficient cortactin could be subject to RBI assay, and we predict a decrease in success rate of growth cone re-orientation by apCAM coated bead.

6.5 Actin dynamics during 3D neurite outgrowth

Due to limitations in the configuration of conventional microscopy, live cell imaging of actin activities has been mostly performed on planer cellular structures such as leading edge of migrating cells and the large growth cone formed by *Aplysia* bag cell neurons on 2D culture (Suter, 2011). However, rapid development in new imaging technologies has made it possible to image with higher resolution in all three dimensions, much faster, and deeper into tissues (Burke et al., 2015, Daetwyler and Huisken, 2016, Heilemann et al., 2008, Huang et al., 2008, Huang et al., 2016, Juette et al., 2008, Park et al., 2015). This will enable direct observation of actin organization and dynamics during three-dimensional neurite outgrowth. Because actin dynamics in *Aplysia* bag cell neuron growth cone has been studied extensively, and the morphology of growth cone from the same cells has been shown to be very different in 3D, live cell imaging of growth cone in 3D with fluorescently labeled actin will uncover how the same force-generating machinery is used differently in different cellular context. Since growth cones are hypothetically optimized for growth in 3D, this direct observation may reveal a more physiologically realistic, or even more efficient utilization of actin-based motility.

REFERENCES

ABEDI, H. & ZACHARY, I. 1998. Cytochalasin D stimulation of tyrosine phosphorylation and phosphotyrosine-associated kinase activity in vascular smooth muscle cells. *Biochem Biophys Res Commun,* 245**,** 646-50.

AHMED, I., PONERY, A. S., NUR-E-KAMAL, A., KAMAL, J., MESHEL, A. S., SHEETZ, M. P., SCHINDLER, M. & MEINERS, S. 2007. Morphology, cytoskeletal organization, and myosin dynamics of mouse embryonic fibroblasts cultured on nanofibrillar surfaces. *Molecular and Cellular Biochemistry,* 301**,** 241-249.

ALESHIN, A. & FINN, R. S. 2010. SRC: a century of science brought to the clinic. *Neoplasia,* 12**,** 599-607.

ATHAMNEH, A. I., CARTAGENA-RIVERA, A. X., RAMAN, A. & SUTER, D. M. 2015. Substrate Deformation Predicts Neuronal Growth Cone Advance. *Biophys J,* 109**,** 1358-71.

ATHAMNEH, A. I. & SUTER, D. M. 2015. Quantifying mechanical force in axonal growth and guidance. *Front Cell Neurosci,* 9**,** 359.

ATHAMNEH, A. I. M., HE, Y., LAMOUREUX, P., FIX, L., SUTER, D. M. & MILLER, K. E. 2017. Neurite elongation is highly correlated with bulk forward translocation of microtubules. *Sci Rep,* 7**,** 7292.

AUDESIRK, T. E. 1979. A Field Study of Growth and Reproduction in Aplysia Californica. *Biol Bull,* 157**,** 407-421.

AYALA, I., BALDASSARRE, M., GIACCHETTI, G., CALDIERI, G., TETE, S., LUINI, A. & BUCCIONE, R. 2008. Multiple regulatory inputs converge on cortactin to control invadopodia biogenesis and extracellular matrix degradation. *J Cell Sci,* 121**,** 369-78.

BAMBURG, J. R. & BERNSTEIN, B. W. 2010. Roles of ADF/cofilin in actin polymerization and beyond. *F1000 Biol Rep,* 2**,** 62.

BENTLEY, D. & O'CONNOR, T. P. 1994. Cytoskeletal events in growth cone steering. *Curr Opin Neurobiol,* 4**,** 43-8.

BLANCHOIN, L., BOUJEMAA-PATERSKI, R., SYKES, C. & PLASTINO, J. 2014. Actin dynamics, architecture, and mechanics in cell motility. *Physiol Rev,* 94**,** 235-63.

BORNSCHLOGL, T. 2013. How filopodia pull: what we know about the mechanics and dynamics of filopodia. *Cytoskeleton (Hoboken),* 70**,** 590-603.

BOVOLENTA, P. & MASON, C. 1987. Growth cone morphology varies with position in the developing mouse visual pathway from retina to first targets. *J Neurosci,* 7**,** 1447-60.

BRANNVALL, K., BERGMAN, K., WALLENQUIST, U., SVAHN, S., BOWDEN, T., HILBORN, J. & FORSBERG-NILSSON, K. 2007. Enhanced neuronal differentiation in a three-dimensional collagen-hyaluronan matrix. *J Neurosci Res,* 85**,** 2138-46.

BREMBS, B., LORENZETTI, F. D., REYES, F. D., BAXTER, D. A. & BYRNE, J. H. 2002. Operant reward learning in Aplysia: neuronal correlates and mechanisms. *Science,* 296**,** 1706-9.

BRYCE, N. S., CLARK, E. S., LEYSATH, J. L., CURRIE, J. D., WEBB, D. J. & WEAVER, A. M. 2005. Cortactin promotes cell motility by enhancing lamellipodial persistence. *Curr Biol,* 15**,** 1276-85.

BUCK, K. B., SCHAEFER, A. W., SCHOONDERWOERT, V. T., CREAMER, M. S., DUFRESNE, E. R. & FORSCHER, P. 2017. Local Arp2/3-dependent actin assembly modulates applied traction force during apCAM adhesion site maturation. *Mol Biol Cell,* 28**,** 98-110.

BURKE, D., PATTON, B., HUANG, F., BEWERSDORF, J. & BOOTH, M. J. 2015. Adaptive optics correction of specimen-induced aberrations in single-molecule switching microscopy. *Optica,* 2**,** 177-185.

BURKE, T. A., CHRISTENSEN, J. R., BARONE, E., SUAREZ, C., SIROTKIN, V. & KOVAR, D. R. 2014. Homeostatic actin cytoskeleton networks are regulated by assembly factor competition for monomers. *Curr Biol,* 24**,** 579-85.

BURMEISTER, D. W., RIVAS, R. J. & GOLDBERG, D. J. 1991. Substrate-bound factors stimulate engorgement of growth cone lamellipodia during neurite elongation. *Cell Motil Cytoskeleton,* 19**,** 255-68.

BURNETTE, D. T., JI, L., SCHAEFER, A. W., MEDEIROS, N. A., DANUSER, G. & FORSCHER, P. 2008. Myosin II activity facilitates microtubule bundling in the neuronal growth cone neck. *Dev Cell,* 15**,** 163-9.

BURNETTE, D. T., SCHAEFER, A. W., JI, L., DANUSER, G. & FORSCHER, P. 2007. Filopodial actin bundles are not necessary for microtubule advance into the peripheral domain of Aplysia neuronal growth cones. *Nat Cell Biol,* 9**,** 1360-9.

CAO, H., CHEN, J., KRUEGER, E. W. & MCNIVEN, M. A. 2010. SRC-mediated phosphorylation of dynamin and cortactin regulates the "constitutive" endocytosis of transferrin. *Mol Cell Biol,* 30**,** 781-92.

CAO, L., HENTY-RIDILLA, J. L., BLANCHOIN, L. & STAIGER, C. J. 2016. Profilin-Dependent Nucleation and Assembly of Actin Filaments Controls Cell Elongation in Arabidopsis. *Plant Physiol,* 170**,** 220-33.

CAREFOOT, T. H. 1987. Aplysia: its biology and ecology. *Oceanography and Marine Biology,* 25**,** 167.

CHAN, C. E. & ODDE, D. J. 2008. Traction dynamics of filopodia on compliant substrates. *Science,* 322**,** 1687-91.

CHEN, T. W., WARDILL, T. J., SUN, Y., PULVER, S. R., RENNINGER, S. L., BAOHAN, A., SCHREITER, E. R., KERR, R. A., ORGER, M. B., JAYARAMAN, V., LOOGER, L. L., SVOBODA, K. & KIM, D. S. 2013. Ultrasensitive fluorescent proteins for imaging neuronal activity. *Nature,* 499**,** 295-300.

CHUNG, K. & DEISSEROTH, K. 2013. CLARITY for mapping the nervous system. *Nat Methods,* 10**,** 508-13.

CLEVERS, H. 2016. Modeling Development and Disease with Organoids. *Cell,* 165**,** 1586-1597.

CONN, P. J. & KACZMAREK, L. K. 1989. The bag cell neurons of Aplysia. A model for the study of the molecular mechanisms involved in the control of prolonged animal behaviors. *Mol Neurobiol,* 3**,** 237-73.

COSEN-BINKER, L. I. & KAPUS, A. 2006. Cortactin: the gray eminence of the cytoskeleton. *Physiology (Bethesda),* 21**,** 352-61.

COWIESON, N. P., KING, G., COOKSON, D., ROSS, I., HUBER, T., HUME, D. A., KOBE, B. & MARTIN, J. L. 2008. Cortactin adopts a globular conformation and bundles actin into sheets. *J Biol Chem,* 283**,** 16187-93.

DAETWYLER, S. & HUISKEN, J. 2016. Fast Fluorescence Microscopy with Light Sheets. *Biol Bull,* 231**,** 14-25.

DAVENPORT, R. W., DOU, P., REHDER, V. & KATER, S. B. 1993. A sensory role for neuronal growth cone filopodia. *Nature,* 361**,** 721-4.

DAVIDSON, A. J. & WOOD, W. 2016. Unravelling the Actin Cytoskeleton: A New Competitive Edge? *Trends Cell Biol,* 26**,** 569-76.

DECOURT, B., MUNNAMALAI, V., LEE, A. C., SANCHEZ, L. & SUTER, D. M. 2009. Cortactin colocalizes with filopodial actin and accumulates at IgCAM adhesion sites in Aplysia growth cones. *J Neurosci Res,* 87**,** 1057-68.

DENT, E. W. & GERTLER, F. B. 2003. Cytoskeletal dynamics and transport in growth cone motility and axon guidance. *Neuron,* 40**,** 209-27.

DENT, E. W., GUPTON, S. L. & GERTLER, F. B. 2011. The growth cone cytoskeleton in axon outgrowth and guidance. *Cold Spring Harb Perspect Biol,* 3.

DENT, E. W., TANG, F. & KALIL, K. 2003. Axon guidance by growth cones and branches: common cytoskeletal and signaling mechanisms. *Neuroscientist,* 9**,** 343-53.

DESAI, A., KISAALITA, W. S., KEITH, C. & WU, Z. Z. 2006. Human neuroblastoma (SH-SY5Y) cell culture and differentiation in 3-D collagen hydrogels for cell-based biosensing. *Biosens Bioelectron,* 21**,** 1483-92.

DEWARD, A. D., EISENMANN, K. M., MATHESON, S. F. & ALBERTS, A. S. 2010. The role of formins in human disease. *Biochim Biophys Acta,* 1803**,** 226-33.

DI CIANO, C., NIE, Z., SZASZI, K., LEWIS, A., URUNO, T., ZHAN, X., ROTSTEIN, O. D., MAK, A. & KAPUS, A. 2002. Osmotic stress-induced remodeling of the cortical cytoskeleton. *Am J Physiol Cell Physiol,* 283**,** C850-65.

DOMINGUEZ, R. & HOLMES, K. C. 2011. Actin structure and function. *Annu Rev Biophys,* 40**,** 169-86.

DOTTI, C. G., SULLIVAN, C. A. & BANKER, G. A. 1988. The establishment of polarity by hippocampal neurons in culture. *J Neurosci,* 8**,** 1454-68.

ENGLE, E. C. 2010. Human genetic disorders of axon guidance. *Cold Spring Harb Perspect Biol,* 2**,** a001784.

EVANS, J. V., AMMER, A. G., JETT, J. E., BOLCATO, C. A., BREAUX, J. C., MARTIN, K. H., CULP, M. V., GANNETT, P. M. & WEED, S. A. 2012. Src binds cortactin through an SH2 domain cystine-mediated linkage. *J Cell Sci,* 125**,** 6185-97.

FAIX, J. & ROTTNER, K. 2006. The making of filopodia. *Curr Opin Cell Biol,* 18**,** 18-25.

FAN, L., DI CIANO-OLIVEIRA, C., WEED, S. A., CRAIG, A. W., GREER, P. A., ROTSTEIN, O. D. & KAPUS, A. 2004. Actin depolymerization-induced tyrosine phosphorylation of cortactin: the role of Fer kinase. *Biochem J,* 380**,** 581-91.

FERGUSON, S. M. & DE CAMILLI, P. 2012. Dynamin, a membrane-remodelling GTPase. *Nat Rev Mol Cell Biol,* 13**,** 75-88.

FORSCHER, P. & SMITH, S. J. 1988. Actions of cytochalasins on the organization of actin filaments and microtubules in a neuronal growth cone. *J Cell Biol,* 107**,** 1505-16.

GALLO, G. 2013. Mechanisms underlying the initiation and dynamics of neuronal filopodia: from neurite formation to synaptogenesis. *Int Rev Cell Mol Biol,* 301**,** 95-156.

GEORGES, P. C., MILLER, W. J., MEANEY, D. F., SAWYER, E. S. & JANMEY, P. A. 2006. Matrices with compliance comparable to that of brain tissue select neuronal over glial growth in mixed cortical cultures. *Biophys J,* 90**,** 3012-8.

GERALDO, S. & GORDON-WEEKS, P. R. 2009. Cytoskeletal dynamics in growth-cone steering. *J Cell Sci,* 122**,** 3595-604.

GOLDBERG, D. J. & BURMEISTER, D. W. 1986. Stages in axon formation: observations of growth of Aplysia axons in culture using video-enhanced contrast-differential interference contrast microscopy. *J Cell Biol,* 103**,** 1921-31.

GOLEY, E. D. & WELCH, M. D. 2006. The ARP2/3 complex: an actin nucleator comes of age. *Nat Rev Mol Cell Biol,* 7**,** 713-26.

GONCALVES-PIMENTEL, C., GOMBOS, R., MIHALY, J., SANCHEZ-SORIANO, N. & PROKOP, A. 2011. Dissecting regulatory networks of filopodia formation in a Drosophila growth cone model. *PLoS One,* 6**,** e18340.

GOODHILL, G. J., FAVILLE, R. A., SUTHERLAND, D. J., BICKNELL, B. A., THOMPSON, A. W., PUJIC, Z., SUN, B., KITA, E. M. & SCOTT, E. K. 2015. The dynamics of growth cone morphology. *BMC Biol,* 13**,** 10.

GRZYWA, E. L., LEE, A. C., LEE, G. U. & SUTER, D. M. 2006. High-resolution analysis of neuronal growth cone morphology by comparative atomic force and optical microscopy. *J Neurobiol,* 66**,** 1529-43.

GU, C., YADDANAPUDI, S., WEINS, A., OSBORN, T., REISER, J., POLLAK, M., HARTWIG, J. & SEVER, S. 2010. Direct dynamin-actin interactions regulate the actin cytoskeleton. *EMBO J,* 29**,** 3593-606.

GUETTA-TERRIER, C., MONZO, P., ZHU, J., LONG, H., VENKATRAMAN, L., ZHOU, Y., WANG, P., CHEW, S. Y., MOGILNER, A., LADOUX, B. & GAUTHIER, N. C. 2015. Protrusive waves guide 3D cell migration along nanofibers. *J Cell Biol,* 211**,** 683-701.

HATCHER, N. G. & SWEEDLER, J. V. 2008. Aplysia bag cells function as a distributed neurosecretory network. *J Neurophysiol,* 99**,** 333-43.

HE, Y., REN, Y., WU, B., DECOURT, B., LEE, A. C., TAYLOR, A. & SUTER, D. M. 2015. Src and cortactin promote lamellipodia protrusion and filopodia formation and stability in growth cones. *Mol Biol Cell,* 26**,** 3229-44.

HEAD, J. A., JIANG, D., LI, M., ZORN, L. J., SCHAEFER, E. M., PARSONS, J. T. & WEED, S. A. 2003. Cortactin tyrosine phosphorylation requires Rac1 activity and association with the cortical actin cytoskeleton. *Mol Biol Cell,* 14**,** 3216-29.

HEILEMANN, M., VAN DE LINDE, S., SCHUTTPELZ, M., KASPER, R., SEEFELDT, B., MUKHERJEE, A., TINNEFELD, P. & SAUER, M. 2008. Subdiffraction-resolution fluorescence imaging with conventional fluorescent probes. *Angew Chem Int Ed Engl,* 47**,** 6172-6.

HELGESON, L. A. & NOLEN, B. J. 2013. Mechanism of synergistic activation of Arp2/3 complex by cortactin and N-WASP. *Elife,* 2**,** e00884.

HELGESON, L. A., PRENDERGAST, J. G., WAGNER, A. R., RODNICK-SMITH, M. & NOLEN, B. J. 2014. Interactions with actin monomers, actin filaments, and Arp2/3 complex define the roles of WASP family proteins and cortactin in coordinately regulating branched actin networks. *J Biol Chem,* 289**,** 28856-69.

HERING, H. & SHENG, M. 2003. Activity-dependent redistribution and essential role of cortactin in dendritic spine morphogenesis. *J Neurosci,* 23**,** 11759-69.

HOLT, C. E. 1989. A single-cell analysis of early retinal ganglion cell differentiation in Xenopus: from soma to axon tip. *J Neurosci,* 9**,** 3123-45.

HOUDUSSE, A. & SWEENEY, H. L. 2016. How Myosin Generates Force on Actin Filaments. *Trends Biochem Sci,* 41**,** 989-997.

HOYE, A. M., COUCHMAN, J. R., WEWER, U. M. & YONEDA, A. 2016. The Phosphorylation and Distribution of Cortactin Downstream of Integrin alpha9beta1 Affects Cancer Cell Behaviour. *Sci Rep,* 6**,** 28529.

HUANG, B., JONES, S. A., BRANDENBURG, B. & ZHUANG, X. 2008. Whole-cell 3D STORM reveals interactions between cellular structures with nanometer-scale resolution. *Nat Methods,* 5**,** 1047-52.

HUANG, C., NI, Y., WANG, T., GAO, Y., HAUDENSCHILD, C. C. & ZHAN, X. 1997. Down-regulation of the filamentous actin cross-linking activity of cortactin by Src-mediated tyrosine phosphorylation. *J Biol Chem,* 272**,** 13911-5.

HUANG, F., HARTWICH, T. M., RIVERA-MOLINA, F. E., LIN, Y., DUIM, W. C., LONG, J. J., UCHIL, P. D., MYERS, J. R., BAIRD, M. A., MOTHES, W., DAVIDSON, M. W., TOOMRE, D. & BEWERSDORF, J. 2013. Video-rate nanoscopy using sCMOS camera-specific single-molecule localization algorithms. *Nat Methods,* 10**,** 653-8.

HUANG, F., SIRINAKIS, G., ALLGEYER, E. S., SCHROEDER, L. K., DUIM, W. C., KROMANN, E. B., PHAN, T., RIVERA-MOLINA, F. E., MYERS, J. R., IRNOV, I., LESSARD, M., ZHANG, Y., HANDEL, M. A., JACOBS-WAGNER, C., LUSK, C. P., ROTHMAN, J. E., TOOMRE, D., BOOTH, M. J. & BEWERSDORF, J. 2016. Ultra-High Resolution 3D Imaging of Whole Cells. *Cell,* 166**,** 1028-1040.

HUISKEN, J., SWOGER, J., DEL BENE, F., WITTBRODT, J. & STELZER, E. H. 2004. Optical sectioning deep inside live embryos by selective plane illumination microscopy. *Science,* 305**,** 1007-9.

HUR, E. M., SAIJILAFU & ZHOU, F. Q. 2012. Growing the growth cone: remodeling the cytoskeleton to promote axon regeneration. *Trends Neurosci,* 35**,** 164-74.

HUTSON, L. D. & CHIEN, C. B. 2002. Pathfinding and error correction by retinal axons: the role of astray/robo2. *Neuron,* 33**,** 205-17.

HYLAND, C., DUFRESNE, E. R. & FORSCHER, P. 2014a. Regeneration of Aplysia bag cell neurons is synergistically enhanced by substrate-bound hemolymph proteins and laminin. *Sci Rep,* 4**,** 4617.

HYLAND, C., MERTZ, A. F., FORSCHER, P. & DUFRESNE, E. 2014b. Dynamic peripheral traction forces balance stable neurite tension in regenerating Aplysia bag cell neurons. *Sci Rep,* 4**,** 4961.

JACQUEMET, G., HAMIDI, H. & IVASKA, J. 2015. Filopodia in cell adhesion, 3D migration and cancer cell invasion. *Curr Opin Cell Biol,* 36**,** 23-31.

JANG, K. J., KIM, M. S., FELTRIN, D., JEON, N. L., SUH, K. Y. & PERTZ, O. 2010. Two distinct filopodia populations at the growth cone allow to sense nanotopographical extracellular matrix cues to guide neurite outgrowth. *PLoS One,* 5**,** e15966.

JANSEN, S., COLLINS, A., YANG, C., REBOWSKI, G., SVITKINA, T. & DOMINGUEZ, R. 2011. Mechanism of actin filament bundling by fascin. *J Biol Chem,* 286**,** 30087-96.

JOHNSON, B. N., LANCASTER, K. Z., HOGUE, I. B., MENG, F., KONG, Y. L., ENQUIST, L. W. & MCALPINE, M. C. 2016. 3D printed nervous system on a chip. *Lab Chip,* 16**,** 1393-400.

JUETTE, M. F., GOULD, T. J., LESSARD, M. D., MLODZIANOSKI, M. J., NAGPURE, B. S., BENNETT, B. T., HESS, S. T. & BEWERSDORF, J. 2008. Three-dimensional sub-100 nm resolution fluorescence microscopy of thick samples. *Nat Methods,* 5**,** 527-9.

KACZMAREK, L. K., FINBOW, M., REVEL, J. P. & STRUMWASSER, F. 1979. The morphology and coupling of Aplysia bag cells within the abdominal ganglion and in cell culture. *J Neurobiol,* 10**,** 535-50.

KERSTEIN, P. C., NICHOL, R. I. & GOMEZ, T. M. 2015. Mechanochemical regulation of growth cone motility. *Front Cell Neurosci,* 9**,** 244.

KINLEY, A. W., WEED, S. A., WEAVER, A. M., KARGINOV, A. V., BISSONETTE, E., COOPER, J. A. & PARSONS, J. T. 2003. Cortactin interacts with WIP in regulating Arp2/3 activation and membrane protrusion. *Curr Biol,* 13**,** 384-93.

KNOLL, B. & DRESCHER, U. 2004. Src family kinases are involved in EphA receptor-mediated retinal axon guidance. *J Neurosci,* 24**,** 6248-57.

KOROBOVA, F. & SVITKINA, T. 2008. Arp2/3 complex is important for filopodia formation, growth cone motility, and neuritogenesis in neuronal cells. *Mol Biol Cell,* 19**,** 1561-74.

KRUEGER, E. W., ORTH, J. D., CAO, H. & MCNIVEN, M. A. 2003. A dynamin-cortactin-Arp2/3 complex mediates actin reorganization in growth factor-stimulated cells. *Mol Biol Cell,* 14**,** 1085-96.

KUPFERMANN, I. & CAREW, T. J. 1974. Behavior patterns of Aplysia californica in its natural environment. *Behav Biol,* 12**,** 317-37.

KUPFERMANN, I. & KANDEL, E. R. 1970. Electrophysiological properties and functional interconnections of two symmetrical neurosecretory clusters (bag cells) in abdominal ganglion of Aplysia. *J Neurophysiol,* 33**,** 865-76.

LAI, F. P., SZCZODRAK, M., OELKERS, J. M., LADWEIN, M., ACCONCIA, F., BENESCH, S., AUINGER, S., FAIX, J., SMALL, J. V., POLO, S., STRADAL, T. E. & ROTTNER, K. 2009. Cortactin promotes migration and platelet-derived growth factor-induced actin reorganization by signaling to Rho-GTPases. *Mol Biol Cell,* 20**,** 3209-23.

LAI, Y., CHENG, K. & KISAALITA, W. 2012. Three dimensional neuronal cell cultures more accurately model voltage gated calcium channel functionality in freshly dissected nerve tissue. *PLoS One,* 7**,** e45074.

LEE, A. C., DECOURT, B. & SUTER, D. 2008a. Neuronal cell cultures from aplysia for high-resolution imaging of growth cones. *J Vis Exp*.

LEE, A. C. & SUTER, D. M. 2008. Quantitative analysis of microtubule dynamics during adhesion-mediated growth cone guidance. *Dev Neurobiol,* 68**,** 1363-77.

LEE, J., CUDDIHY, M. J. & KOTOV, N. A. 2008b. Three-dimensional cell culture matrices: state of the art. *Tissue Eng Part B Rev,* 14**,** 61-86.

LEE, Y. S., COLLINS, G. & ARINZEH, T. L. 2011. Neurite extension of primary neurons on electrospun piezoelectric scaffolds. *Acta Biomater,* 7**,** 3877-86.

LEWIS, A. K. & BRIDGMAN, P. C. 1992. Nerve growth cone lamellipodia contain two populations of actin filaments that differ in organization and polarity. *J Cell Biol,* 119**,** 1219-43.

LI, G. N., LIVI, L. L., GOURD, C. M., DEWEERD, E. S. & HOFFMAN-KIM, D. 2007. Genomic and morphological changes of neuroblastoma cells in response to three-dimensional matrices. *Tissue Eng,* 13**,** 1035-47.

LIN, C. H., ESPREAFICO, E. M., MOOSEKER, M. S. & FORSCHER, P. 1996. Myosin drives retrograde F-actin flow in neuronal growth cones. *Neuron,* 16**,** 769-82.

LIN, C. H. & FORSCHER, P. 1995. Growth cone advance is inversely proportional to retrograde F-actin flow. *Neuron,* 14**,** 763-71.

LIU, J., HUANG, C. & ZHAN, X. 1999. Src is required for cell migration and shape changes induced by fibroblast growth factor 1. *Oncogene,* 18**,** 6700-6.

LOWERY, L. A. & VAN VACTOR, D. 2009. The trip of the tip: understanding the growth cone machinery. *Nat Rev Mol Cell Biol,* 10**,** 332-43.

LUA, B. L. & LOW, B. C. 2005. Cortactin phosphorylation as a switch for actin cytoskeletal network and cell dynamics control. *FEBS Lett,* 579**,** 577-85.

LUO, Y. & SHOICHET, M. S. 2004. A photolabile hydrogel for guided three-dimensional cell growth and migration. *Nat Mater,* 3**,** 249-53.

MACGRATH, S. M. & KOLESKE, A. J. 2012. Cortactin in cell migration and cancer at a glance. *J Cell Sci,* 125**,** 1621-6.

MAGALHAES, M. A., LARSON, D. R., MADER, C. C., BRAVO-CORDERO, J. J., GIL-HENN, H., OSER, M., CHEN, X., KOLESKE, A. J. & CONDEELIS, J. 2011. Cortactin phosphorylation regulates cell invasion through a pH-dependent pathway. *J Cell Biol,* 195**,** 903-20.

MAHAJAN, S. & ATHALE, C. A. 2012. Spatial and temporal sensing limits of microtubule polarization in neuronal growth cones by intracellular gradients and forces. *Biophys J,* 103**,** 2432-45.

MALLAVARAPU, A. & MITCHISON, T. 1999. Regulated actin cytoskeleton assembly at filopodium tips controls their extension and retraction. *J Cell Biol,* 146**,** 1097-106.

MARTINEZ-QUILES, N., HO, H. Y., KIRSCHNER, M. W., RAMESH, N. & GEHA, R. S. 2004. Erk/Src phosphorylation of cortactin acts as a switch on-switch off mechanism that controls its ability to activate N-WASP. *Mol Cell Biol,* 24**,** 5269-80.

MARTINEZ-QUILES, N., ROHATGI, R., ANTON, I. M., MEDINA, M., SAVILLE, S. P., MIKI, H., YAMAGUCHI, H., TAKENAWA, T., HARTWIG, J. H., GEHA, R. S. & RAMESH, N. 2001. WIP regulates N-WASP-mediated actin polymerization and filopodium formation. *Nat Cell Biol,* 3**,** 484-91.

MASON, C. A. & WANG, L. C. 1997. Growth cone form is behavior-specific and, consequently, position-specific along the retinal axon pathway. *J Neurosci,* 17**,** 1086-100.

MATTILA, P. K. & LAPPALAINEN, P. 2008. Filopodia: molecular architecture and cellular functions. *Nat Rev Mol Cell Biol,* 9**,** 446-54.

MCCONNELL, R. E., EDWARD VAN VEEN, J., VIDAKI, M., KWIATKOWSKI, A. V., MEYER, A. S. & GERTLER, F. B. 2016. A requirement for filopodia extension toward Slit during Robo-mediated axon repulsion. *J Cell Biol,* 213**,** 261-74.

MEJEAN, C. O., SCHAEFER, A. W., BUCK, K. B., KRESS, H., SHUNDROVSKY, A., MERRILL, J. W., DUFRESNE, E. R. & FORSCHER, P. 2013. Elastic coupling of nascent apCAM adhesions to flowing actin networks. *PLoS One,* 8**,** e73389.

MELLOR, H. 2010. The role of formins in filopodia formation. *Biochim Biophys Acta,* 1803**,** 191-200.

MITCHISON, T. J. & CRAMER, L. P. 1996. Actin-based cell motility and cell locomotion. *Cell,* 84**,** 371-9.

MOGILNER, A. & RUBINSTEIN, B. 2005. The physics of filopodial protrusion. *Biophys J,* 89**,** 782-95.

MOROZ, L. L. 2011. Aplysia. *Curr Biol,* 21**,** R60-1.

NAVRATIL, A. M., DOZIER, M. G., WHITESELL, J. D., CLAY, C. M. & ROBERSON, M. S. 2014. Role of cortactin in dynamic actin remodeling events in gonadotrope cells. *Endocrinology,* 155**,** 548-57.

NICK, T. A., KACZMAREK, L. K. & CAREW, T. J. 1996a. Ionic currents underlying developmental regulation of repetitive firing in Aplysia bag cell neurons. *J Neurosci,* 16**,** 7583-98.

NICK, T. A., MOREIRA, J. E., KACZMAREK, L. K., CAREW, T. J. & WAYNE, N. L. 1996b. Developmental dissociation of excitability and secretory ability in Aplysia bag cell neurons. *J Neurophysiol,* 76**,** 3351-9.

NIETO-PELEGRIN, E. & MARTINEZ-QUILES, N. 2009. Distinct phosphorylation requirements regulate cortactin activation by TirEPEC and its binding to N-WASP. *Cell Commun Signal,* 7**,** 11.

O'CONNOR, T. P. & BENTLEY, D. 1993. Accumulation of actin in subsets of pioneer growth cone filopodia in response to neural and epithelial guidance cues in situ. *J Cell Biol,* 123**,** 935-48.

OLAZABAL, I. M. & MACHESKY, L. M. 2001. Abp1p and cortactin, new "hand-holds" for actin. *J Cell Biol,* 154**,** 679-82.

OMOTADE, O. F., POLLITT, S. L. & ZHENG, J. Q. 2017. Actin-based growth cone motility and guidance. *Mol Cell Neurosci,* 84**,** 4-10.

OSER, M., MADER, C. C., GIL-HENN, H., MAGALHAES, M., BRAVO-CORDERO, J. J., KOLESKE, A. J. & CONDEELIS, J. 2010. Specific tyrosine phosphorylation sites on cortactin regulate Nck1-dependent actin polymerization in invadopodia. *J Cell Sci,* 123**,** 3662-73.

OSER, M., YAMAGUCHI, H., MADER, C. C., BRAVO-CORDERO, J. J., ARIAS, M., CHEN, X., DESMARAIS, V., VAN RHEENEN, J., KOLESKE, A. J. & CONDEELIS, J. 2009.

Cortactin regulates cofilin and N-WASp activities to control the stages of invadopodium assembly and maturation. *J Cell Biol,* 186**,** 571-87.

PARK, J. H., SUN, W. & CUI, M. 2015. High-resolution in vivo imaging of mouse brain through the intact skull. *Proc Natl Acad Sci U S A,* 112**,** 9236-41.

PARSONS, S. J. & PARSONS, J. T. 2004. Src family kinases, key regulators of signal transduction. *Oncogene,* 23**,** 7906-9.

PHILLIPS, M. J. & OTTESON, D. C. 2011. Differential expression of neuronal genes in Muller glia in two- and three-dimensional cultures. *Invest Ophthalmol Vis Sci,* 52**,** 1439-49.

PINSKER, H., KUPFERMANN, I., CASTELLUCCI, V. & KANDEL, E. 1970. Habituation and dishabituation of the gill-withdrawal reflex in Aplysia. *Science,* 167**,** 1740-2.

POLLARD, T. D. 1986. Rate constants for the reactions of ATP- and ADP-actin with the ends of actin filaments. *J Cell Biol,* 103**,** 2747-54.

PRAGER-KHOUTORSKY, M. & SPIRA, M. E. 2009. Neurite retraction and regrowth regulated by membrane retrieval, membrane supply, and actin dynamics. *Brain Res,* 1251**,** 65-79.

RADHAKRISHNAN, V. M., KOJS, P., YOUNG, G., RAMALINGAM, R., JAGADISH, B., MASH, E. A., MARTINEZ, J. D., GHISHAN, F. K. & KIELA, P. R. 2014. pTyr421 cortactin is overexpressed in colon cancer and is dephosphorylated by curcumin: involvement of non-receptor type 1 protein tyrosine phosphatase (PTPN1). *PLoS One,* 9**,** e85796.

REN, X. L., QIAO, Y. D., LI, J. Y., LI, X. M., ZHANG, D., ZHANG, X. J., ZHU, X. H., ZHOU, W. J., SHI, J., WANG, W., LIAO, W. T., DING, Y. Q. & LIANG, L. 2018. Cortactin recruits FMNL2 to promote actin polymerization and endosome motility in invadopodia formation. *Cancer Lett,* 419**,** 245-256.

ROBLES, E., WOO, S. & GOMEZ, T. M. 2005. Src-dependent tyrosine phosphorylation at the tips of growth cone filopodia promotes extension. *J Neurosci,* 25**,** 7669-81.

ROCHLIN, M. W., DAILEY, M. E. & BRIDGMAN, P. C. 1999. Polymerizing microtubules activate site-directed F-actin assembly in nerve growth cones. *Mol Biol Cell,* 10**,** 2309-27.

ROSKOSKI, R., JR. 2004. Src protein-tyrosine kinase structure and regulation. *Biochem Biophys Res Commun,* 324**,** 1155-64.

SABRY, J. H., O'CONNOR, T. P., EVANS, L., TOROIAN-RAYMOND, A., KIRSCHNER, M. & BENTLEY, D. 1991. Microtubule behavior during guidance of pioneer neuron growth cones in situ. *J Cell Biol,* 115**,** 381-95.

SCHAEFER, A. W., KABIR, N. & FORSCHER, P. 2002. Filopodia and actin arcs guide the assembly and transport of two populations of microtubules with unique dynamic parameters in neuronal growth cones. *J Cell Biol,* 158**,** 139-52.

SCHAEFER, A. W., SCHOONDERWOERT, V. T., JI, L., MEDERIOS, N., DANUSER, G. & FORSCHER, P. 2008. Coordination of actin filament and microtubule dynamics during neurite outgrowth. *Dev Cell,* 15**,** 146-62.

SCHNOOR, M., STRADAL, T. E. & ROTTNER, K. 2018. Cortactin: Cell Functions of A Multifaceted Actin-Binding Protein. *Trends Cell Biol,* 28**,** 79-98.

SITON, O., IDESES, Y., ALBECK, S., UNGER, T., BERSHADSKY, A. D., GOV, N. S. & BERNHEIM-GROSWASSER, A. 2011. Cortactin releases the brakes in actin- based motility by enhancing WASP-VCA detachment from Arp2/3 branches. *Curr Biol,* 21**,** 2092-7.

SMALL, J. V., STRADAL, T., VIGNAL, E. & ROTTNER, K. 2002. The lamellipodium: where motility begins. *Trends Cell Biol,* 12**,** 112-20.

STARNES, T. W., BENNIN, D. A., BING, X., EICKHOFF, J. C., GRAHF, D. C., BELLAK, J. M., SEROOGY, C. M., FERGUSON, P. J. & HUTTENLOCHER, A. 2014. The F-BAR protein PSTPIP1 controls extracellular matrix degradation and filopodia formation in macrophages. *Blood,* 123**,** 2703-14.

SUETSUGU, S. 2013. Activation of nucleation promoting factors for directional actin filament elongation: allosteric regulation and multimerization on the membrane. *Semin Cell Dev Biol,* 24**,** 267-71.

SUTER, D. M. 2011. Live cell imaging of neuronal growth cone motility and guidance in vitro. *Methods Mol Biol,* 769**,** 65-86.

SUTER, D. M., ERRANTE, L. D., BELOTSERKOVSKY, V. & FORSCHER, P. 1998. The Ig superfamily cell adhesion molecule, apCAM, mediates growth cone steering by substrate-cytoskeletal coupling. *J Cell Biol,* 141**,** 227-40.

SUTER, D. M. & FORSCHER, P. 1998. An emerging link between cytoskeletal dynamics and cell adhesion molecules in growth cone guidance. *Curr Opin Neurobiol,* 8**,** 106-16.

SUTER, D. M. & FORSCHER, P. 2001. Transmission of growth cone traction force through apCAM-cytoskeletal linkages is regulated by Src family tyrosine kinase activity. *J Cell Biol,* 155**,** 427-38.

SUTER, D. M., SCHAEFER, A. W. & FORSCHER, P. 2004. Microtubule dynamics are necessary for SRC family kinase-dependent growth cone steering. *Curr Biol,* 14**,** 1194-9.

SVITKINA, T. 2018. The Actin Cytoskeleton and Actin-Based Motility. *Cold Spring Harb Perspect Biol,* 10.

SVITKINA, T. M., BULANOVA, E. A., CHAGA, O. Y., VIGNJEVIC, D. M., KOJIMA, S., VASILIEV, J. M. & BORISY, G. G. 2003. Mechanism of filopodia initiation by reorganization of a dendritic network. *J Cell Biol,* 160**,** 409-21.

TEHRANI, S., TOMASEVIC, N., WEED, S., SAKOWICZ, R. & COOPER, J. A. 2007. Src phosphorylation of cortactin enhances actin assembly. *Proc Natl Acad Sci U S A,* 104**,** 11933-8.

THOMPSON, C., LIN, C. H. & FORSCHER, P. 1996. An Aplysia cell adhesion molecule associated with site-directed actin filament assembly in neuronal growth cones. *J Cell Sci,* 109 (Pt 12)**,** 2843-54.

URIBE, R. & JAY, D. 2009. A review of actin binding proteins: new perspectives. *Mol Biol Rep,* 36**,** 121-5.

URUNO, T., LIU, J., ZHANG, P., FAN, Y., EGILE, C., LI, R., MUELLER, S. C. & ZHAN, X. 2001. Activation of Arp2/3 complex-mediated actin polymerization by cortactin. *Nat Cell Biol,* 3**,** 259-66.

VAN DAMME, H., BROK, H., SCHUURING-SCHOLTES, E. & SCHUURING, E. 1997. The redistribution of cortactin into cell-matrix contact sites in human carcinoma cells with 11q13 amplification is associated with both overexpression and post-translational modification. *J Biol Chem,* 272**,** 7374-80.

VITRIOL, E. A. & ZHENG, J. Q. 2012. Growth cone travel in space and time: the cellular ensemble of cytoskeleton, adhesion, and membrane. *Neuron,* 73**,** 1068-81.

WAYNE, N. L., KIM, Y. J. & YONG-MONTENEGRO, R. J. 1998. Seasonal fluctuations in the secretory response of neuroendocrine cells of Aplysia californica to inhibitors of protein kinase A and protein kinase C. *Gen Comp Endocrinol,* 109**,** 356-65.

WEAVER, A. M., KARGINOV, A. V., KINLEY, A. W., WEED, S. A., LI, Y., PARSONS, J. T. & COOPER, J. A. 2001. Cortactin promotes and stabilizes Arp2/3-induced actin filament network formation. *Curr Biol,* 11**,** 370-4.

WEED, S. A., KARGINOV, A. V., SCHAFER, D. A., WEAVER, A. M., KINLEY, A. W., COOPER, J. A. & PARSONS, J. T. 2000. Cortactin localization to sites of actin assembly in lamellipodia requires interactions with F-actin and the Arp2/3 complex. *J Cell Biol,* 151**,** 29-40.

WEED, S. A. & PARSONS, J. T. 2001. Cortactin: coupling membrane dynamics to cortical actin assembly. *Oncogene,* 20**,** 6418-34.

WEIDMANN, M. D., SURVE, C. R., EDDY, R. J., CHEN, X., GERTLER, F. B., SHARMA, V. P. & CONDEELIS, J. S. 2016. Mena(INV) dysregulates cortactin phosphorylation to promote invadopodium maturation. *Sci Rep,* 6**,** 36142.

WHITE, B. H., NICK, T. A., CAREW, T. J. & KACZMAREK, L. K. 1998. Protein kinase C regulates a vesicular class of calcium channels in the bag cell neurons of aplysia. *J Neurophysiol,* 80**,** 2514-20.

WILLIAMS, D. K. & COHAN, C. S. 1994. The role of conditioning factors in the formation of growth cones and neurites from the axon stump after axotomy. *Brain Res Dev Brain Res,* 81**,** 89-104.

WINCKLER, B., FORSCHER, P. & MELLMAN, I. 1999. A diffusion barrier maintains distribution of membrane proteins in polarized neurons. *Nature,* 397**,** 698-701.

WU, B., DECOURT, B., ZABIDI, M. A., WUETHRICH, L. T., KIM, W. H., ZHOU, Z., MACISAAC, K. & SUTER, D. M. 2008. Microtubule-mediated Src tyrosine kinase trafficking in neuronal growth cones. *Mol Biol Cell,* 19**,** 4611-27.

WU, D. Y., WANG, L. C., MASON, C. A. & GOLDBERG, D. J. 1996. Association of beta 1 integrin with phosphotyrosine in growth cone filopodia. *J Neurosci,* 16**,** 1470-8.

WU, H. & PARSONS, J. T. 1993. Cortactin, an 80/85-kilodalton pp60src substrate, is a filamentous actin-binding protein enriched in the cell cortex. *J Cell Biol,* 120**,** 1417-26.

XIONG, Y., LEE, A. C., SUTER, D. M. & LEE, G. U. 2009. Topography and nanomechanics of live neuronal growth cones analyzed by atomic force microscopy. *Biophys J,* 96**,** 5060-72.

YAMADA, H., ABE, T., SATOH, A., OKAZAKI, N., TAGO, S., KOBAYASHI, K., YOSHIDA, Y., ODA, Y., WATANABE, M., TOMIZAWA, K., MATSUI, H. & TAKEI, K. 2013. Stabilization of actin bundles by a dynamin 1/cortactin ring complex is necessary for growth cone filopodia. *J Neurosci,* 33**,** 4514-26.

YAMADA, H., TAKEDA, T., MICHIUE, H., ABE, T. & TAKEI, K. 2016. Actin bundling by dynamin 2 and cortactin is implicated in cell migration by stabilizing filopodia in human non-small cell lung carcinoma cells. *Int J Oncol,* 49**,** 877-86.

YAN, W., LIU, W., QI, J., FANG, Q., FAN, Z., SUN, G., HAN, Y., ZHANG, D., XU, L., WANG, M., LI, J., CHEN, F., LIU, D., CHAI, R. & WANG, H. 2017. A Three-Dimensional Culture System with Matrigel Promotes Purified Spiral Ganglion Neuron Survival and Function In Vitro. *Mol Neurobiol*.

YANG, Q., ZHANG, X. F., POLLARD, T. D. & FORSCHER, P. 2012. Arp2/3 complex-dependent actin networks constrain myosin II function in driving retrograde actin flow. *J Cell Biol,* 197**,** 939-56.

YANG, Q., ZHANG, X. F., VAN GOOR, D., DUNN, A. P., HYLAND, C., MEDEIROS, N. & FORSCHER, P. 2013. Protein kinase C activation decreases peripheral actin network density and increases central nonmuscle myosin II contractility in neuronal growth cones. *Mol Biol Cell,* 24**,** 3097-114.

YIN, M., MA, W. & AN, L. 2017. Cortactin in cancer cell migration and invasion. *Oncotarget,* 8**,** 88232-88243.

ZHANG, X., YUAN, Z., ZHANG, Y., YONG, S., SALAS-BURGOS, A., KOOMEN, J., OLASHAW, N., PARSONS, J. T., YANG, X. J., DENT, S. R., YAO, T. P., LANE, W. S. & SETO, E. 2007. HDAC6 modulates cell motility by altering the acetylation level of cortactin. *Mol Cell,* 27**,** 197-213.

ZHAO, J., WEI, J., MIALKI, R., ZOU, C., MALLAMPALLI, R. K. & ZHAO, Y. 2012. Extracellular signal-regulated kinase (ERK) regulates cortactin ubiquitination and degradation in lung epithelial cells. *J Biol Chem,* 287**,** 19105-14.

ZHAO, Y., WANG, D. O. & MARTIN, K. C. 2009. Preparation of Aplysia sensory-motor neuronal cell cultures. *J Vis Exp*.

ZHOU, F. Q., WATERMAN-STORER, C. M. & COHAN, C. S. 2002. Focal loss of actin bundles causes microtubule redistribution and growth cone turning. *J Cell Biol,* 157**,** 839-49.

ZHU, J., ZHOU, K., HAO, J. J., LIU, J., SMITH, N. & ZHAN, X. 2005. Regulation of cortactin/dynamin interaction by actin polymerization during the fission of clathrin-coated pits. *J Cell Sci,* 118**,** 807-17.

VITA

Education

2012-present PhD. candidate in Neuroscience, Purdue University. Advisor: Dr. Daniel Suter

2012 M.S. in Cell Biology, Nankai University, Tianjin, China. Advisor: Dr. Jun Zhou

2009 B.S. in Biochemistry and Molecular Biology, Honors Program
China Agricultural University, Beijing, China

Research Experience

2012-present Department of Biological Sciences, Purdue University

I study how a tyrosine kinase (Src2) and its substrate (cortactin) regulate the motility of neuronal growth cones by altering actin organization and dynamics. I also developed novel three-dimensional (3D) culture systems for *Aplysia* bag cell neurons.

2009-2012 Department of Cell Biology and Genetics, Nankai University

I participated in multiple projects looking into the role of microtubule binding proteins in development and disease. For my thesis, I studied angiogenesis using epithelial cells and chick embryo, and did tumor angiogenesis studies in transgenic mice. Co-advisor: Dr. Dengwen Li.

2008-2009 Laboratory of Cytoskeleton and Signal Transduction, Tsinghua University

I characterized flagella defects after silencing a novel gene in green algae *Chlamydomonas reinhardtii*. Advisor: Dr. Junmin Pan.

Professional course

2017 Physical biology of the cell. Marine Biological Laboratory. Woods Hole, MA
Directors: Dr. Hernan Garcia, Dr. Rob Phillips.

Awards

2017 ASCB Travel Award, American Society for Cell Biology
2017 Yeunkyung Woo Achieve Excellence Travel Award, Purdue University
2017 Purdue Research Foundation (PRF) Research Grant, Purdue Univeristy
2015 Graduate School Summer Research Grant, Purdue University
2012 Ross Fellowship, Purdue University
2009 Top Graduate Scholarship, Nankai University

Teaching Experience

2017	Teaching assistant in BIOL 110 “Fundamentals of Biology I”, spring semester. Instructor: Dr. Mark Browning; Dr. Alan Friedman. Purdue University
2016	Teaching assistant in BIOL 203 “Human Anatomy and Physiology”, fall semester. Instructor: Dr. C David Bridges. Purdue University
2015	Teaching assistant in BIOL 111 “Fundamentals of Biology II”, fall semester. Instructor: Dr. Mark Browning; Dr. Alan Friedman. Purdue University
2014	Teaching assistant in BIOL 436 “Introduction to Neurobiology”, fall semester. Instructor: Dr. Daniel Suter. Purdue University
2014	Teaching assistant in BIOL 367 “Principles of Development”, spring semester. Instructor: Dr. Donna Fekete. Dr. Yuk Fai Leung. Purdue University
2010	Teaching assistant in “Experimental Cell Biology”, fall semester. Instructor: Dr. Chunguo Wang. Nankai University

Mentoring

Graduates	Sabbir Alam, Kristi McElmurry, Sanniv Ganguly
Undergraduates	Halie Alexandria Szilagyi, Amber Lee, Shannon Eileen Roberts

Presentations

2018	"Src-mediated cortactin tyrosine phosphorylation regulates filopodia formation in neuronal growth cones." *Poster* at Chicago Cytoskeletal Meeting. Chicago, IL. 16/03/2017
2018	"Src-mediated cortactin tyrosine phosphorylation regulates filopodia formation in neuronal growth cones." *Talk* at Cellular Dynamics meeting. Purdue University, West Lafayette, IN. 02/23/2018
2018	"Src-mediated cortactin tyrosine phosphorylation regulates filopodia formation in neuronal growth cones." *Talk* at FLAME (Fish group joint lab meeting). Purdue University, West Lafayette, IN. 02/02/2018
2017	"Src-mediated cortactin tyrosine phosphorylation regulates filopodia formation in neuronal growth cones." *Poster* at Joint Annual Meeting of American Society for Cell Biology and European Molecular Biology Organization. Philadelphia, PA. 12/03/2017

2017 "Src-mediated cortactin tyrosine phosphorylation regulates filopodia formation in neuronal growth cones." *Poster* at Department of Biological Sciences Annual Retreat. Bloomington, IN. 11/11/2017

2017 "Cortactin phosphorylation promotes filopodia formation in growth cone." *Talk* at FLAME (Fish group joint lab meeting). Purdue University, West Lafayette, IN. 09/01/2017

2017 "Morphological changes in growth cones derived from cultured *Aplysia* bag cell neuron." *Talk* at Neuroscience & Physiology Seminar Series in the Department of Biological Sciences. Purdue University, West Lafayette, IN. 03/14/2017

2017 "Morphological change of growth cone of cultured *Aplysia* bag cell neuron." *Talk* at FLAME (Fish group joint lab meeting). Purdue University, West Lafayette, IN. 01/20/2017

2016 "Three dimensional culture of bag cell neuron." *Talk and poster* at Annual Biology Graduate Student Retreat. Purdue University, West Lafayette, IN. 08/16/2016

2016 "High-resolution analysis of cortactin co-localization with activated Src2 and Arp3 in growth cones." *Poster* at Chicago Cytoskeleton Meeting. Chicago, IL. 03/18/2016

2016 "Three dimensional culture of bag cell neuron." *Poster* at Sigma Xi poster competition. Purdue University, West Lafayette, IN. 03/02/2016

2015 "High-resolution analysis of cortactin co-localization with activated Src2 and Arp3 in growth cones." *Poster* at Annual Meeting of American Society for Cell Biology. San Diego, CA. 12/14/2015

2015 "Correlation between size and motility of growth cone." *Poster* at Department of Biological Sciences Annual Retreat. Plymouth, IN. 11/21/2015

2015 "Correlation between size and motility of *Aplysia* bag cell neuron growth cones."*Talk* at Cellular Dynamics Meeting. Purdue University, West Lafayette, IN. 10/09/2015

2011 "Regulation of paclitaxel sensitivity in breast cancer by microtubule-binding proteins." *Talk* at Workshop on Chemistry and Biology of Microtubules and Microtubule-interacting Agents. Beijing, China. 09/11/11

Publications

2018 Fligor CM, Edler MC, Sridhar A, **Ren Y**, Shields PK, Langer KB, Ohlemacher SK, Sluch VM, Zack DJ, Zhang C, Suter DM, and Meyer JS. Extensive neurite outgrowth and pathfinding from retinal ganglion cells derived from human pluripotent stem cells. Submitted.

2018 **Ren Y**, Athamneh A, Suter DM. Src mediated generation of traction force in growth cone turning. In preparation.

2018 **Ren Y**, He Y, Mlodzianoski MJ, Ma D, Huang F, Suter, DM. A single tyrosine phosphorylation site in cortactin is critical for filopodia formation in neuronal growth cones. Submitted.

2018 **Ren Y**, Mlodzianoski MJ, Lee AC, Huang F, Suter DM. A low-cost microwell device for high-resolution imaging of neurite outgrowth in 3D. Journal of neural engineering. 2018 Jan 24.

2017 Liu S, Mlodzianoski MJ, Hu Z, **Ren Y**, McElmurry K, Suter DM, Huang F. sCMOS noise-correction algorithm for microscopy images. Nature methods. 2017 Jul 28;14(8):760.

2016 **Ren Y**, Suter DM. Increase in Growth Cone Size Correlates with Decrease in Neurite Growth Rate. Neural plasticity. 2016 May 4; 2016.

2015 He Y, **Ren Y**, Wu B, Decourt B, Lee AC, Taylor A, Suter DM. Src and cortactin promote lamellipodia protrusion and filopodia formation and stability in growth cones. Molecular biology of the cell. 2015 Sep 15;26(18):3229-44.

2012 Shi X, Wang J, Yang Y, **Ren Y**, Zhou J, Li D. Cep70 promotes microtubule assembly in vitro by increasing microtubule elongation. Acta Biochim. Biophys. Sin.(Shanghai). 2012 May 1;44:450-4.

2012 Zhang C, Sun X, **Ren Y**, Lou Y, Zhou J, Liu M, Li D. Validation of Polo-like kinase 1 as a therapeutic target in pancreatic cancer cells. Cancer biology & therapy. 2012 Oct 1;13(12):1214-20.

2012 Peng G, **Ren Y**, Sun X, Zhou J, Li D. Inhibition of farnesyltransferase reduces angiogenesis by interrupting endothelial cell migration. Biochemical pharmacology. 2012 May 15;83(10):1374-82.

2012 Zhang SX, Zhu C, Ba Y, Chen D, Zhou XL, Cao R, Wang LP, **Ren Y**, Wu XZ. Gekko-sulfated glycopeptide inhibits tumor angiogenesis by targeting basic fibroblast growth factor. Journal of Biological Chemistry. 2012 Apr 13;287(16):13206-15.

2012 Sun X, Li D, Yang Y, **Ren Y**, Li J, Wang Z, Dong B, Liu M, Zhou J. Microtubule‐binding protein CLIP‐170 is a mediator of paclitaxel sensitivity. The Journal of pathology. 2012 Mar 1;226(4):666-73.

2011 Li D, Xie S, **Ren Y**, Huo L, Gao J, Cui D, Liu M, Zhou J. Microtubule-associated deacetylase HDAC6 promotes angiogenesis by regulating cell migration in an EB1-dependent manner. Protein & cell. 2011 Feb 1;2(2):150-60.

Outreach

2017 Guest graduate speaker. Purdue Neuroscience Society. Purdue University.11/07/2017

2016 Volunteer. Spring Fest. Purdue University. 04/16/16

2016 Volunteer. Nanodays. Purdue University. 04/14/16

2016 Volunteer. Grad Hosts for Recruitment/Interview Weekend for Department of Biological Sciences. Purdue University. 01/28-01/30/16

2015 Volunteer. Spring Fest. Purdue University. 04/18/15

2015 Volunteer. Nanodays. Purdue University. 04/17/15

2015 Member. Boiler out volunteer program. Purdue University

2014 Volunteer. The Big Ten+ Graduate School Exposition. Purdue University. 09/22/14

2014 Volunteer. Big Brother/Sisters for the incoming Graduate Students of Department of Biological Sciences. Purdue University.

2014 Volunteer. Spring Fest. Purdue University. 04/12/14

2014 Volunteer. Nanodays. Purdue University. 04/11/14

2013 Member. International friendship program. Purdue University